2-1-2012

Fabrication and characterization of synthetic substrates for use in rigidity cell culture studies of valvular interstitial cells for aortic valve tissue engineering

Alexander T. Leonard

Alexander T. Leonard

Candidate

Chemical and Nuclear Engineering

Department

This thesis is approved, and it is acceptable in quality and form for publication:

Approved by the Thesis Committee:

Dr. Elizabeth L. Dirk , Chairperson

Dr. Steven Graves

Dr. Heather Canavan

FABRICATION AND CHARACTERIZATION OF SYNTHETIC SUBSTRATES FOR USE IN RIGIDITY CELL CULTURE STUDIES OF VALVULAR INTERSTITIAL CELLS FOR AORTIC VALVE TISSUE ENGINEERING

By

ALEXANDER T. LEONARD

B.S. CHEMICAL ENGINEERING, COLORADO STATE UNIV

THESIS

Submitted in Partial Fulfillment of the
Requirements for the Degree of

Master of Science
Chemical Engineering

The University of New Mexico
Albuquerque, New Mexico

December, 2011

ACKNOWLEDGMENTS

I acknowledge Dr. Elizabeth Hedberg-Dirk, my advisor and committee chair, for her continuing support to push the limits of my knowledge, requiring my best at all times. Her encouragement to attend graduate school in the first place has helped me to grow professionally and personally. I will carry these experiences with me for life.

I thank Dr. Heather Canavan for her professional guidance and uncompensated time, instructing me in and out of the classroom. Her willingness to extend a helping hand is a quality I hope to reflect in the future. To Dr. Steven Graves, thank you for your valuable time, serving on my committees. Your advice and guidance has proven to be invaluable.

My editors and group members; Dr. Linnea Ista, Dr. Thomas Corbitt, Dr. Dimitri Dascier, Dr. Eunkyung Ji, Scott Spangler, Kirsten Cicotte, Mathew Rush, and Kristen Wilde this document is a direct reflection of your time and thoughtful inputs.

Additional thanks to Michael Brumbach (Sandia National Laboratories, SNL) for obtaining XPS spectra, Dr. Kateryna Artyushkova and Dr. Jamie Reed (University of New Mexico, UNM) for assistance in the analysis of XPS spectra and Dr. C. Jeffrey Brinker (UNM, SNL) for access to the AFM which was performed by Matthew Rush. The data for the compressive modulus and glass transition was obtained by Kirsten Cicotte at SNL. Spectral images for the quantification of ICC staining were obtained by Genevieve Phillips at the UNM Cancer Research Facility. Your experience and knowledge has enabled the incorporation of a variety of techniques otherwise unavailable. These few words cannot portray my thankfulness. Special thanks to Dr. Kristi Anseth (University of Colorado, Boulder) for insightful discussions.

I extend a great appreciation to my family who has supplied unlimited support and love throughout my graduate career.

A heartfelt thank you to my friends, who have always offered temporary escapes from reality to maintain my sanity. Finally, my mountain bike race sponsors, Bikeworks ABQ and Tomac Mountain Bikes, who thought highly enough of my abilities and personality to support me, although my fitness varied based on my workload.

Fabrication and Characterization of Synthetic Substrates for Use in Rigidity Cell Culture Studies of Valvular Interstitial Cells for Aortic Valve Tissue Engineering

By

Alexander T. Leonard

B.S. Chemical Engineering, Colorado State University, 2008

M.S. Chemical Engineering, University of New Mexico, 2011

ABSTRACT

More than 100,000 Americans each year undergo aortic valve (AV) replacement due to valve failure. An AV can become diseased, impairing the proper function of the valve. Common treatments for a defective valve are either replacement with a decellularized biologic or a synthetic valve. These treatments options are limited by short functional lifetime and thrombogenic surfaces. Tissue engineered heart valve will have the ability to integrate with the surrounding tissue as well as to repair and remodel. However, a greater understanding of valve cell biology is required to induce analogous tissue formation. A diseased valve is associated with stiffening of the tissue. Researchers have probed the impact of stiffness on cell function, but have had results complicated by *in vitro* models used.

The synthetic materials commonly used to fabricate cell culture platforms with varied moduli are limited in applicability due to a restricted range of achievable moduli and/or surface instabilities. The copolymer network n-octyl methacrylate (nOM) and diethylene glycol dimethacrylate (DEGDMA) offers attractive material properties that overcome these limitations. We have fabricated co-polymer networks with 3 to 33 wt%

DEGDMA with bulk compressive modulus of 25±2 to 4700±300 kPa. Nanoindentation determined cellular level mechanics of the nOM / DEGDMA ranged from 6.5 ± 0.00 to 1,562.5 ± 192 MPa. The networks demonstrated consistent surface properties of wettability/hydrophobicity, chemical composition and topography. The nOM/DEGDMA substrates vary in modulus over three orders of magnitude while maintaining comparable chemical and topographical surface features.

The primary cells of the AV, valvular interstitial cells (VICs), were cultured on the nOM/DEGDMA substrates. It was found that the rate of proliferation was not impacted by the stiffness of the culture platform. Expression levels of phenotypic markers for the active and osteoblastic-like were not affected by the stiffness of the substrates. Production of collagen-I and sulfated glycosaminoglycans did not change between the different substrate moduli. However, elastin production was significantly upregulated on the softest materials. We have fabricated a cell culture platform that is capable of varying over a three orders of magnitude of a physiologically relevant range, and used it to study the changes of VIC functions.

Table of Contents

List of Figures

List of Tables

Chapter 1 : Aortic Heart Valve and 2D Substrates

1. Introduction

Approximately 100,000 Americans each year must undergo aortic valve (AV) replacement due to disease or dysfunction.[3, 5, 6] An improperly functioning AV increases the strain on the heart from improper opening or closing of the valve.[6-9] Common treatment of a defective valve is replacement with either a biologically isolated or a synthetic valve.[7, 10] Bio-prosthetic valves have the drawback of a limited functional lifetime of ~10-15 years. This limited lifetime is attributed to the decellularization process, removing the cells that continually remodel structural components of the AV. The decellularization process also damages the extracellular matrix (ECM), further limiting the valves' ability to last in the body. Synthetic valves are structurally reliant, but have thrombogenic surfaces that can cause blood clots, requiring the patient to remain on lifetime anticoagulation therapy.[7] The generation of living AV constructs that are capable of integration with surrounding tissue, growth and maintenance of homeostasis will overcome the limitations of these current therapies. However, an incomplete understanding exists of how to induce the cells that occupy the AV to produce ECM.

Development of materials that are capable of directing the cellular functions of the native cells of the AV to promote normal cell functions is necessary to develop a living prosthesis. Heart valve cells (and other mammalian cells) respond to multiple influences including soluble factors and substrate interactions.[11, 12] The interactions cells have with a substrate are dependent on the mechanics, topography and/or chemistry of an underlying substrate.[13-15] Although mammalian cells are on the order of magnitude of tens of microns, changes in substrates on the nanometer scale can have a profound impact on many cellular functions.[16, 17] With this knowledge, cellular environments can be

engineered to direct cell functions. However, the problem is complicated by the fact that each type of cell will respond differently to the same stimulations. This makes it critically important to independently engineer each material for each cell type.

Substrate modulation of cell response begins with cellular adhesion. The attachment of cells through adsorbed proteins on a material's surface begins a cascade of intercellular and extracellular signaling.[14, 18] Once a cell is attached to a surface, tension generated by the cells cytoskeleton mediates the many intercellular signaling cascades through trans-membrane force sensing proteins. This type of cellular response to its environment is defined as mechanosensing. Changes of the mechanical environment of the cell can lead to alterations in the genetic and protein expression patterns of the cell through mechanosensing.[14, 18-20] For example, exposure to various substrate moduli has been shown to cause fibroblasts and osteoblasts to adapt by reorganizing the internal cytoskeleton.[19] Mechanosensing is critical in the human body as it allows cells to operate in a wide range of tissues, all with different mechanical properties directly related to the function. The soft tissues in the body can range from very soft (such as the liver with a elastic modulus of ~1 kPa[21]) to the arterial wall (~1 MPa[22]) and finally cortical bone (~5 GPa[23]).

2. Aortic Heart Valve

2.1. Anatomy and Function

The heart has four unidirectional valves that control both the flow of blood within the heart as well as in the entire cardiovascular system. The heart valves are divided into two categories: the artioventricular and semilunar.[1] The artioventricular valves are

responsible for controlling flow into the ventricles from the left (mitral valve) and right (tricuspid valve) atria. Simultaneously, the three cusped, semilunar valves control the flow leaving the heart from the left (aortic) and the right (pulmonary) ventricles into the aorta and pulmonary arteries, respectively.[24, 25] Figure 1-1 shows the anatomy of the heart with the left and right atria removed to display the valves.

The left and right sides of the heart serve different purposes; the patient's right atrium receives venous blood passes it to the right ventricle pressurizing it to approximately 20 mmHg to deliver blood to the lungs through the pulmonary artery. The left atrium receives oxygenated blood from the lungs and further pressurizes the flow to approximately 120 mmHg in the aorta.[3] The AV must withstand the most demanding hydrodynamic environment of the heart with the highest pressures and blood flows to deliver blood to the rest of the body.

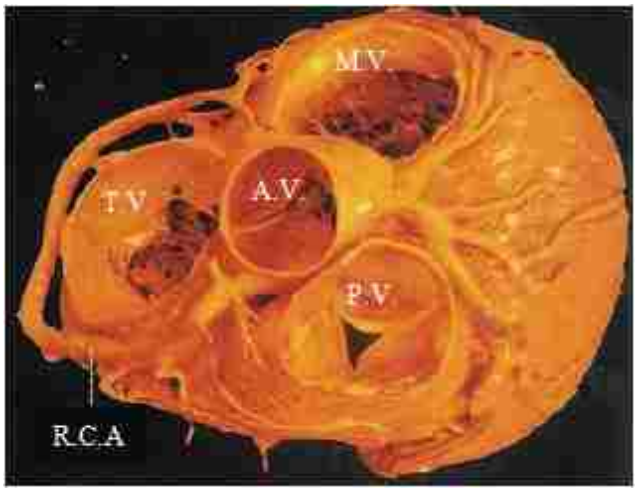

Figure 1-1. Top view of the heart with the left and right artiums removed to view the atrioventricular valves, tricuspid (T.V.) and mitral (M.V.) valve. The semilunar valves pulmonary (P.V.) and aortic (A.V.) are seen near the center of the image. The right coronary artery (R.C.A.) descends off the aorta after the aortic valve. Heart is seen with patient's right on the left side of the image.[1]

The aortic valve is composed of three leaflets, which separate during opening (systole) and come back together to create a seal when closed (diastole). The three cusps meet in the center of the aorta at a thickened area of the valve called the node of Arantii.[26] The AV cycles approximately 70 times per minute with fluid velocities as high as 5 liters per minute.[3] The AV is opened when the left ventricle contracts, increasing pressure within the ventricle. When blood has exited the left ventricle, pressure differential between the aorta and the empty ventricle causes the AV to close. An AV is subjected to three distinct types of forces during a single cardiac cycle: tension (closure), flexural (opening), and shear (blood ejection).[7, 8] As seen in Figure 1-2, each cusp is approximately 1 mm thick, and is comprised of three distinct layers: the fibrosa, ventricularis and the spongiosa.[2, 27, 28] These layers provide the valves ability to resist all of the forces applied on it and move anisotropically. The valve leaflets in healthy normal function are avascular and rely on the diffusion of nutrients and oxygen to support normal function. The AV is able to withstand these different forces and anisotropic movements by the macro and micro structure of the ECM, which is maintained by the cells of the valve.[2, 28, 29] Thus, an engineered heart valve must mimic these properties for optimal function.

Figure 1-2. Histological cross section of an aortic valve cusp, with the three distict layers. The fibrosa on the aortic side of the valve, spongiosa fills the interstitial space and the ventricularis on the ventricle side. (http://cohesion.rice.edu)

2.2. Disease and Current Treatments

Disease of the AV results in approximately 15,000 patient deaths per year in the United States. In addition to complete valve failure, 30% of adults over 65 years old suffer from early stages of valve malfunction.[30] This results in 100,000 heart valve surgeries per year, at an approximate total cost of $14 billion.[5, 31] Function of the AV can become impaired by congenital defects, age related failure and infection. Failure of the AV is classified in two different categories, stenosis (valve is unable to fully open) and regurgitation (valve is unable to fully close). Both types of disease increase the load on the left ventricle, as well as strain on the rest of the cardiovascular system. A malfunctioning AV increases the likelihood of death related to a cardiovascular disease (heart attack, stroke, etc.) by 50%.[32] Cures of AV disease by pharmaceuticals is still in early stages and treatments had limited success, leaving surgical replacement as the only treatment option, either with a synthetic or a decellularized biologic valve.[3]

Synthetic valves are currently fabricated using pyrolytic carbon coated metal. These mechanical valves are structurally dependent, but are limited by their complex geometries that induce thrombosis. [33] The thrombogenic surfaces of these valves require a patient stay on anticoagulant therapy for the remainder of their life.[34] An attractive alternative is the use of biologically isolated valves: autografts (Ross procedure), homografts (transplant) or xenografts (porcine, bovine).[9] Examples of both a synthetic and biologic valve are shown in Figure 1-3, with the fabric suture ring shown on both samples. While the biologic valve offers non-thrombogenic surfaces, the durability of the valve is limited. In adults older than 65 that are relatively inactive, a decellularized biologic valve can last 20 years. In younger, more active patients, the functional lifetime of the valve can be

decreased to less than five years.[35] The failure of a decellularized biologic valve results in either patient death or reoperation. The limitations of current treatments with biologic and synthetic valve replacements have spurred research to develop a tissue engineering solution that could produce a living valve capable of recapitulating the healthy structure and function of the AV. These valves will be populated by native cells, integrating with surrounding tissues of the patient.

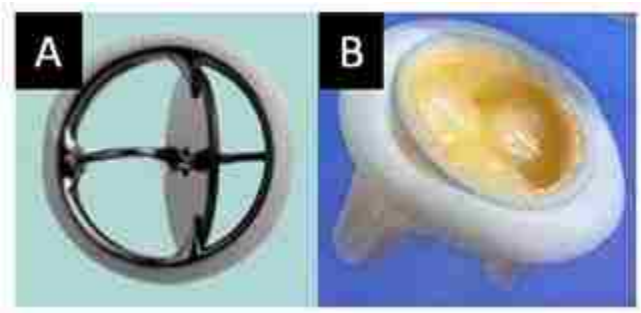

Figure 1-3. Examples of a mechanical (A) and biologic (B) heart valve replacement. (http://www.medtronic.com)

2.3. Microstructure of the Extra Cellular Matrix

The structure and the arrangement of the ECM components in the valve are critical to withstand the forces that are placed on it during healthy function. Microstructure components responsible for function and durability range from sheets of aligned fibers to hydrogel networks. Each of the three layers of the valve contains different amounts of collagen, elastin and glycosaminoglycans (GAG) that provide the needed functionality. The ventricularis dominates the elastic response during the end of the diastole phase.[29] The elastin fibers of the ventricularis give the valve its flexibility to return to the closed position at the end of the diastole phase. These fibers are radially aligned and stretch during opening and contract during closing. (Figure 1-4A).[2] Elastin is highly extensible (ε_{max} 150%) changing chain conformations based on tensile forces. This high

extensibility is attributed to a highly- crosslinked network of alternating hydrophobic and hydrophilic domains. A measure of single elastin fibers by Aaron and Gosline found an approximate Young's modulus of 1 MPa.[36]

In contrast, the fibrosa withstands the tension that is placed on the valve by the high pressure in the aorta by behaving inelastically through circumferentially aligned collagen fibers packed into bundles. These collagen bundles resist tension along the axis of the fiber. (Figure1-4 B and C).[37] However, to allow the valve to move as required the collagen fibers exist in two conformations. During systole, the collagen fibers are corrugated and offer little resistance to opening the valve. When the valve is placed under tension, the collagen fibers uncrimp and prevent the valve from collapsing into the ventricle.[4] The very low extensibility of type I collagen (ε_{max} 10 -50%, depending of extent of crosslinking) gives the fibrosa ability to resist the strain associated with diastole. Type I collagen self-assembles into arrays of fibrils which are then enzymaticaly crosslinked to form 'solid' fibers. These fibers can then be assembled into bundles The extent of crosslinking can vary the Young's modulus of the collagen fiber from 200 to 7500 MPa, allowing the tissue to be locally tuned to resist strains.[38]

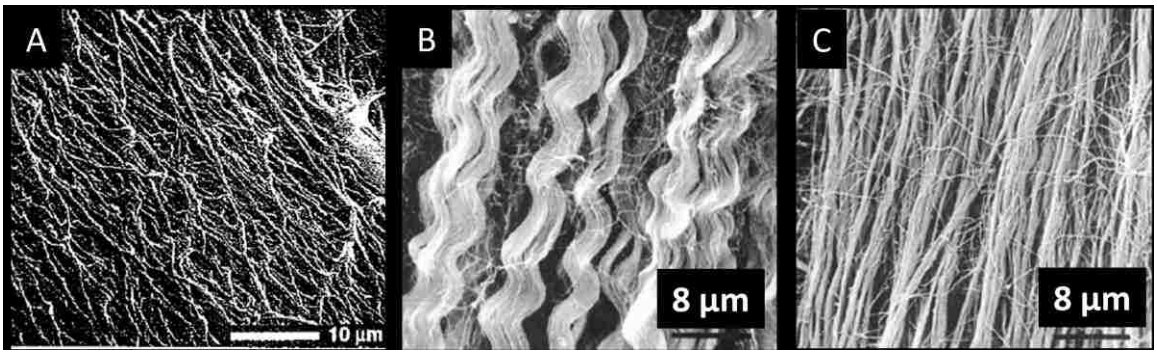

Figure 1-4. Electron micrographs of isolated structural fibers in the aortic valve. The structure and composition of the valve varries to allow for the highly anisotropic movements. Alligned elastin fibers from the ventricularis (A) allows the valve to stretch during systole while the crimped collagen fibers (B) allow the valve to open but then during diastole uncrimp and resists the tensions during diastole (C). [1, 2]

The spongiosa serves as the lubrication between the fibrosa and ventricularis. Highly hydrated glycosaminoglycans (GAGs) (chondroitin sulfate, dermatan sulfate, hyaluronan) in the spongiosa allow for the anisotropic movement of the valve cusps.[39] Isolated free standing hydrogels composed of GAG have been found to have a bulk modulus an order of magnitude lower (10 kPa) than the fibril components of the valve. The relationship between these different layers during cyclic movement of the valve is represented in Figure 1-5. To function properly, the valve is highly dependent on the orientation and arrangement of the structural components of the valve. The mechanics of the individual collagen, elastin and GAGs allow for the proper anisotropic movements of the valve. The array of structures and mechanics of a native healthy valve provide a highly diverse structural environment for the cells that occupy the valve.

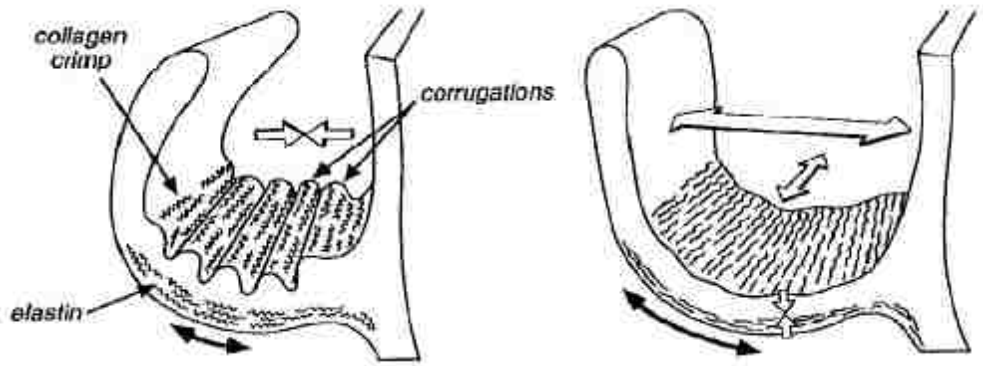

Figure 1-5. Pictorials diagram of a single leaflet in opening and closing in relation to the movements of the internal fibers of the valve.[4]

2.4. Aortic Valve Cells

The micro and macrostructure of the AV is extremely important to maintain function in the demanding environment at the base of the aorta. The highly cyclic movement of the valve puts large stresses and strains on the structural components of the valve and without continuous remolding of these structural proteins it would be impossible to maintain function over an entire lifetime. The remolding and the regulation is performed by two primary cell types that occupy the AV. The cells are the valvular interstitial cells (VICs) and valvular endothelial cells (VECs).[40]

The ideal cells to use in research for tissue engineering of the AV would be healthy and disease-free human cells. However, due to the inaccessibility of the AV, as well as the high degree of valve co-morbidity in chronic cases, healthy human cells are extremely rare. Sources for disease free human cells are, thus limited to acute traumatic non-cardiac injuries and rejected donor tissue. The amount of usable tissue is further limited as many rejected donor tissues contain inflammation or pathology from either the recipient or the donor.[41, 42] Other cell types have been evaluated as potential model cell sources, such as bone marrow mesenchymal stem cells (MSCs) and smooth muscle cells (SMCs) of the ascending aorta. The SMC displayed similar rates of proliferation, but VICs produced ECM components at a much higher rate in collagen hydrogels.[43] While MSCs showed similar response of collagen production to mechanical forces, the MSCs were more sensitive to any osteogenic compounds.[44] All of these factors require that animal models must be used to acquire healthy cells. Cells of the AV have been isolated from porcine, bovine, ovine, canine, and rodents (mouse, rat, hamster and chinchilla).[3] Cells isolated from the porcine model have become the primary *in vitro* model. The

porcine model is selected as it has similar cell size, valve hemodynamics, and homologous genome to a human.[45] For these reasons the remaining work discussed is regarding the cells of the porcine model.

The outer most layer of the AV is composed of a single layer of VECs. The VECs and other cardiac endothelial cells share the similar responsibility: to maintain the non-thrombogenic outer surface of the valve. The AV endothelium is distinct from that of the aorta and the ventricle, which is attributed to a distinctive linage during embryonic development.[3] While other cardiac cells are aligned parallel to the flow of blood, VECs align themselves circumferentially across the surfaces of the valve.[46] The VECs not only provide a non-thrombogenic surface, but also transmit nutrients and biochemical signals into the AV. [47] It has been shown that VECs are highly responsive to shear stress from surrounding fluid. The average shear stress associated with the ventricular surface is approximately 20 dynes/cm^2, with the arterial side having an order of magnitude lower stress.[24] The difference in shear stress is believed to be the cause of site specific VEC expression of many factors including caspase-3, tumor necrosis factor-α and bone morphogenetic factor-4.[31] The VECs are believed to regulate the homeostasis of the AV by signaling to the VICs through these cytokines.

The VICs are present in all layers of the valve and are responsible for the remodeling of structural valve components. To contend with the need to continually repair the micro failures of the structural components of the valve, VICs have a higher level of protein and GAG turnover coupled with a higher rate of proliferation as compared to many other cell types.[48] Any cell in the AV that is not a VEC is classified as a VIC, and as a result, the VIC population is highly heterogeneous.[49] This diverse

population is broken into five different phenotypes: embryonic (eVIC), progenitor (pVIC), quiescent (qVIC), activated (aVIC), and osteoblastic (obVIC).[49] The eVICs are only present in the developmental stage of the aortic valve; all other types can co-exist in a single valve.[50] In healthy valves, the predominant VIC phenotype is considered the qVIC which is characterized as fibroblast-like with elongated spindle-shaped morphology.[49] The qVIC population in the valve is thought to regulate low levels of ECM turnover and inhibit angiogenesis into the leaflet.[51] During injury or disease, qVIC are activated to become aVICs; characterized as smooth muscle cell-like with round-rhomboid to elongated morphologies.[49] The aVICs are associated with higher rate of ECM turnover, proliferation and migration marked by alpha-smooth muscle actin (αSMA) expression.[52] After repair of damaged/diseased tissues, aVICs are deactivated or undergo apoptosis. If the deactivation of aVICs to qVICs is disrupted, disease (fibrosis, angiogenesis, inflammation and calcification) of the valve tissue can result. *In vivo*, obVICs are observed in later stages of disease and are associated with regions that contain cartilaginous nodules and mature lamellar bone. [53, 54]

To study the transition between the aVIC and obVIC states, *in vitro* studies require the addition of specific cytokines (BMP-2 and -4, TGF-β1) and organic calcium (ascorbic acid, β-glycerol phosphate). [55] Representative images of these phenotypes in two-dimensional culture are shown in Figure 1-6. The final phenotype pVIC, can account for as much as 10% of the VIC population and has markers associated with bone marrow derived mesenchymal stem cells.[3] It has been hypothesized that these cells are associated with valve disease and the differentiation into obVICs. A subset of these pVICs are positive for both αSMA and collagen. The relationship between the cells and the

underlying substrate has also been shown to facilitate the transition of the VICs from one phenotype to another.[49]

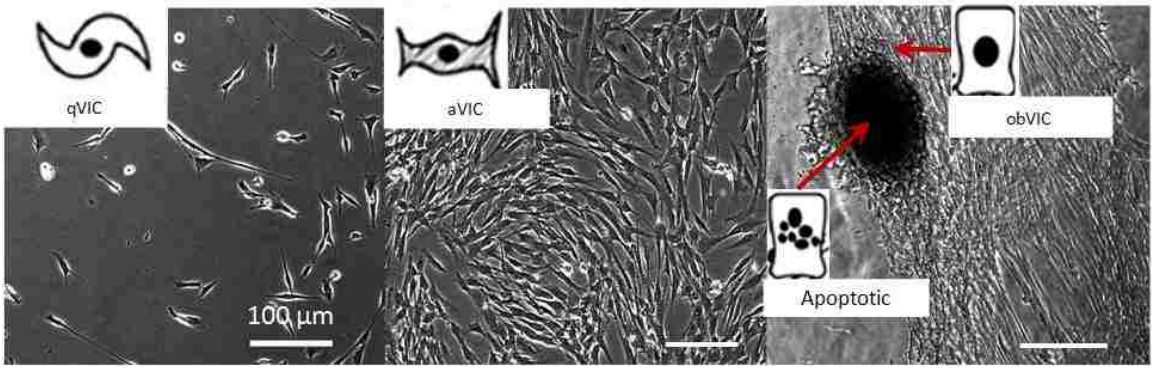

Figure 1-6. Images of the different phenotypes of VICs in vitro culture, qVIC , aVIC, obVIC.[3]

The influence of soluble factors on VIC phenotype has been extensively studied.[44, 49, 50, 54, 56] It has also been demonstrated that the substrate on which the cells are cultured also plays a large role in regulation the phenotypes. Yip *et. al* examined the relationship between the substrate material stiffness and VIC phenotypic expression. Two different substrates were fabricated using collagen fibers (~0.12 µm) with matrices of varying thicknesses to produce a compliant (2 kPa bulk modulus) and stiff (6.0 kPa bulk modulus) substrates. VICs cultured in media with components (β-glycerophosphate, ascorbic acid, dexamathesone) known to induce differentiation to obVIC lineage on the substrates showed that the compliant matrices promote osteoblastic differentiation and aggregation; however, cells cultured on stiffer matrices showed an increase in apoptosis, calcium deposition and proliferation. The stiffer matrices also made the cells more sensitive to the addition of TGF-β1, increasing the number of cellular aggregates. These results indicate that VIC function is related to the stiffness of the culture matrix as well as soluble factors.[55] Benton *et al.* compared tissue culture polystyrene (TCPS) and

poly(ethylene glycol) hydrogels coated with either fibrin or fibronectin and found that the unmodified and modified TCPS increased expression of markers associated with calcification and osteoblastic differentiation (alkaline phosphatase, αSMA, core binding factor-1 (CBFa-1)). The more compliant PEG hydrogels showed decreased levels of all for osteoblastic markers.[57] These two studies exemplify the importance of defining cell culture substrate properties.

The response of VICs to a substrate is not limited to the rigidity but is also affected by the hydrophobicity and roughness. Pedron *et al.* fabricated a gradient hydrogel capable of variations in modulus, roughness and hydrophobicity on a single surface to determine if preferential attachment of VICs occurred.[58] After a 48 hour culture period, it was observed that VICs tended to gravitate to the stiffer (E_r ~100 MPa), rougher (R_{rms} ~20 nm) and hydrophilic (Contact angle ~20°) regions of the gel.[58] These studies have indicated that the relationship between the culture substrate and cellular function of VICs requires a greater understanding and must be explored more. However, the substrates currently used do not isolate individual variables and it is difficult to deconvolute the actual substrate variations inducing the changes in VIC behavior.

3. 2D Cell Culture Platforms

3.1. 2D Materials to Study Impact of Rigidity and Topography

It has been demonstrated through numerous experiments using a wide variety of cell types that the material properties of an underlying substrates play a vital role in modulating cellular response both *in vivo* and *in vitro*[59-63]. Cellular functions such as adhesion and spreading, proliferation, and gene expression are affected by many

chemical and physical factors of a substrate, including but not limited to exposed chemical groups, surface topography, and mechanical properties.[13] Studies that have focused on the effects of mechanical properties have been limited due to a lack of materials that are capable of isolating the effects of stiffness over a wide range without changes in surface chemistry and/or topography.[64] To mimic the environments presented to VICs *in vivo*, a specific material platform is required to engineer topography and rigidity independently. The wide range of mechanics that exists in the AV structural components (kPa to GPa) as well as the variation of topographical features requires a material platform that can be easily fabricated to have the specific properties to mimic the native valve.

3.2. Materials Based on Natural Polymers for Rigidity

Materials commonly used for examining the effects of substrate rigidity can either be classified as natural or synthetic. Natural materials are generally crosslinked extracellular matrix polymers. These materials can be tailored with various moduli by varying protein concentration, stiffening cofactors, crosslinking density and substrate mounting.[65] Some natural substrates used for rigidity manipulation consist of fibrin, collagen and polysaccharides.[60] Substrates composed of natural polymers have been shown to exhibit elastic moduli of 0.001 kPa to a maximum of 150 kPa. Collagen and fibronectin substrates cover the lowest range with elastic moduli of 0.001 to 1 kPa and alginate gels ranging from 0.1 to 150 kPa.[65] Natural polymers offer the benefits of biocompatibility and cell adhesion. The reason that natural polymers make such a good cell substrate also makes them poor substrates for rigidity manipulation studies. The complex and bioactive

extracellular matrix proteins can directly interact with the cell. These interactions make it difficult to discern if the resulting cell response is due to the variation of cell/material adhesion or substrate rigidity.[13] These reasons make natural polymer based substrates difficult to use as a model platforms to understand the role of rigidity in cell functions.

3.3. Materials based on Synthetic Polymers for Rigidity

Synthetic substrates are able to overcome the limitations of low modulus and complex cell adhesion associated with natural polymer based substrates. Synthetic substrates can be fabricated with precise surface features for localized adhesion.[60] Synthetic substrates can be made from a variety of materials such as ceramics, metals and polymers.[66] We are focused on polymeric substrates due to the relative ease by which the materials can be chemically and mechanically altered. The modulus of these networks can be varied by co-polymerization of different monomers and/or addition of a crosslinking agent and polymer blending.[13, 60, 64, 65]

Some synthetic polymer networks used for rigidity manipulation include polyacrylamide (PA), polydimethylsiloxane (PDMS) and more recently poly(ethylene glycol) (PEG).[64] The substrates based on PA and PDMS have been some of the more widely studied. The moduli can be easily modified by the crosslinker to polymer ratio. Acrylamide monomers are crosslinked with bis-acrylamide using radical polymerization, and have been characterized with elastic moduli of 0.1 to 100 kPa.[65] As soft tissues in the body range 1kPa to 1 MPa, this limits PA gels to the study of the lower range of soft tissue.[64, 65] PDMS is able to overcome this limitation with elastic moduli in the range of 10 kPa to 1 MPa. A simple variation in base to curing agent ratio produces this wide

range of material modulus.[67] PDMS covers a much broader range of the soft tissue moduli range than PA. However, PDMS is unable to support a long-term cell adhesion layer, due to its hydrophobicity and high chain mobility at the surface.[64, 67] Poly(ethylene glycol) (PEG) hydrogels allow for independent control of biochemical and mechanical properties, but require additional functionalization of the material to allow for cellular adhesion.[64, 68, 69] A summary of the synthetic materials used for cell rigidity studies is shown in Figure 1-7. To further the understanding of the relationship between a substrate's rigidity and cellular functions, it is necessary to develop a substrate with an easily tunable modulus that maintains stable surface chemistry and topography over a broad range of moduli.

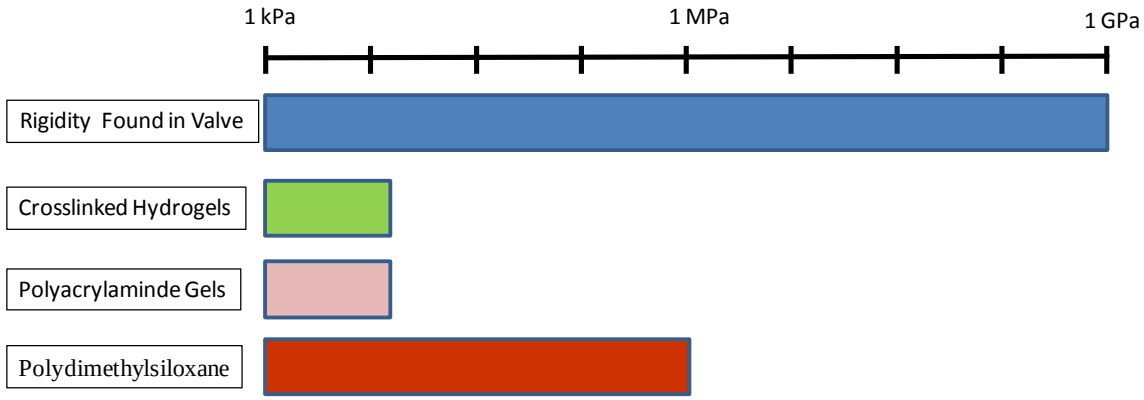

Figure 1-7. Summary of materials commonly used in cell rigidity studies along with the general range of achievable elastic modulus for each material.[64, 65]

3.4. Ordered Nanoscale Surface Topography Cell Culture Substrates

The conformation and orientation of the proteins adsorbed on a surface influence how a cell interacts with the surface. The addition of nanotopography to a surface affects either specific or nonspecific adsorbed proteins. The topography changes the conformation, orientation, and spacing of the proteins and thus the resulting cell

interactions. [70] Methods to fabricate submicron topography produce either ordered or unordered topography, each applicable for different interactions. Unordered topography methods exploit topographies that spontaneously occur under controlled processing conditions. Examples of techniques that produce unordered topography include polymer demixing, colloidal self-assembly and chemical etching.[16, 71, 72] Ordered topographies produce prescribed patterns and geometries capable of closely mimicking natural structures. The precise features are generated with electron beam lithography, photolithography or focused ion beam lithography.[16, 71]

The current work focuses on the ordered methods that produce substrates with structural features that mimic the native heart valve ECM. Producing these ordered features is generally time consuming, requires expensive equipment and precise knowledge of the submicron structure of tissues.[16, 70] Directly writing ordered patterns on materials for cell culture is impractical because the time and materials required to fabricate an individual substrate.[71] This limitation can be overcome by coupling the ordered techniques in series with nanoimprint lithography (NIL). NIL allows for the production of a single master mold that is used to pattern multiple subsequent materials by mechanical contact.[73] Several variations exist of NIL, however, the basic use of the same using a master mold to shape a liquid then varying methodologies to cure the liquid while the liquid is still in contact with the mold. When the mold is removed the negative of the mold structures remains on the imprinted surface. [73-75] A schematic is shown in Figure 1-8, where the master is brought into contact with the material to be patterned. The printed material is cured generally through changes in temperature of exposure to ultra violet light.

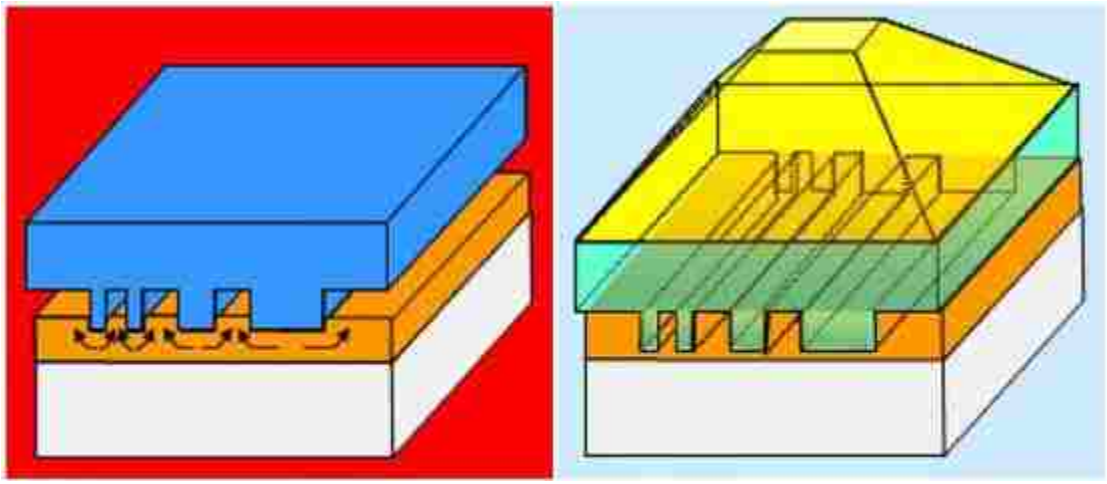

Figure 1-8. Schematic of NIL, bringing a mold fabricated with a 3D structure that is into mechanical contact with a liquid material that is cured into the negative shape of the master.[72]

Examples of materials that have been successfully printed using NIL include silicon, poly(methylmethacrylate) (PMMA) and poly(dimethylsiloxane) (PDMS). [71] Feature sizes down to 100 nm have been reported imprinting with PDMS. The feature size is limited by the elasticity of the bulk material. As a PDMS mold is pressed into the material to be imprinted the mold deforms and resolution of the original mold is decreased.[76] Use of rigid mold increases the resolution possible, as the mold does not deform with the pressure of mechanical contact. Silicon wafers and PMMA can be used to produce feature sizes down below 25 nm.[77] The trade off is that rigid molds become more difficult to release from the cured material, and damage to both the mold and imprinted material can occur when separating the materials.[74] The development of techniques for sub-micron patterning has now given bioengineers new tools to expand the type of cell culture substrates that can be produced to mimic native structures.

4. Summary

The VICs of the AV exist in a highly diverse mechanical and topographical environment. It is necessary to engineer substrates with control of both topography and bulk modulus. The natural tissue of the AV has a hierarchical structure critical for proper function of the valve: the macro structure (1 mm thickness), the micro-structure (1 μm – 1 mm) and nano-structure (< 1 μm). The culture environment plays a large role in the regulation of the VIC phenotype. The studies that have been preformed to study these impacts have been limited. Previous test substrata were plagued with problems of variation of surface properties as a result of the changes in the modulus, and thus affected the protein adsorption properties on the surface and finally the cell-material interface. With the exception of PDMS, there is little crossover between substrates used to engineer submicron surface topography and bulk material modulus. To truly understand the relationship that the VICs have with the physical environment, it is necessary to design a cell substrate capable of mimicking both topographical features and the mechanical environment present in a healthy valve. New cell culture platforms are needed to discover the appropriate conditions to induce specified cell functions. These new cell platforms will allow for the expansion of knowledge to develop a living tissue alternative to the current replacement therapies for valve disease.

5. References

1. Misfeld, M.; Sievers, H. H., Heart valve macro- and microstructure. *Phil Trans R Soc B* **2007,** 362, (1484), 1421-1436.

2. Scott, M. J.; Vesely, I., Morphology of porcine aortic valve cusp elastin. *J Heart Valve Dis* **1996,** 5, (5), 464-471.

3. Butcher, J. T.; Mahler, G. J.; Hockaday, L. A., Aortic valve disease and treatment: The need for naturally engineered solutions. *Adv Drug Deliver Rev* **2011,** 63, (4-5), 242-268.

4. Schoen, F. J., Aortic valve structure-function correlations: Role of elastic fibers no longer a stretch of the imagination. *J Heart Valve Dis* **1997,** 6, (1), 1-6.

5. Nkomo, V. T.; Gardin, J. M.; Skelton, T. N.; Gottdiener, J. S.; Scott, C. G.; Enriquez-Sarano, M., Burden of valvular heart diseases: A population-based study. *Lancet* **2006,** 368, (9540), 1005-1011.

6. Vesely, I., Heart valve tissue engineering. *Circ Res* **2005,** 97, (8), 743-755.

7. Sacks, M. S.; Schoen, F. J.; Mayer, J. E., Bioengineering challenges for heart valve tissue engineering. *Annu Rev Biomed Eng* **2009,** 11, (1), 289-313.

8. Michael, S. S.; Merryman, W. D.; David, E. S., On the biomechanics of heart valve function. *J Biomech* **2009,** 42, (12), 1804-1824.

9. Mol, A.; Smits, A. I. P. M.; Bouten, C. V. C.; Baaijens, F. P. T., Tissue engineering of heart valves: Advances and current challenges.(report). *Expert Rev Med Devic* **2009,** 6, (3), 259(17).

10. Masters, K. S.; Shah, D. N.; Leinwand, L. A.; Anseth, K. S., Crosslinked hyaluronan scaffolds as a biologically active carrier for valvular interstitial cells. *Biomaterials* **2005,** 26, (15), 2517-2525.

11. Hallab, N. J.; Bundy, K. J.; Oconnor, K.; Clark, R.; Moses, R. L., Cell adhesion to biomaterials: Correlations between surface charge, surface roughness, adsorbed protein, and cell morphology. *J Long-Term Eff Med Implants* **1995,** 5, (3), 209-231.

12. Shiu, J. Y.; Kuo, C. W.; Whang, W. T.; Chen, P. L., Observation of enhanced cell adhesion and transfection efficiency on superhydrophobic surfaces. *Lab Chip* **2010,** 10, (5), 556-558.

13. Wong, J. Y.; Leach, J. B.; Brown, X. Q., Balance of chemistry, topography, and mechanics at the cell-biomaterial interface: Issues and challenges for assessing the role of substrate mechanics on cell response. *Surf Sci* **2004,** 570, (1-2), 119-133.

14. Discher, D. E.; Janmey, P.; Wang, Y. l., Tissue cells feel and respond to the stiffness of their substrate. *Science* **2005,** 310, (5751), 1139-1143.

15. Curtis, A.; Wilkinson, C., Topographical control of cells. *Biomaterials* **1997,** 18, (24), 1573-1583.

16. Norman, J.; Desai, T., Methods for fabrication of nanoscale topography for tissue engineering scaffolds. *Ann Biomed Eng* **2006,** 34, (1), 89-101.

17. Curtis, A.; Wilkinson, C., Nantotechniques and approaches in biotechnology. *Trends in Biotechnol* **2001,** 19, (3), 97-101.

18. Vogel, V.; Sheetz, M., Local force and geometry sensing regulate cell functions. *Nat Rev Mol Cell Biol* **2006,** 7, (4), 265-275.

19. Fletcher, D. A.; Mullins, R. D., Cell mechanics and the cytoskeleton. *Nature* **2010,** 463, (7280), 485-492.

20. Janmey, P. A.; McCulloch, C. A., Cell mechanics: Integrating cell responses to mechanical stimuli. *Annu Rev Biomed Eng* **2007,** 9, (1), 1-34.

21. Yeh, W. C.; Li, P. C.; Jeng, Y. M.; Hsu, H. C.; Kuo, P. L.; Li, M. L.; Yang, P. M.; Lee, P. H., Elastic modulus measurements of human liver and correlation with pathology. *Ultrasound Med Biol* **2002,** 28, (4), 467-474.

22. Silver, F. H.; Kato, Y. P.; Ohno, M.; Wasserman, A. J., Analysis of mammalian connective-tissue - relationship between hierarchical structures and mechanical-properties. *J Long-Term Eff Med Implants* **1992,** 2, (2-3), 165-198.

23. Choi, K.; Kuhn, J. L.; Ciarelli, M. J.; Goldstein, S. A., The elastic-moduli of human subchondral, tranecular, and cortical bone tissue and the size-dependency of cortical bone modulus. *J Biomech* **1990,** 23, (11), 1103-1113.

24. Kilner, P. J.; Yang, G. Z.; Wilkes, A. J.; Mohiaddin, R. H.; Firmin, D. N.; Yacoub, M. H., Asymmetric redirection of flow through the heart. *Nature* **2000,** 404, (6779), 759-761.

25. Merryman, W. D.; Engelmayr, J. G. C.; Liao, J.; Sacks, M. S., Defining biomechanical endpoints for tissue engineered heart valve leaflets from native leaflet properties. *Prog Pediatr Cardiol* **2006,** 21, (2), 153-160.

26. Clark, R. E.; Finke, E. H., Scanning and light-microscopy of human aortic leaflets in stressed and relaxed states. *J Thorac Cardiov Sur* **1974,** 67, (5), 792-804.

27. Clark, R. E.; Finke, E. H., Morphology of stressed and relaxed human aortic leaflets. *T Am Soc Art Int Org* **1974,** B 20, 437-448.

28. Scott, M.; Vesely, I., Aortic-valve cusp microstructure - the role of elastin. *Ann of Thorac Surg* **1995,** 60, (2), S391-S394.

29. Vesely, I., The role of elastin in aortic valve mechanics. *J Biomech* **1998,** 31, (2), 115-123.

30. Messika-Zeitoun, D.; Bielak, L. F.; Peyser, P. A.; Sheedy, P. F.; Turner, S. T.; Nkomo, V. T.; Breen, J. F.; Maalouf, J.; Scott, C.; Tajik, A. J.; Enriquez-Sarano, M., Aortic valve calcification - determinants and progression in the population. *Arterioscl Throm Vas* **2007,** 27, (3), 642-648.

31. Butcher, J. T.; Markwald, R. R., Valvulogenesis: The moving target. *Philos Trans R Soc Lond B* **2007,** 362, (1484), 1489-1503.

32. *Heart disease and strokes statistics - 2009 update*; American Heart Association: Dallas, TX, 2009.

33. Zilla, P.; Brink, J.; Human, P.; Bezuidenhout, D., Prosthetic heart valves: Catering for the few. *Biomaterials* **2008,** 29, (4), 385-406.

34. Grunkemeier, G. L.; Li, H. H.; Naftel, D. C.; Starr, A.; Rahimtoola, S. H., Long-term performance of heart valve prostheses. *Curr Prob Cardiology* **2000,** 25, (2), 78-154.

35. Grunkemeier, G. L.; Li, H. H.; Starr, A., Heart valve replacement: A statistical review of 35 years' results. *J Heart Valve Dis* **1999,** 8, (5), 466-470.

36. Aaron, B. B.; Gosline, J. M., Elastin as a random-network elastomer - a mechanical and optical analysis of single elastin fibers. *Biopolymers* **1981,** 20, (6), 1247-1260.

37. Doehring, T. C.; Kahelin, M.; Vesely, I., Mesostructures of the aortic valve. *J Heart Valve Dis* **2005,** 14, (5), 679-86.

38. Guthold, M.; Liu, W.; Sparks, E.; Jawerth, L.; Peng, L.; Falvo, M.; Superfine, R.; Hantgan, R.; Lord, S., A comparison of the mechanical and structural properties of fibrin fibers with other protein fibers. *Cell Biochem Biophys* **2007,** 49, (3), 165-181.

39. Grande-Allen, K. J.; Osman, N.; Ballinger, M. L.; Dadlani, H.; Marasco, S.; Little, P. J., Glycosaminoglycan synthesis and structure as targets for the prevention of calcific aortic valve disease. *Cardiovasc Res* **2007,** 76, (1), 19-28.

40. Brody S, M. J., Yao L, O'Brien M, Dockery P, Pandit A, The effect of cholecyst-derived extracellular matrix on the phenotypic behaviour of valvular endothelial and valvular interstitial cells. *Biomaterials* **2007,** 28, (8), 1461-1469.

41. Hafizi, S.; Taylor, P. M.; Chester, A. H.; Allen, S. P.; Yacoub, M. H., Mitogenic and secretory responses of human valve interstitial cells to vasoactive agents. *J Heart Valve Dis* **2000,** 9, (3), 454-458.

42. Osman, L.; Yacoub, M. H.; Latif, N.; Amrani, M.; Chester, A. H., Role of human valve interstitial cells in valve calcification and their response to atorvastatin. *Circulation* **2006,** 114, (1_suppl), I-547-552.

43. Butcher, J. T.; Nerem, R. M., Porcine aortic valve interstitial cells in three-dimensional culture: Comparison of phenotype with aortic smooth muscle cells. *J Heart Valve Dis* **2004,** 13, (3), 478-485.

44. Ku, C.-H.; Johnson, P. H.; Batten, P.; Sarathchandra, P.; Chambers, R. C.; Taylor, P. M.; Yacoub, M. H.; Chester, A. H., Collagen synthesis by mesenchymal stem cells and aortic valve interstitial cells in response to mechanical stretch. *Cardiovasc Res* **2006,** 71, (3), 548-556.

45. Johnson, C. M.; Hanson, M. N.; Helgeson, S. C., Porcine cardiac valvular subendothelial cells in culture - cell isolation and growth-characteristics. *J Mol and Cell Cardiol* **1987,** 19, (12), 1185-1193.

46. Deck, J. D., Endothelial-cell orientation on aortic-valve leaflets. *Cardiovas Res* **1986,** 20, (10), 760-767.

47. Frater, R. W. M.; Gong, G.; Hoffman, D.; Liao, K., Endothelial covering of biologival artificial-heart valves. *Ann Thorac Surg* **1992,** 53, (3), 371-372.

48. Schneider, P. J.; Deck, J. D., Tissue and cell renewal in the natural aortic-valve of rats - an autoradiographic study. *Cardiovasc Res* **1981,** 15, (4), 181-189.

49. Liu, A. C.; Joag, V. R.; Gotlieb, A. I., The emerging role of valve interstitial cell phenotypes in regulating heart valve pathobiology. *Am J of Pathol* **2007,** 171, (5), 1407-1418.

50. Chiu, Y. N.; Norris, R. A.; Mahler, G.; Recknagel, A.; Butcher, J. T., Transforming growth factor beta, bone morphogenetic protein, and vascular endothelial growth factor mediate phenotype maturation and tissue remodeling by

embryonic valve progenitor cells: Relevance for heart valve tissue engineering. *Tissue Eng Part A* **2010,** 16, (11), 3375-3383.

51. Lester, W. M.; Damji, A. A.; Gedeon, I.; Tanaka, M., Interstitial-cells from the atrial and ventricular sides of the bovine mitral-valve respond differently to denuding endocardial injury. *In Vitro Cell Dev-An* **1993,** 29A, (1), 41-50.

52. Durbin, A. D.; Gotlieb, A. I., Advances towards understanding heart valve response to in injury. *Cardiovasc Pathol* **2002,** 11, (2), 69-77.

53. Mohler, E. R.; Gannon, F.; Reynolds, C.; Zimmerman, R.; Keane, M. G.; Kaplan, F. S., Bone formation and inflammation in cardiac valves. *Circulation* **2001,** 103, (11), 1522-1528.

54. Rajamannan, N. M.; Subramaniam, M.; Rickard, D.; Stock, S. R.; Donovan, J.; Springett, M.; Orszulak, T.; Fullerton, D. A.; Tajik, A. J.; Bonow, R. O.; Spelsberg, T., Human aortic valve calcification is associated with an osteoblast phenotype. *Circulation* **2003,** 107, (17), 2181-2184.

55. Yip, C. Y. Y.; Chen, J.-H.; Zhao, R.; Simmons, C. A., Calcification by valve interstitial cells is regulated by the stiffness of the extracellular matrix. *Arterioscler Thromb Vasc Biol* **2009,** 29, (6), 936-942.

56. Cushing, M. C.; Liao, J.-T.; Anseth, K. S., Activation of valvular interstitial cells is mediated by transforming growth factor-[beta]1 interactions with matrix molecules. *Matrix Biol* **2005,** 24, (6), 428-437.

57. Benton, J. A.; Kern, H. B.; Anseth, K. S., Substrate properties influence calcification in valvular interstitial cell culture. *J Heart Valve Dis* **2008,** 17, (6), 689-699.

58. Pedron, S.; Peinado, C.; Bosch, P.; Benton, J. A.; Anseth, K. S., Microfluidic approaches for the fabrication of gradient crosslinked networks based on poly(ethylene glycol) and hyperbranched polymers for manipulation of cell interactions. *J Biomed Mater Res A* **2011,** 96A, (1), 196-203.

59. Shieh, A., Biomechanical forces shape the tumor microenvironment. *Ann Biomed Eng* **2011,** 39, (5), 1379-1389.

60. Georges, P. C.; Janmey, P. A., Cell type-specific response to growth on soft materials. *J Appl Physiol* **2005,** 98, (4), 1547-1553.

61. Meital Levy-Mishali, J. Z., Shulamit Levenberg, Effect of scaffold stiffness on myoblast differentiation. *Tissue Eng Part A* **2009,** 15, (4), 935-944.

62. Genes, N. G.; Rowley, J. A.; Mooney, D. J.; Bonassar, L. J., Effect of substrate mechanics on chondrocyte adhesion to modified alginate surfaces. *Arch Biochem Biophys* **2004,** 422, (2), 161-167.

63. Stephens, E. H.; Durst, C. A.; West, J. L.; Grande-Allen, K. J., Mitral valvular interstitial cell responses to substrate stiffness depend on age and anatomic region. *Acta Biomater* **2011,** 7, (1), 75-82.

64. Nemir, S.; West, J. L., Synthetic materials in the study of cell response to substrate rigidity. *Ann Biomed Eng* **2010,** 38, (1), 2-20.

65. Rehfeldt, F.; Engler, A. J.; Eckhardt, A.; Ahmed, F.; Discher, D. E., Cell responses to the mechanochemical microenvironment--implications for regenerative medicine and drug delivery. *Adv Drug Delivery Rev* **2007,** 59, (13), 1329-1339.

66. Shin, H.; Jo, S.; Mikos, A. G., Biomimetic materials for tissue engineering. *Biomaterials* **2003,** 24, (24), 4353-4364.

67. Brown, X. Q.; Ookawa, K.; Wong, J. Y., Evaluation of polydimethylsiloxane scaffolds with physiologically-relevant elastic moduli: Interplay of substrate mechanics and surface chemistry effects on vascular smooth muscle cell response. *Biomaterials* **2005,** 26, (16), 3123-3129.

68. Flanagan, L. A.; Ju, Y. E.; Marg, B.; Osterfield, M.; Janmey, P. A., Neurite branching on deformable substrates. *Neuroreport* **2002,** 13, (18), 2411-2415.

69. Leach, J. B.; Brown, X. Q.; Jacot, J. G.; DiMilla, P. A.; Wong, J. Y., Neurite outgrowth and branching of pc12 cells on very soft substrates sharply decreases below a threshold of substrate rigidity. *J Neural Eng* **2007,** 4, (2), 26-34.

70. Lord, M. S.; Foss, M.; Besenbacher, F., Influence of nanoscale surface topography on protein adsorption and cellular response. *Nano Today* **2010,** 5, (1), 66-78.

71. Ni, M.; Tong, W. H.; Choudhury, D.; Rahim, N. A. A.; Iliescu, C.; Yu, H., Cell culture on mems platforms: A review. *Int J Mol Sci* **2009,** 10, (12), 5411-5441.

72. Zhang, S.; Marini, D. M.; Hwang, W.; Santoso, S., Design of nanostructured biological materials through self-assembly of peptides and proteins. *Curr Opin Chem Biol* **2002,** 6, (6), 865-871.

73. Truskett, V. N.; Watts, M. P. C., Trends in imprint lithography for biological applications. *Trends Biotechnol* **2006,** 24, (7), 312-317.

74. Schift, H., Nanoimprint lithography: An old story in modern times? A review. *J Vac Sci Technol B* **2008,** 26, (2), 458-480.

75. Guo, L. J., Nanoimprint lithography: Methods and material requirements. *Adv Mater* **2007,** 19, (4), 495-513.

76. Bender, M.; Plachetka, U.; Ran, J.; Fuchs, A.; Vratzov, B.; Kurz, H.; Glinsner, T.; Lindner, F. In *High resolution lithography with pdms molds*, San Diego, California (USA), 2004; AVS: San Diego, California (USA), 2004; pp 3229-3232.

77. Chou, S. Y.; Krauss, P. R.; Renstrom, P. J., Imprint lithography with 25-nanometer resolution. *Science* **1996,** 272, (5258), 85-87.

Chapter 2 : Fabrication and Characterization of Synthetic Substrates

Prepared for Submission to the journal Biomaterials

Fabrication and Characterization of Synthetic Substrates for Use in Rigidity Cell Culture Studies

Alexander T. Leonard [a, b]; Kirsten N. Cicotte [b]; Jared R. Funston [a, b]; Matthew N. Rush[b] and Elizabeth L. Hedberg-Dirk,[a, b]

[a] *Department of Chemical and Nuclear Engineering, University of New Mexico, Albuquerque, NM*

[b] *Center for Biomedical Engineering, University of New Mexico, Albuquerque, NM*

1. Introduction

The fabrication and characterization of a new cell culture substrate is examined. The goal was to fabricate a cell culture platform that varies material modulus over several orders of magnitude, while maintaining similar surface features across the mechanical range and is easily fabricated. Here we examine the use of mono and di-methacrylate system as a cell culture platform. The platform is capable of variations in bulk modulus while maintaining the surface features.

Changes in surface topography, surface energies, and chemical functional groups usually accompany changes in a material's stiffness.[1-3] The alterations in surface properties will all affect the way that biomolecules adsorb onto a surface and that can affect how the cells adhere to those biomolecules.[4] It is therefore required to have precise control of substrate's surface properties to control cellular interactions and manage cellular response. The variation of surface properties is a major limitation of previous substrates used to study the impact of substrate modulus on cellular function.

Current materials in use to evaluate the cellular function impact from the material's mechanical properties include cross-linked hydrogels, polyacrylamide (PA), and polydimethylsiloxane (PDMS).[5, 6] For example, hydrogels with an elastic modulus ranging from 0.001 to 150 kPa lack the rigidity to model stiff tissues. [2, 5] Specifically, hydrogels fabricated from natural polymers can increase cell adhesion, but the complexity of the chemical structure can have unknown interactions with the adhered cell.[5, 7, 8] Synthetic substrates such as PA and PDMS are capable of achieving elastic moduli of 0.1 to 1000 kPa and have the benefit of precise control of mechanics via

crosslinking ratios.[5] However, it has been observed that PA gels and PDMS require surface modification to allow cell adhesion.[2, 9-11]

The co-polymer network of n-octyl methacrylate (nOM) and diethyleneglycol dimethacrylate (DEGDMA) was chosen based on the proven biocompatibility as dental restorative material.[12, 13] Young et al. showed that an increase from 5 to 20 wt% DEGDMA at 37°C corresponds to an increase in the storage modulus from 10^3 to $10^{4.1}$ kPa.[14] Initially, a trimethacrylate system was also investigated, using trimethylolpropane trimethacrylate as the crosslinker. This system has also been shown to be biocompatible and has an increase in storage modulus with increase in crosslinker content. The trimethacrylate system was not chosen for this platform as the 3.5 wt% crosslinker materials have a storage modulus nearly an order of magnitude larger than the 5 wt% dimethacrylate system.[15] The much larger storage material modulus would limit the trimethacrylate based system to the upper range of tissues. The use of these studies as the basis for our work, the dimethacrylate system was chosen. The dimethacrylate system offers a physiologically relevant moduli range and the ability to fabricate substrates that are homogenous in the material properties.

The values of DEGDMA content were chosen based on the glass transition temperatures determined by Young *et al*.[16] It was observed that at approximately 33 wt% DEGDMA that poly(nOM-co-DEGDMA) has a glass transition temperature of 37°C, body temperature. Although the substrates were based on Young's poly(nOM-co-DEGDMA), adaptations of the photoinitator and fabrication techniques were necessary for poly(nOM-co-DEGDMA) substrates to be used as a cell culture platform. These changes will have an impact on the properties of the resulting polymer substrate. For

example the photoinitator was changed from 2,2-dimethoxy-2-phenylacetophenone (DMPA) in the Young studies to IRGACURE 2959 in the current study. The change of the photoinitator has an impact on the reaction kinetics and thus the final internal structure of the polymer networks. The bulk material properties of compressive modulus and glass transition temperature were tested to determine the range of achievable modulus. The surfaces of these materials were evaluated to determine relative hydrophobicty, chemical composition and topography across a single formulation as well as between the different formulations. Finally, the polymer networks were verified as a viable cell culture platform.

2. Materials and Methods

2.1. Substrate Fabrication

Substrates were polymerized from n-octyl methacrylate (nOM; Scientific Polymer Products (SPP), Ontario, NY) and diethyleneglycol dimethacrylate (DEGDMA; SPP). n-Octyl methacrylate and DEGDMA were received inhibited with monomethyl ether hydroquinone (MEHQ) and hydroquinone (HQ), respectively. The radical inhibitor was removed with HQ/MEHQ removal columns (SPP) immediately before use. The photoinitiator used for these studies was 1-[4-(2-hydroxyethoxy)phenyl]-2-hydroxy-2-methylpropan-1-one (IRGACURE 2959, Ciba, Florham Park, NJ). Four substrate formulations were fabricated with 3, 19, 25 or 33 wt% DEGDMA and 0.25 wt% IRGACURE 2959, with the remaining being nOM.

Monomers and radical initiator were added to a glass vial and heated to slightly above room temperature to allow the IRGACURE 2959 to dissolve. The reaction mixture

was allowed to stir overnight at room temperature. The reaction mixture was poured into glass molds, 3 x 5 x 0.1 cm, and polymerized in a UV crosslinking box (CL-1000, UVP, Upland, CA) for 300 minutes with a maximum wavelength emission at 365 nm and exposure energy of 999.9 mJ/cm^2. Substrates were removed from molds by sonication in ethanol (200 proof, Fisher Scientific, Waltham, MA). Circular samples of diameter 6 mm were cut out of the cured sheet using a biopsy punch (96-1125, Sklar, West Chester, PA). These circular samples were used to determine glass transition temperature (Tg), contact angle measurements, X-ray photoelectron spectroscopy (XPS), atomic force microscopy (AFM), protein adsorption and biocompatibility. Samples intended for compressive modulus testing were fabricated in glass vials with an inner diameter of 6 mm. To obtain a 2:1 height to diameter ratio the crosslinked cylindrical samples were cut to a length of 12 mm with a wet saw (TechCut 5™, Allied High Tech Products Inc., Rancho Dominguez, CA). Before testing all samples were submerged in 200 proof ethanol (Fisher) for 48 hours, degassed overnight under vacuum, and submerged in 18 MΩ water (Synergy UV, Millipore, Billerica, MA) for 1 week.

2.2. Bulk Compressive Modulus

Compressive modulus of the bulk material was determined for the four formulations (n=5) using an Instron (5500R, Instron, Norwood, MA) following ASTM 695 – 02a. The experiment was performed using MTS ReNew software (Eden Prairie, MN). Stress – strain curves were analyzed in the linear region (5 – 20% strain) using Microsoft Excel (Microsoft Croporation, Redmond, WA) to determine sample modulus.

2.3. Glass Transition Temperature (Tg)

The Tg was measured using differential scanning calorimetry (DSC Q100, TA Instruments, New Castle, DE). Material samples were cut down from the 6 mm disks to 1 mm^2 squares to fit in the sample pans (900779.901, TA Instruments). The samples were heated from -50°C to 150°C at a rate of 10°C/min for 3 cycles. The Tg calculated from the DSC heat flow trace from the midpoint of step function using the instrument software (Universal Analysis, TA Instruments).

2.4. Contact Angle Measurement

Samples were dried under vacuum overnight. Contact angles were determined using the sessile drop technique on a goniometer (Model 100-00-115, ramé-hart Inc., Netcong, NJ). Briefly, 3 μL of ultrapure water was pipetted onto the center of the sample surface to avoid edge effects. The contact angle between the water droplet and the sample surface was determined using the DROPimage Standard program (ramé-hart). The contact angles were measured immediately after drop formation to minimize the effect of dynamic surface wetting and evaporation. Four samples of each formulation were tested with one drop per sample and three measurements per drop.

2.5. X-ray Photoelectron Spectroscopy (XPS)

XPS survey and high resolution spectra were obtained using Kratos Axis Ultra spectrometer with a monochromatic Al K(α) (1486.6 eV) source at 225W. High-resolution spectra of carbon and oxygen were obtained for two areas for each sample. Survey spectra were obtained at pass energy 80 eV and high-resolution spectra at pass

energy 20 eV. Base pressure was less than 5 x 10^{-9} Torr. Charge compensation was accomplished using low energy electrons. Linear background was used for elemental quantification of C1s and O1s spectra. Quantification utilized sensitivity factors provided by the manufacturer. All the spectra were charge referenced to the aliphatic carbon at 285 eV. Curve fitting was carried out using individual peaks of constrained width, position and 70% Gaussian/30% Lorentzian line shape.

2.6. Atomic Force Microscopy (AFM)

Samples for the AFM were incubated with 5 mL ethanol while sonicated for 2 minutes. The ethanol wash was followed by rinsing in 5 mL of deionized H_2O (dH_2O). The cleaned samples were mounted on a glass coverslip using silicon vacuum grease and inserted in a liquid cell (BioHeater Closed Fluid Cell, Asylum Research, Santa Barbara, CA). The fluid cell was mounted on the AFM instrument (MFP-3D Version 050810, Asylum Research (AR), Santa Barbara, CA) and filled with dH_2O. The liquid cell was heated to 37°C (AFM Environmental Controller, AR). Surface scanning was performed at 2.50 µm per second at 0.2 Hz with a 40 nm radius cantilever tip (TR400PB, Olympus, Center Valley, PA). Scans were analyzed using Igor Pro (MFP-3D, Asylum Research).

2.7. Total Protein Adsorption

Four substrates of each of the four formulations were mounted onto the bottom of flat bottom 96 well plate (3370, Corning Inc., Corning, NY) with a small amount of silica vacuum grease. The loaded plate was placed under UV (NU-430-600, Nuaire, Plymouth, MN) radiation for 30 min to sterilize the plate. Each substrate was incubated

with 2 mg/mL bovine serum albumin (BSA, A9418-5G, Sigma-Aldrich, St, Louis, MO) in 1X phosphate buffer saline (PBS, C001N22, Thomas Scientific, Swedesboro, NJ) for 45 minutes at 37°C. The BSA/PBS solution was removed, and substrates were washed three times with 200µL of PBS to remove non-adsorbed proteins. Substrates were then incubated in 150µL 2% SDS solution overnight at 37°C. The 2% SDS was removed from the substrates and placed in a black walled clear bottom plate (3370, Corning), and protein content determined with the Micro BCA Protein Assay Kit (23235, Thermo Scientific, Fremont, CA) as per the manufacturers' instructions, and compared to a BSA standard curve. The analysis of the assay was performed using the SpectraMax M2 Microplate Reader (Molecular Devices, Sunnyvale, CA) at 562nm.

2.8. Cellular Seeding

The murine cell line MC3T3-E1 (CRL-2593, ATCC, Manassas, VA) was used as a model cell line for all cell studies. All tissue culture solutions were purchased from Fisher Scientific. Cells were cultured in 75 cm^2 tissue culture polystyrene (TCPS) medium consisting of MEM alpha modification media (1X) supplemented with 10% (v/v) fetal bovine serum (FBS), 1% (v/v) penicillin/streptomycin (P/S), and 1% (v/v) fungizone at 37°C and 5.0% carbon dioxide. At ~80% confluence, cells were rinsed with 2 mL Dulbecco's phosphate buffered solution (DPBS). Cells were lifted with 2 mL of 0.25% (w/v) trypsin incubated at 37°C for 15 minutes. The cell solution was transferred to two micro centrifuge tubes and centrifuged at 2000 rpm for 5 minutes. The supernatants were removed and the pelleted cells were resuspended in 2 mL of fresh culture media, the cell solutions were recombined. Cell concentrations were determined

using a hemocytometer (1483, Hausser Scientific, Horsham, PA). Four samples of each substrate formulation were loaded into a flat bottom non-tissue culture polystyrene 96 well plates (3370,Corning, Lowell, MA). Samples were covered with 200 µL of ultra pure water and sterilized through exposure to UV radiation (Nuaire) overnight. After removal of the water, surfaces were seeded with MC3T3-E1 cells at a density of 25,000 cells/cm^2.

2.9. Cellular Attachment and Viability

Cellular attachment and viability were assessed after 6 and 96 hours, respectively, using the Live/Dead® Cell Viability Assay (Invitrogen, Carlsbad, CA) as per the manufacturer's instructions. Four samples of each substrate formulation were used per time point. Live and dead cell controls consisted of cells seeded at the same density on regular (non-tissue culture treated) polystyrene 96 well plates (3370, Corning). Dead controls were incubated with 100 µL of 70% methanol/30% water for 30 minutes prior to staining. All samples were incubated with 100 µL of 4 µM ethidium homodimer-1 (ex 495nm/em 515nm) and 1 µM calcein AM (ex 495nm/em 635nm) for one hour, thereby staining the live cells green and dead cells red. The fluorescently labeled cells were imaged on an inverted microscope (Eclipse TS-100, Nikon, Melville, NY) with a mercury light source (X-Cite Series 120, Lumen Dynamics, Mississauga, Ontario). Images were captured with a 14.2 Color Mosaic camera and processed using Spot software (Diagnostic Instruments Inc. Sterling Heights, MI).

2.10. Statistical Analysis

Compressive modulus and protein adsorption results were analyzed using the Kruskal-Wallis one-way nonparametric analysis of variance (ANOVA) with values of $p < 0.05$ considered statistically significant. Contact angle measurements were compared for significance using a Friedman Test (nonparametric repeated measures ANOVA) with values of $p < 0.05$ considered statistically significant. All analysis was done with InStat 3 (GraphPad Software, La Jolla, CA).

3. Results

3.1. Bulk Compressive Modulus

The uniaxial compressive modulus was determined from the slope of the linear region of the stress-strain curves.[17] Compressive moduli of all four formulations (3, 19, 25 and 33 wt% DEGDMA) are presented in Figure 2-1. All formulations were found to be significantly different with $p < 0.01$.

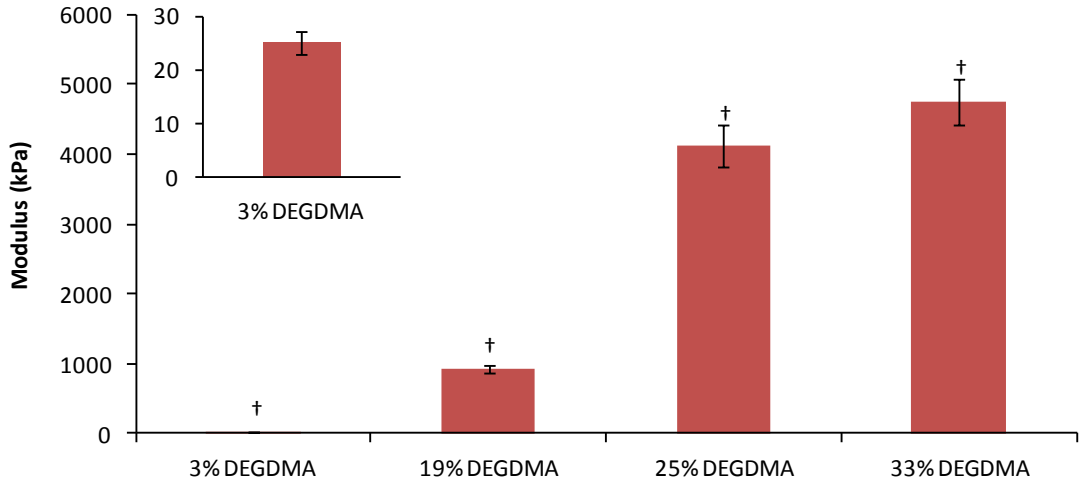

Figure 2-1. Compressive modulus for the four formulations studied, 3, 19, 25 and 33 wt% DEGDMA substrates. Slight increase or decrease in DEGDMA content can be used to achieve a tunable material modulus. n=5, † $p < 0.01$

3.2. Glass Transition Temperature

Glass transition temperatures (T_g) for the four formulations are shown in Figure 2-2. The T_g was determined from the heat flow traces between -50 and 150°C heated at a rate of 10°C/min. The midpoint of the step functions observed from the heat flow traces were used to establish the T_g. The increase in T_g with the increase of DEGDMA content is expected as an increase of crosslinking density is proportional to the increase in crosslinker content. This phenomenon is due to the decrease in the degrees of freedom of each chain. Figure 2-2 demonstrates the T_g increase from -7 to 53°C between the 3 and 33 wt% DEGDMA substrates.

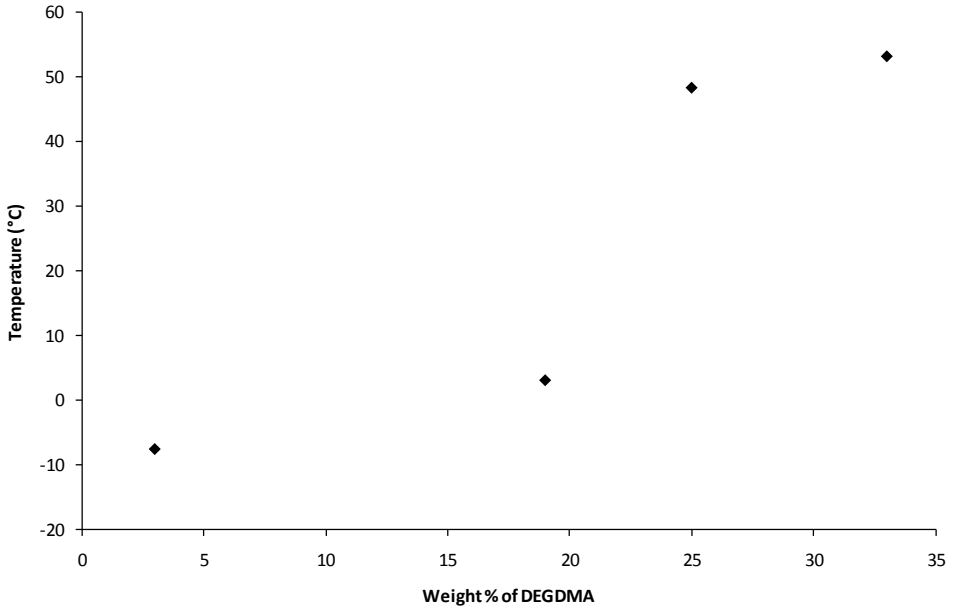

Figure 2-2. Glass transition temperatures (Tg) for the four formulations of varying DEGDMA content substrates tested. The Tg varies proportionally with the measured compressive modulus.

3.3. Contact Angle Measurement

Using the Sessile drop technique, the water contact angles were used to determine the surface wettabilty with a 3 μL drop of 18 MΩ water. Contact angle is a simple method to approximate solid-vapor and solid-liquid interfacial tensions by measuring the tangent angle where the three phases intersect.[18] Contact angles for 3, 19, 25 and 33 wt% DEGDMA substrate formulations are presented in Figure 2-3. No statistical difference was found across all of the four different substrate formulations. Consistent contact angle indicates that the surface energetics and topography are similar between different material formulations. The similarity in contact angle suggests that the amount of protein adsorption and conformation will be comparable across the different formulations.

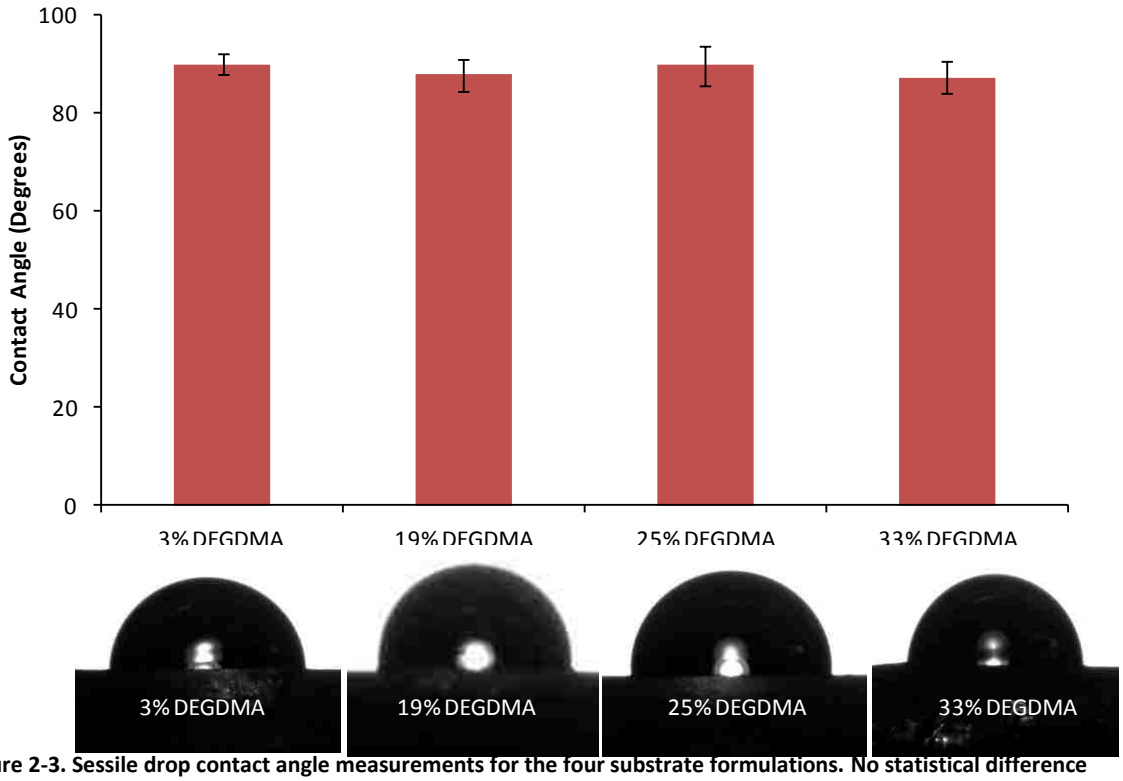

Figure 2-3. Sessile drop contact angle measurements for the four substrate formulations. No statistical difference between formulations was observed, indicating consistent surface wettability/hydrophobicity across the range of formulations. n=4 for each formulation.

3.4. X-ray photoelectron spectroscopy

Quantification of the elemental composition and functional groups was performed using XPS. The position of the peak (i.e., binding energy) and the peak intensity were used to identify surface elemental composition, the chemical bond environment, and quantity of each of the DEGDMA formulations. Solid samples of 3 and 33 wt% DEGDMA formulations were analyzed to validate that the differences between the substrates chemical surface was minimal. For each sample, two spots were analyzed to confirm consistency across a single formulation. Heterogeneities in the material were observed with the initial material evaluation by Young *et al.*, primarily believed to be due to cyclization of the polymer network as the amount of crosslinking agent was increased past a critical point.[19] Surface characterization was performed at multiple spots on the surface to verify that these cyclizations would not have a negative impact on poly(nOM-co-DEGDMA) ability to be used for cell culture.. Several surface analysis techniques were employed to verify homogenous surfaces on a single substrate and across multiple substrate formulations.

The elemental compositions of the substrates are shown in Table 2-1. Briefly, the compositions of both formulations are nearly identical (79.2% C and 16.4% O for the 3% DEGDMA formulation; 80.7% C and 17.4% O for the 33wt% DEGDMA formulation). The variation between samples is well within the experimental error of the technique.[20-22] From this data, the ratio of C/O was calculated and compared to that of the predicted by the stoichiometry of the monomers. The observed ratio of C/O of the 33wt% DEGDMA formulation (4.6) is nearly identical to the value predicted by stoichiometry of the

monomers (4.3). The 3wt% DEGDMA formulation C/O ratio differs slightly from the expected value (4.7 to 5.7, respectively); this difference is most likely due to the presence of hydroxyl groups on the surface from incomplete conversion of free radicals during polymerization.

Table 2-1. Elemental composition of the maximum and minimum DEGDMA content substrates made determined by XPS analysis. Values represent the relative atomic percentage of each species present on the surface averaged from two locations. Trace amounts of (<1%) nitrogen and silicon (<4%) was also detected.

	C 1s	O 1s	C / O Ratio
3% DEGDMA Experimental	79.2	16.4	4.7
3% DEGDMA Stoichiometric	85	15	5.7
33% DEGDMA Experimental	80.7	17.4	4.6
33% DEGDMA Stoichiometric	81	19	4.3

In addition to obtaining elemental information, high-resolution spectra were obtained for carbon and oxygen to observe the chemical species of these elements. High-resolution O1s spectra in Figure 2-4B show similar shapes between the 3 (top) and 33 (bottom) wt% DEGDMA formulations. Table 2-2 contains the oxygen binding environment quantification values. Peak assignments were as follows: O=C, 532.3 eV; C-O-C, 533.9 eV; O-(C=O), 534.4 eV; O-H, 536 eV.[23] The location of the peak fits for the α-oxygen (O-(C=O)) and the ether (C-O-C) are within 1 eV, which is below the resolution of the instrument. [30% C-O-C and 24% O-(C=O) for 3 wt% DEGDMA, 31% C-O-C and 23% O-(C=O) for 33 wt% DEGDMA]. It is necessary to combine the two quantification values; from this adjusted data the ratio of ester to ether was calculated. For both the 3 and 33 wt% DEGDMA formulations the ratio of ester to ether functionalities are almost identical between the experimental and the values predicted by the stoichiometry of the

monomers (0.6 to 1.0 for 3wt% DEGDMA, 0.7 to 0.9 for 33wt% DEGDMA). The observed peak for hydroxyl (O-H, 536 eV) is most likely due to oxidization at the surface from incomplete conversion of free radicals from the polymerization.

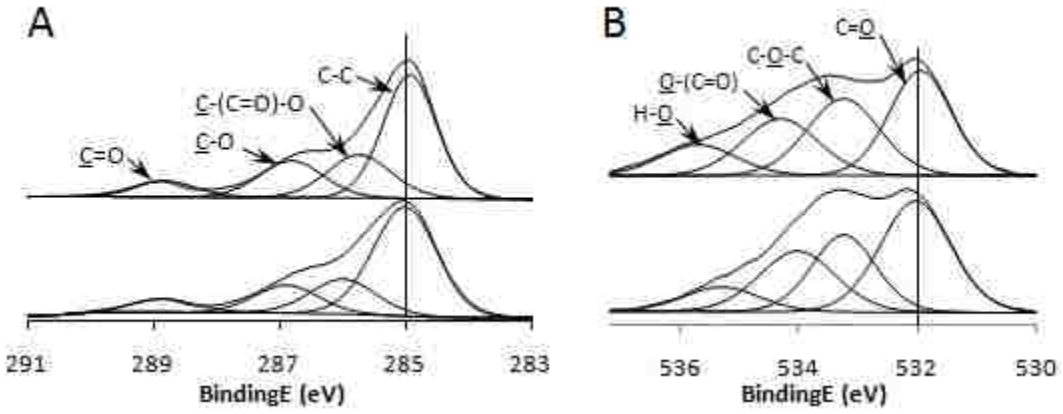

Figure 2-4. Representative high-resolution scans from 3 (top) and 33 (bottom) wt% DEGDMA formulations for C1s (left) and O1s (right). The surface reproducibility is confirmed by the C1s high-resolution scans (A) of the 3 and 33 wt% DEGDMA substrates. The O1s high-resolution spectra (B) for 3 and 33 wt% DEGDMA demonstrate similar peak shapes between the two formulations.

The high-resolution C1s spectra (Figure 2-4A) have similar shapes between the 3 (top) and 33 (bottom) wt% DEGDMA formulations. The peak assignments for the carbon high resolution peak are as follows: aliphatic carbon, 285 eV; C-(C=O)-O, 285.7 eV; C-O, 286.8 eV, C=O, 288.8 eV.[23] As with the O1s spectra, the peaks for the α-carbon (C-(C=O)-O, 285.7 eV) and the aliphatic carbons (C-C, 285 eV) are separated by less than 1 eV at the peak maxima. The separation necessitates the combination of the peak fit parameters (46% C-C and 23% C-(C=O)-O for the 3 wt% DEGDMA formulation; 45% C-C and 25% C-(C=O)-O for the 3 wt% DEGDMA formulation) and is shown as a calculated value in Table 2-3 (69% and 70% for 3% and 33% DEGDMA formulation, respectively). The adjusted value for the aliphatic carbon was used to calculate the ratio of C-C/C-O and C-C/C=O. The variation between the C-C/C-O value for the 3 and 33

wt% DEGDMA formulations (3.3 and 3.6, respectively) is an excellent demonstration of the limited variation between the two extremes of material rigidity.

Table 2-2. High-resolution spectra of oxygen quantification. Oxygen binding environment of 3 and 33 wt% DEGDMA content substrates. Values represent the relative percent of each species present on the surface averaged from two different locations on the surface. The experimental values are shows for 3 and 33 wt% DEGDMA for each formulation.

	O=C 532.3	C-O-C 533.9	O-(C=O) 534.4	O-H 536	C-O-C + O-(C=O)	O=C / O-C
3% DEGDMA Experimental	33	30	24	13	54	0.6
3% DEGDMA Stoichiometric	50	1	49	-	50	1.0
33% DEGDMA Experimental	35	31	23	24	54	0.7
33% DEGDMA Stoichiometric	47	6	47	-	53	0.9

Table 2-3. High-resolution spectra of carbon quantification. Carbon binding environment of 3 wt% and 33 wt% DEGDMA content substrates. Values represent the relative percent of each species present on the surface averaged from two different locations on the the surface. The experimental values are shows for 3 wt% and 33 wt% DEGDMA for each formulation.

	C-C 285.0	C-(C=O)-O 285.7	C-O 286.8	C=O 288.8	C-C + C-(C=O)-O	C-C/ C-O	C-C/ C=O
3% DEGDMA Experimental	46	23	21	7	69	3.3	9.8
3% DEGDMA Stoichiometric	74	8	8	8	82	10.3	10.3
33% DEGDMA Experimental	45	25	19	12	70	3.6	5.8
33% DEGDMA Stoichiometric	66	10	12	10	76	6.3	7.6

3.5. Atomic Force Microscopy

To ensure consistent surface topography over the range of substrate formulations, AFM was used to map the substrate's topography at three different locations on each of the lowest and highest content DEGDMA formulations. Figure 2-5 presents representative AFM micrographs of the substrate's surface for 3 and 33 wt% DEGDMA (Figure 2-5A & B, respectively). Amorphous surface features on the order of 0.5μm in diameter are can be observed on both formulations. The AFM scans were also used to

quantify the surface roughness. Surface roughness was evaluated at the three random spots on each substrate. Roughness was calculated from the three 50 x 50 µm area, approximating the surface area occupied by a single mammalian cell. The root mean squared roughness (R_{rms}) values were measured to be 14 ± 1 nm and 17 ± 6 nm for 3 and 33 wt% DEGDMA formulations, respectively.

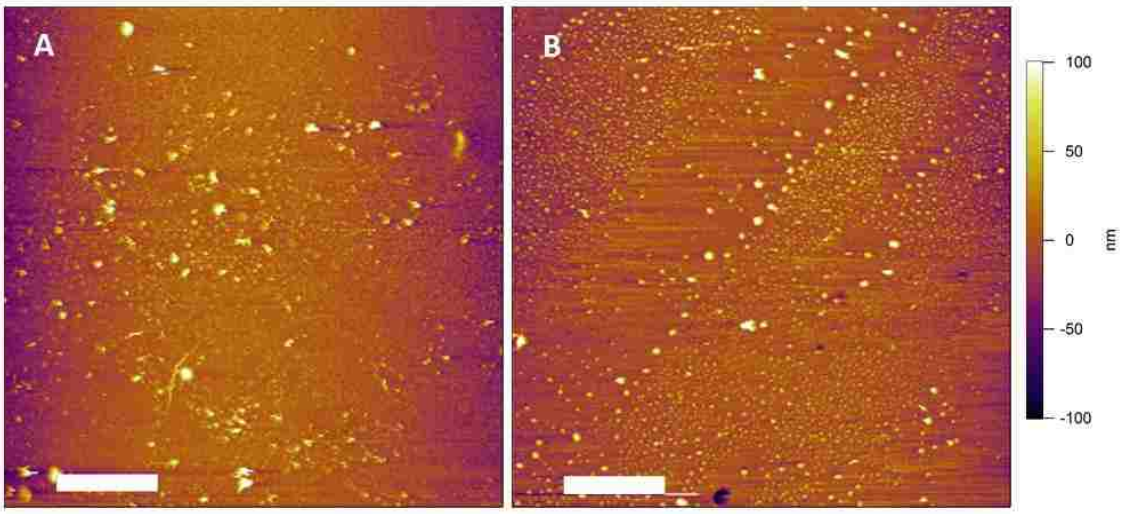

Figure 2-5. Representive atomic force microscopy scans of (A) 3% DEGDMA, and (B) 33% DEGDMA. Three 50 x 50 µm AFM scans were performed on each formulation to verify consistent surface topography across each sample. The average R_{rms} was calculated from the three a reas of each formulation and found to 14±1 and 17±6 nm for 3 and 33 wt% DEGDMA formulations, respectively. Similar surface features are observed between the upper and lower limit of DEGDMA content substrates that are imparted to the polymer surface from the surface of quartz mold.

3.6. Total Protein Adsorption

Bovine serum albumin (BSA) was chosen as a model protein to demonstrate consistent protein adsorption. The bicinchoninic acid assay (BCA) is a colorimetric protein assay that detects cuprous ions (+1) generated from cupric ions (+2) by reduction in the presences of proteins in an alkaline environment.[24] The BCA assay was selected over the use of radiolabeling followed by scintillation counting for the long term stability

of the BCA while still maintaining a sufficiently low detection limit of 0.5µg/mL.[24] Figure 2-6 shows the quantities of BSA that were adsorbed onto the surfaces of the different formulations of substrates at 37°C for 45 minutes using initial protein concentrations of 2 mg/mL. The amounts of protein adsorbed onto the substrate surfaces ranged from 17.8±1.8 to 19.7±1.7 µg/cm^2. No statistically significant difference was found between the four different substrate formulations. This confirms the results as predicted by water contact angle, XPS and AFM that protein adsorption is not affected by the rigidity of the substrate surface.

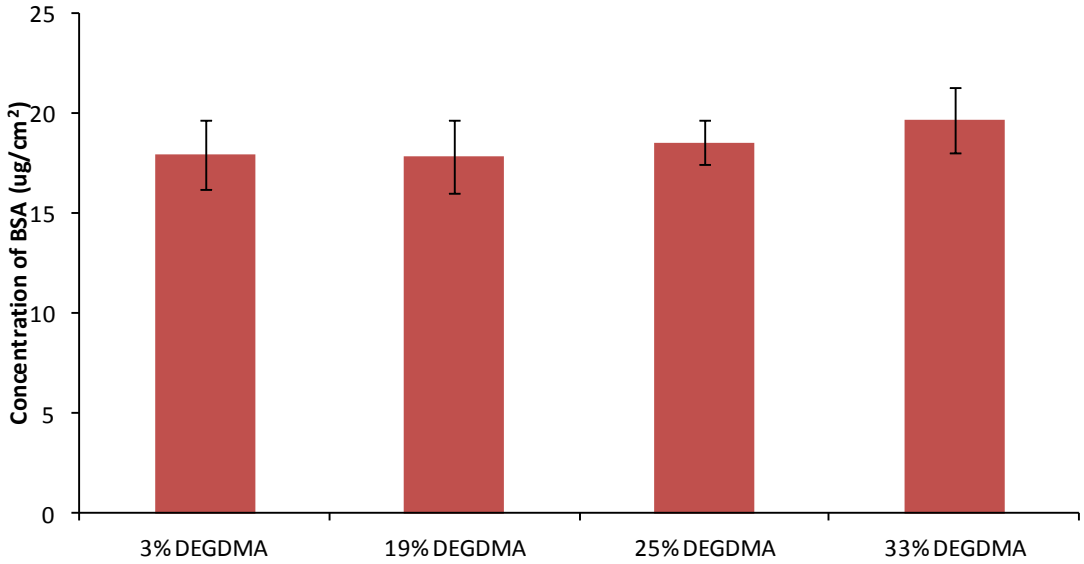

Figure 2-6. Adsorption of BSA onto the four different substrate formulations after 45 minute incubation at an intital protein concentration of 2 mg/mL measured with Micro BCA assay. No statistically significant difference was found between the different formulations. n=4.

3.7. Cell Attachment and Viability

A murine pre-osteoblastic cell line (MC3T3-E1) was used to demonstrate cellular attachment and proliferation of a monolayer cell culture on all four formulations. Viable cells were stained green and cells undergoing cell death were stained red. Viable cells were seen adhered to all formulations six hours after seeding (Figure 2-7 A-D). Figure 2-7 E-H show representative images of stained cells 96 hours after initial seeding on substrates. All formulations show an increase in green fluorescence indicating an increase in the number of viable cells.

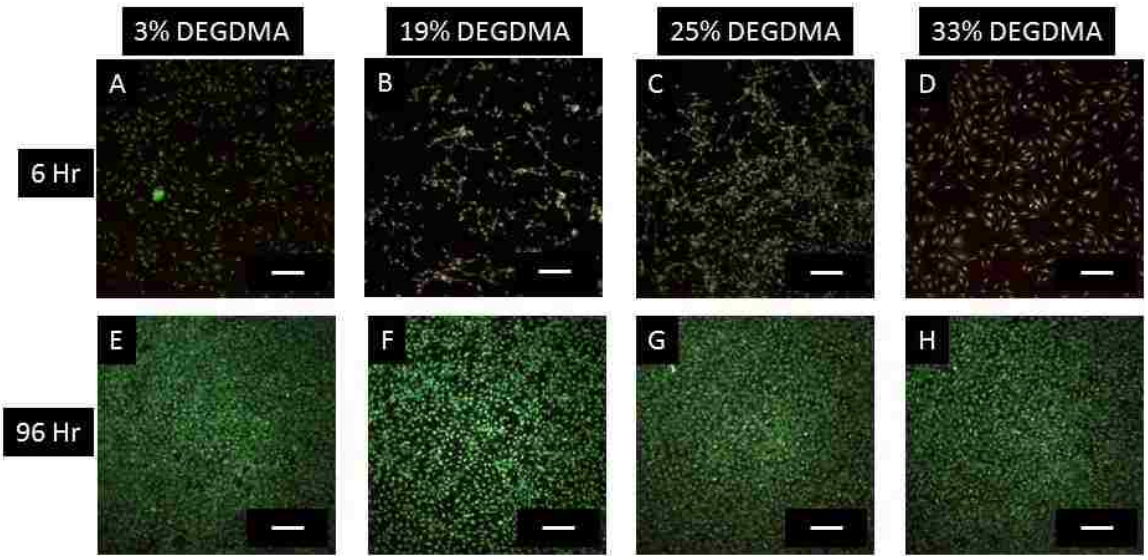

Figure 2-7. MC3T3-E1 cell line visualized with Live/Dead® fluorescence staining. Green = live, Red = dead, cells seeded at 25,000 cells/cm2. Live and dead images false pseudo colored and then merged into a single image using Adobe Photoshop CS2. Images were obtained at 6 hours post cell sedding (top row) and 96 hours post seeding (bottom row). A) 3 wt% DEGDMA 6hr, B) 19 wt% DEGDMA 6hr, C) 25 wt% DEGDMA 6hr, D) 33 wt% DEGDMA 6hr, E) 3 wt% DEGDMA 96hr, F) 19 wt% DEGDMA 96hr, G) 25 wt% DEGDMA 96hr, H) 33 wt% DEGDMA 96hr. Scale Bar = 100 µm in all images.

4. Discussion

The uniaxial compressive modulus exhibited a two order of magnitude increase in the materials compressive modulus, from 25 ± 2 to 4700 ± 300 kPa, with an increase of 3 to 33 wt% DEGDMA content (Figure 2-1). The lower limit of 3 wt% DEGDMA content was selected to obtain the softest stable free standing substrate. Research by Kannurpatti *et al.* showed that the inner two formulations (19 and 25 wt% DEGDMA) bounds a critical point for poly(nOM-co-DEGDMA). These bounding points designate a change in the dominating property controlling the bulk modulus.[19] For the lower two substrate formulations, 3 and 19 wt% DEGDMA, there is a decrease in the degrees of freedom of the polymer chains due to an increase in the crosslinking density. The polymer backbone is primarily nOM with DEGDMA crosslinks. While in the upper two formulations, 25 and 33 wt% DEGDMA, the mechanical properties are controlled by co-polymerization. The co-polymerization effect is purely based on the stiffness of the polymer backbones; which is based on the monomers and the fractions in which they are present.[16, 19, 25] Co-polymerization dominates when DEGDMA is no longer just a crosslink between polymer chains of nOM, but is a repeat unit in the polymer backbone. This is further supported by the work of Young *et al.*, as the plot of polymer molecular weight between crosslinks and DEGDMA content asymptotically levels out.[16] As seen in Figure 2-1, the modulus of the 3 and 19 wt% DEGDMA substrates increases from 25 ± 2 to 920 ± 60 kPa. The next jump from 19 to 25 wt% DEGDMA shows a ~3000 kPa increase in the compressive modulus crossing over the transition between the 'crosslinking effect' and the 'co-polymerization effect' of poly(nOM-co-DEGDMA). An increase of DEGDMA content

to 33 wt% DEGDMA results in an increase of 600 kPa from the 25 wt% DEGDMA substrate and gives this studies highest achievable modulus of 4700 ±300 kPa.

A higher glass transition temperature equates to a lower molecular weight between crosslinks and an increase in modulus. The change in the bulk material properties is due to the decrease in the degree of freedom of the chains between crosslinks.[14] The values of DEGDMA content were chosen based on the glass transition temperatures determined by Young et al.[16] The Tg was observed to be 37°C with approximately 33 wt% DEGDMA body temperature.

Substrate surface evaluation was begun by measuring water contact angles in sessile drop mode. Contact angles are largely dictated by relative surface hydrophobicity, but can also be impacted by the topography and chemical functional groups presented at the surface of the substrate.[18] A consistent angle from the range of formulations indicates similarities of topography and chemical features on all of the substrates. The contact angles measured show no statistical difference across the range of DEGDMA formulations (Figure 2-3), with all measured to be approximately 90°. The consistency in the surface energetics gives indication that biomolecular adsorption onto the surface will be similar for all of the substrates. To achieve a quantified understanding of the substrates surface it was necessary to independently interrogate the surface topography and chemical features.

Quantification of the chemical surface composition by XPS provides the elemental and chemical binding environment present on the substrate's surface. Elemental composition was observed at two different locations on each formulation, (Table 2-1) both formulations have similar elemental composition (79.2% C, 16.4% O for 3%

DEGDMA and 80.7% C, 17.4% O for 33 wt% DEGDMA). The carbon-oxygen ratio for the 3wt% DEGDMA formulation shows a higher than predicted amount of oxygen present on the surface (4.7 experimental to 5.7 stoichiometry). Possible explanations for this could be the polymer presents the ester and ether side groups on the surface while burying the alkyl carbon or an additional oxygen functional group is on the surface. The latter of these two possible explanations is supported by the detection of O-H species at 536 eV (Figure 2-4B). It is likely that the incomplete conversion of the free radicals for polymerization produce an alcohol terminal when exposed to air. Ratios of ether to ester functional groups allowed evaluation independently from the peak at 356 eV. The ratios are close to that of the predicted values (0.6 to 1.0 for the 3% DEGDMA and 0.7 to 0.9 for the 33% DEGDMA formulation), Table 2-2. The increased amount of ether groups compared to the esters is seen at each of the separate analysis points. The most likely explanation for the difference is the presence of polydimethylsiloxane (PDMS). The silicon-oxygen bond present in the backbone of PDMS can contribute electrons from the oxygen with similar binding energy to carbon-oxygen bonds. The trace amounts of PDMS can be transferred to the substrate by handling with tweezers and drying the samples in a vacuum oven that may have been used for PDMS gas evacuation. The presence of PDMS would increase the amount of ether (peak at 534 eV) observed from the O1s high-resolution spectra curve fits. Further analysis of the sample using high-resolution C1s spectra showed similar amounts of carbon in the specified chemical environments between the different formulations in Table 2-3 (69% and 70% C-C for 3 and 33 %DEGDMA, respectively). The ratios of carbon binding states are not near the values predicted my stoichiometric analysis. This also was likely due to the presence of

trace amounts of PDMS on the surface. The silicon-carbon binding environment for carbon can possibly alter the amounts of ether and aliphatic carbon observed in the spectra. Even with the differences between the experimental values and the predicted values, analysis shows the surface chemistry varies little across each formulation as well as across the 3 and 33 wt% DEGDMA substrates (3.3 to 3.6 C-C/C-O for 3 and 33 % DEGDMA, respectively). The two extremes of formulation were evaluated first; we found no significant difference between the two. This did not require the further use of the technique for surface evaluation of the two intermediate formulations.

Consistent surface topography was confirmed using AFM. This method was chosen as it allows for the assessment of the micro sized features with no need to further modify the surface for evaluation. All AFM scans were performed in a liquid cell filled with deionized water at 37°C. Heated liquid AFM was performed to ensure that the use of environmental conditions consistent with cell culture conditions did not alter the surface. As with XPS analysis, the 3 and 33 wt% DEGDMA formulations were analyzed to verify that the substrates with the most drastic difference in modulus had similar topography. Surface features observed with the AFM in the liquid cell were comparable with scanning electron microscopy images (not shown) of dried substrates, suggesting that the substrates are not undergoing swelling or other alteration when heated and wetted. The observed features were amorphous and random, from the nanometer to millimeter length scales (Figure 2-5). The surface roughness was measured using AFM and calculated through R_{rms} for three areas on each formulation. It was observed that the similar features of randomly spaced high points without consistent height were seen on the AFM scans of the different formulations. Roughness values were seen below 20 nm with standard

deviation less than 6 nm obtained for the 3 and 33 wt% DEGDMA formulations. This data shows that the surface topography are consistent across a single sample, as well as between the different formulations. It is believed that any of the surface topography observed was imprinted on the substrates because of the mold materials surface topography.

Protein adsorption on a surface is dependent on the properties of electrostatic interactions, and dictates how cells will interact with a surface.[26-29] Bovine serum albumin was chosen as a model protein because the globular protein will adsorb onto surfaces and based on the electrostatics of the substrate will induce structural changes in the BSA.[30-32] Relatively hydrophobic substrates of polystyrene (water sessile drop contact angle ~85°) were found to form 58% of a complete protein monolayer.[32] Conversely hydrophilic substrates form 95% of a complete protein monolayer.[32] The difference in the amount of protein adsorbed is due to the differences in the conformation of the adsorbed BSA. The hydrophobic substrates attract the non-polar regions of BSA molecules, inducing denaturation of the protein.[31] Hydrophilic substrates allow for retention of the native structure increasing the packing density.[31] The difference in the amount of protein adsorbed can be used to infer the conformation of the protein when adsorbed to the surface. The drastic difference between BSA adsorbed on varying substrates allows for a greater sensitivity when determining protein substrate interactions, over proteins (i.e. ECM components) that have secondary and tertiary structure stabilization by covalent bonding.

The adsorption of BSA on nOM/DEGDMA (water sessile drop contact angle ~90°) should be similar to that of the polystyrene suggesting the formation of partial protein

monolayers. Measurements of the model protein BSA adsorption onto the four different formulations demonstrated that there is no statistically significant difference between the amounts of protein adsorbed (17.8±1.8 to 19.7±1.7 μg/cm^2). This implies that when substrates are formed from varying ratios of nOM/DEGDMA and incubated with cell culture media that contain proteins (i.e. FBS), similar quantities of those proteins will adsorb to the surface.

Murine MC3T3-E1 cells were chosen to demonstrate that this material as fabricated is not only biocompatible, but supports cell attachment and proliferation. This cell line was chosen because it is a well studied cell line, with many substrate interactions already understood.[33] Live/Dead® staining allowed the simultaneous testing of cytotoxic effects as well as observation of cell attachment and proliferation. Cell attachment was observed six hours post seeding across all four sample formulations A separate sample set was stained after 96 hours. The later time point confirmed that cells were still adhered to the surface and proliferated, corresponding with an increase in the fluorescence signal. The preferential attachment of 3T3s to a stiffer material has been demonstrated by Lo and Pelham.[9, 33] This can be generally seen across the different substrate formulations (Figure 2-7), as it appears the cell density increases with the increase of material modulus.

5. Conclusion

Herein we have successfully fabricated substrates by photopolymerization of nOM and DEGDMA. The substrates' mechanical properties are independently varied without significant impact on the topography or chemical composition of the surface. The variation of previous substrate's mechanical properties induced changes in the surface

properties, making them non-ideal for use as model systems. Rather than continue to modify existing materials with limited success, we developed a synthetic culture substrate to fill these needs. The amount of DEGDMA was varied to produce substrates with compressive modulus over three orders of magnitude, ranging from ~20 to 5000 kPa. The relative surface hydrophobicity, elemental/functional composition and topography were shown to be extremely consistent across a single substrate and between the different formulations. Maintenance of the surface physical and chemical features enables for the systematic evaluation of the effects of material stiffness on cellular functions. This model platform can be used to screen polymer formulations with a large range of moduli while maintaining consistent surface (chemistry, topography and relative hydrophobicty). This will allow for the systematic evaluation in order to identify appropriate rigidity for the engineering and design of biomaterials for aortic valve tissue engineering. Additionally, this platform will find utility in studies of cellular biology associated with initiation and progression of diseases which are characterized by a stiffening of the tissue, including calcification of the heart valve,[34] liver fibrosis,[35] and many cancers.[2]

6. References

1. Brown, X. Q.; Ookawa, K.; Wong, J. Y., Evaluation of polydimethylsiloxane scaffolds with physiologically-relevant elastic moduli: Interplay of substrate mechanics and surface chemistry effects on vascular smooth muscle cell response. *Biomaterials* **2005,** 26, (16), 3123-3129.

2. Nemir, S.; West, J. L., Synthetic materials in the study of cell response to substrate rigidity. *Ann Biomed Eng* **2010,** 38, (1), 2-20.

3. Pedron, S.; Peinado, C.; Bosch, P.; Benton, J. A.; Anseth, K. S., Microfluidic approaches for the fabrication of gradient crosslinked networks based on poly(ethylene glycol) and hyperbranched polymers for manipulation of cell interactions. *J Biomed Mater Res A* **2011,** 96A, (1), 196-203.

4. Janmey, P. A.; McCulloch, C. A., Cell mechanics: Integrating cell responses to mechanical stimuli. *Annu Rev Biomed Eng* **2007,** 9, (1), 1-34.

5. Rehfeldt, F.; Engler, A. J.; Eckhardt, A.; Ahmed, F.; Discher, D. E., Cell responses to the mechanochemical microenvironment--implications for regenerative medicine and drug delivery. *Adv Drug Delivery Rev* **2007,** 59, (13), 1329-1339.

6. Wong, J. Y.; Leach, J. B.; Brown, X. Q., Balance of chemistry, topography, and mechanics at the cell-biomaterial interface: Issues and challenges for assessing the role of substrate mechanics on cell response. *Surf Sci* **2004,** 570, (1-2), 119-133.

7. Balgude, A. P.; Yu, X.; Szymanski, A.; Bellamkonda, R. V., Agarose gel stiffness determines rate of drg neurite extension in 3d cultures. *Biomaterials* **2001,** 22, (10), 1077-1084.

8. Seliktar, D., Extracellular stimulation in tissue engineering. *Ann NY Acad Sci* **2005,** 1047, (1), 386-394.

9. Pelham, R. J.; Wang, Y.-l., Cell locomotion and focal adhesions are regulated by substrate flexibility. *P Natl Acad Sci USA* **1997,** 94, (25), 13661-13665.

10. Wang, H. B.; Dembo, M.; Wang, Y. L., Substrate flexibility regulates growth and apoptosis of normal but not transformed cells. *Am J Physiol Cell Physiol* **2000,** 279, (5), C1345-1350.

11. Alauzun, J. G.; Young, S.; D'Souza, R.; Liu, L.; Brook, M. A.; Sheardown, H. D., Biocompatible, hyaluronic acid modified silicone elastomers. *Biomaterials* **2010,** 31, (13), 3471-3478.

12. Meriç, G.; Dahl, J. E.; Ruyter, I. E., Cytotoxicity of silica-glass fiber reinforced composites. *Dent Mater* **2008,** 24, (9), 1201-1206.

13. Yoo, S. H.; Kim, C. K., Effects of various diluents included in the resin matrices on the characteristics of the dental composites. *Polym-Korea* **2009,** 33, (2), 153-157.

14. Young, J. S.; Bowman, C. N., Effect of polymerization temperature and cross-linker concentration on reaction diffusion controlled termination. *Macromolecules* **1999,** 32, (19), 6073-6081.

15. Kannurpatti, A. R.; Anderson, K. J.; Anseth, J. W.; Bowman, C. N., Use of "living" radical polymerizations to study the structural evolution and properties of highly crosslinked polymer networks. *J Polym Sci Pol Phys* **1997,** 35, (14), 2297-2307.

16. Young, J. S.; Anandkumar, K. R.; Bowman, C. N., Effect of comonomer concentration and functionality on photopolymerization rates, mechanical properties and heterogeneity of the polymer. *Macromol Chem Physic* **1998,** 199, (6), 1043-1049.

17. Sperling, L. H., *Introduction to physical polymer science*. Fourth Edition ed.; John Wiley & Sons: Hoboken, 2006.

18. Kwok, D. Y.; Neumann, A. W., Contact angle measurement and contact angle interpretation. *Adv Colloid Inrerface Sci* **1999,** 81, (3), 167-249.

19. Kannurpatti, A. R.; Anseth, J. W.; Bowman, C. N., A study of the evolution of mechanical properties and structural heterogeneity of polymer networks formed by photopolymerizations of multifunctional (meth)acrylates. *Polymer* **1998,** 39, (12), 2507-2513.

20. Escamilla, R.; Huerta, L., X-ray photoelectron spectroscopy studies of non-stoichiometric superconducting nbb2+x. *Supercond Sci Technol* **2006,** 19, (6), 623-628.

21. Hesse, R.; Chassé, T.; Streubel, P.; Szargan, R., Error estimation in peak-shape analysis of xps core-level spectra using unifit 2003: How significant are the results of peak fits? *Surf Interface Anal* **2004,** 36, (10), 1373-1383.

22. Ratner, B. D.; Castner, D. G., Electron spectroscopy for chemical analysis. In *Surface analysis: The principal techniques*, Vickerman, J. C., Ed. John Wiley and Sons: Chichester, 1997; pp 43 - 98.

23. Beamson, G.; Briggs, D., *High resolution xps of organic polymers*. John Wiley & Sons: Chichester, 1992.

24. Smith, P. K.; Krohn, R. I.; Hermanson, G. T.; Mallia, A. K.; Gartner, F. H.; Provenzano, M. D.; Fujimoto, E. K.; Goeke, N. M.; Olson, B. J.; Klenk, D. C., Measurement of protein using bicinchoninic acid. *Anal Biochem* **1985,** 150, (1), 76-85.

25. Elliott, J. E.; Anseth, J. W.; Bowman, C. N., Kinetic modeling of the effect of solvent concentration on primary cyclization during polymerization of multifunctional monomers. *Chem Eng Sci* **2001,** 56, (10), 3173-3184.

26. Hallab, N. J.; Bundy, K. J.; Oconnor, K.; Clark, R.; Moses, R. L., Cell adhesion to biomaterials: Correlations between surface charge, surface roughness, adsorbed protein, and cell morphology. *J Long-Term Eff Med Implants* **1995,** 5, (3), 209-231.

27. Satomi, T.; Nagasaki, Y.; Kobayashi, H.; Otsuka, H.; Kataoka, K., Density control of poly(ethylene glycol) layer to regulate cellular attachment. *Langmuir* **2007,** 23, (12), 6698-6703.

28. Horbett, T. A.; Waldburger, J. J.; Ratner, B. D.; Hoffman, A. S., Cell adhesion to a series of hydrophili–hydrophobic copolymers studies with a spinning disc apparatus. *J Biomed Mater Res* **1988,** 22, (5), 383-404.

29. Ayala, R.; Zhang, C.; Yang, D.; Hwang, Y.; Aung, A.; Shroff, S. S.; Arce, F. T.; Lal, R.; Arya, G.; Varghese, S., Engineering the cell-material interface for controlling stem cell adhesion, migration, and differentiation. *Biomaterials* **2011,** 32, (15), 3700-3711.

30. Jeyachandran, Y. L.; Mielczarski, J. A.; Mielczarski, E.; Rai, B., Efficiency of blocking of non-specific interaction of different proteins by bsa adsorbed on hydrophobic and hydrophilic surfaces. *J Colloid Interf Sci* **2010,** 341, (1), 136-142.

31. Kim, J.; Somorjai, G. A., Molecular packing of lysozyme, fibrinogen, and bovine serum albumin on hydrophilic and hydrophobic surfaces studied by infrared-visible sum frequency generation and fluorescence microscopy. *J Am Chem Soc* **2003,** 125, (10), 3150-3158.

32. Jeyachandran, Y. L.; Mielezarski, E.; Rai, B.; Mielczarski, J. A., Quantitative and qualitative evaluation of adsorption/desorption of bovine serum albumin on hydrophilic and hydrophobic surfaces. *Langmuir* **2009,** 25, (19), 11614-11620.

33. Lo, C. M.; Wang, H. B.; Dembo, M.; Wang, Y. l., Cell movement is guided by the rigidity of the substrate. *Biophys J* **2000,** 79, (1), 144-152.

34. Yip, C. Y. Y.; Chen, J.-H.; Zhao, R.; Simmons, C. A., Calcification by valve interstitial cells is regulated by the stiffness of the extracellular matrix. *Arterioscler Thromb Vasc Biol* **2009,** 29, (6), 936-942.

35. Wells, R. G., The role of matrix stiffness in hepatic stellate cell activation and liver fibrosis. *J Clin Gastroenterol* **2005,** 39, (4), S158-S161.

Chapter 3 : Isolating Effect of Substrate Rigidity on Valvular Interstitial Cells

Prepared for Submission to Cardiovascular Engineering and Technology

Isolated Effect of Substrate Rigidity on Valvular Interstitial Cells

Alexander T. Leonard [a, b]; Kirsten N. Cicotte [b];Genevieve Phillips[c] and Elizabeth L. Hedberg-Dirk,[a, b]

[a] *Department of Chemical and Nuclear Engineering, University of New Mexico, Albuquerque, NM*

[b] *Center for Biomedical Engineering, University of New Mexico, Albuquerque, NM*

[c] *Fluorescence Microscopy Shared Resource, Cancer Research Facility, University of New Mexico, Albuquerque, NM*

1. Introduction

The limitations of current aortic heart valve (AV) replacement therapies necessitate the development of a living biologic replacement.[1] Neither mechanical nor decellularized biological valve replacements offer a patient an unimpeded lifestyle after therapy.[2, 3] Decellularized biological valves are limited in functional lifetime, while synthetic valves require anti-coagulants to reduce the risk of thrombosis.[4] The goal of creating a tissue engineered (TE) valve is to yield a cell populated construct that possess the capability to integrate with surrounding tissues as well as grow and repair over time. In recent years, a number of AV TE strategies employing both natural and synthetic scaffold materials with different cell sources have been explored. To date, however, success has been limited in the demanding position of the AV.[1] The biggest restriction for developing TE replacements has been an incomplete understanding of normal and pathological valve cell biology.

The main cell types present in the AV are the valvular endothelial cells (VECs) and valvular interstitial cells (VICs).[5, 6] The VECs line the blood contacting surfaces and have been implicated in the regulation of inflammation, thrombosis, and remolding through cytokine release.[7-9] The VICs are found throughout the valve and are a heterogeneous population consisting of fibroblast-like, myofibroblasts, smooth muscle cell-like and in disease osteoblastic-like cells.[5, 10] The diverse behavior of VICs phenotypic expression, extracellular matrix (ECM) production, apoptosis and contraction have been shown to be influenced by environmental factors such as cytokines, growth factors and mechanical factors.[11-14]

VICs exist in a variety of phenotypes *in vivo*, the patterns of which vary spatially in the valve as well as temporally during development, wound repair and disease.[15] In the adult AV 3 primary VIC phenotypes have been identified, quiescent (qVIC), activated (aVIC), and, in disease the osteoblastic (obVIC).[16] Changes in the combination of mechanical stresses and soluble factors have been shown to mediate the transition of the VICs between the phenotypes.[17-19] For example, aVICs predominate during periods of high ECM production during valve development and wound healing, marked by expression of α-smooth muscle actin (αSMA).[20] On the other hand, qVICs dominate during healthy valve functions secreting low levels of ECM components.[3, 21] Finally, the obVICs have been associated with valve pathologies and calcification that results in stiffening of the tissue, marked by expression of αSMA and core binding factor-1 (CBFa-1).[14, 16, 22] Of the three different phenotypes, the aVIC is desired for tissue engineering applications for the high rates of proliferation and ECM turnover.[16] By presenting the VICs with the appropriate physical cues, it should induce the aVIC phenotype and ECM synthesis *in vitro.*

When a healthy valve becomes diseased, there is commonly a stiffening of the tissue and formation of calcified tissue.[22] The change in the tissue compliance associated with disease progression has peaked researchers' interest in the effects of substrate rigidity on VIC phenotypic expression. To conduct these experiments, a number of natural and synthetic materials have been employed. Natural materials have been used by varying crosslinking density, thickness, and mounting to achieve a model material with varied stiffness.[23, 24] However, natural materials are inherently bioactive and may therefore transmit additional signals to the cells not associated with the substrate mechanics.[25]

Synthetic materials used previously for rigidity studies include polyethylene glycol (PEG), polyacrylamide (PA), and polydimethylsiloxane (PDMS). These materials are limited in application because of their small range of acheivable moduli and/or surface instabilities.[17, 25-29] The previsouly characterized dental cement co-polymer network of n-octyl methacrylate (nOM) and diethylene glycol dimethacrylate (DEGDMA) has recently been shown in our laboratory to be an *in vitro* cell culture substrate which possesses a wide range of moduli with minimal variation in surface properties.[30-32]

The work presented here focuses on the isolated impact of substrate rigidity on the cellular functions of the VICs. While a few published studies have examined the differences in substrate rigidities on VIC cellular functions, they have been limited because the models used bioactive surfaces, providing additional signals to the VICs. [10, 24] Previous studies have used fibronectin, fibrin, and collagen to functionalize a substrates for cell adhesion.[14, 24] The varied substrata moduli of these studies was purposed to be the major contributing factor to the cell response. However, the addition of the different substrate functionalization proteins induced different cell responses independent of the substrate moduli. Additionally, a number of studies used application of tension or substrate thickness to increase substrate rigidity. These methods introduce structural changes to the substrates.[23, 24]

The use of the nOM / DEGDMA substrates will allow for the independent evaluation of substrate rigidity on VIC functions. Proliferation and phenotypic expression were examined as a function of bulk substrate compressive modulus over the range of 20 to 5000 kPa. Major ECM components glycosaminoglycans (GAG), elastin and collagen-I were also investigated to understand how substrate stiffness could be used to induce

ECM production *in vitro* for TE applications without the application of additional growth factors or cytokines. We hypothesize that softer materials stiffness similar to healthy AV would promote the qVIC with low levels of proliferation and ECM secretion. Additionally, it was hypothesized that as the material stiffness increased, the aVIC phenotype will predominate with higher levels of proliferation and ECM secretion. To evaluate our hypotheses VIC proliferation, phenotypic expression and ECM production were examined on nOM / DEGDMA substrate with bulk moduli ranging from 20 to 5000 kPa.

2. Materials and Methods

2.1. Substrate Fabrication

Substrates were fabricated following the procedure described in detail of Chapter 2, Section 2.1. Substrates were fabricated with monomers of n-octyl methacrylate (nOM; Scientific Polymer Products (SPP), Ontario, NY) and diethyleneglycol dimethacrylate (DEGDMA; SPP). Four substrate formulations were fabricated with 3, 19, 25 or 33 wt% DEGDMA and 0.25 wt% IRGACURE 2959 (Ciba, Florham Park, NJ), with the remaining being nOM, in glass molds for 300 minutes in a UV crosslinking box (CL-1000, UVP, Upland, CA). Circular samples of diameter 6 mm were cut out of the cured sheet using a biopsy punch (96-1125, Sklar, West Chester, PA), incubated in 200 proof ethanol (Fisher Scientific, Waltham, MA) for 48 hours, degassed overnight under vacuum, and submerged in 18 MΩ water (Synergy UV, Millipore, Billerica, MA) for 1 week.

2.2. Nanoindentation

A Micro Materials NanoTest nanomechanical instrument (Platform 2, Version 1, Wrexham, UK) was used to perform depth vs. load-controlled experiments on the different nOM / DEGDMA material formulations (3, 19, 25 and 33 wt.% DEGDMA with the remaining wt% being nOM) using a diamond tip Berkovich probe. All samples were indented at a force that provided a contact depth of 4000 nm. Table 3-1 gives the loading and unloading conditions for each formulation. Initial testing was performed to determinate testing parameters that would ensure accurately measure the reduced modulus to limit interference of plastic modulus, tip adhesion and sink-in.[33-36] Each formulation need test conditions because of the differences in the interaction between the indentation tip and the materials. The linear range of the unloading curve was analyzed with the Oliver-Pharr method to calculate the reduced modulus of each formulation.[34] The Oliver Pharr method uses a plot of applied load, P, and penetration depth, h, to find the slope of material unloading, $\frac{dP}{dh}$. The unloading slope is then used with the projected contact area of the tip, A, to calculate a materials reduced modulus, E_r (Equation 3-1).[33-36] The unloading curves between 100 - 60 % of maximum load were used for analysis. Ten indentations per sample were performed.

Equation 3-1

$$E_r = \frac{(\frac{dP}{dh})\sqrt{\pi}}{2\sqrt{A}}$$

Table 3-1. Testing Parameters for Nanoindentation

	Load / Unload Rate (mN/s)	Hold Time (s)
3% DEGDMA	0.1	120
19% DEGDMA	0.01	120
25% DEGDMA	0.005	60
33% DEGDMA	0.05	60

2.3. Primary Valvular Interstitial Cell Isolation

All tissue culture solutions and supplies were purchased from Fisher Scientific unless otherwise specified. VICs were isolated following the procedure of Hanson and Helgeson.[37] Porcine aortic valve leaflets were surgically isolated from whole hearts (Hormel Foods Corp., Austin, MN). Leaflets were cleaned in Dulbecco's phosphate buffered saline (DPBS) with 1% (v/v) penicillin/streptomycin (P/S), followed by digestion in a 250 units/mL collagenase solution (LS004174, Worthington Biochemical Grp., Lakewood, NJ) digestion for 15 minutes at 37°C. Both sides of the leaflets were mechanically scraped to remove the VEC layer. A second collagenase digestion was performed for 1 hour at 37° C. Digested valve solutions were passed through a 70 µm strainer to remove undigested valve pieces and the cell suspension solution was spun down at 1,000 rpm for 10 minutes. The cell pellet was resuspended in Media 199 with 10% (v/v) fetal bovine serum (FBS), 1% (v/v) of P/S, 1% (v/v) fungizone (culture media) and plated into T75 tissue culture polystyrene (TCPS) culture flasks. Cells were grown to ~70% confluency and lifted after incubation with a 2 mL of 0.25% (w/v) trypsin solution at 37° C for 15 minutes. The cell/trypsin solution was transferred to a 15 mL conical tube

and centrifuged at 2000 rpm for 3 minutes. The supernatant was removed and the pelleted cells were resuspended in 5 mL of DPBS.

To remove any residual VECs, cell solutions were incubated with 50 µL of magnetic bead suspension labeled with CD31 antibodies (Dynabead CD31, Invitrogen, Carslbad, CA) in 15 mL conical tubes at 4° C for 30 minutes with occasional mixing. The tubes were placed in a donut shaped separation magnet for 2 minutes, allowing VECs labeled with magnetic beads to migrate to the sides of the tubes. The VIC solutions were removed and placed in new conical tubes. VIC solutions were centrifuged at 2000 rpm for 3 minutes and the supernatant was discarded. Pelleted cells were resuspended in M199 media with 10% FBS (v/v), 10% dimethyl sulfoxide and cryogenically frozen until use.

2.4. Cell Culture

Cryogenically frozen cells were allowed to thaw at room temperature and then centrifuged at 2000 rpm for 3 minutes. The supernatant was removed and the pelleted cells were resuspended in culture media (Media 199 with 10% (v/v) FBS, 1% (v/v) of P/S, 1% (v/v) fungizone) and plated into T75 TCPS culture flasks. Cells were grown to ~80% confluency and lifted with 2 mL of 0.25% (w/v) trypsin incubated at 37° C for 15 minutes. The cell solution was transferred to a 15 mL conical tube and centrifuged at 2000 rpm for 3 minutes. The supernatant was removed and the pelleted cells were resuspended in 2 mL of fresh culture media. Cell concentrations were determined using a hemocytometer (1483, Hausser Scientific, Horsham, PA). Cell solutions were diluted with media to obtain proper seeding densities for the variable serum, proliferation,

phenotypic, sulfanted GAG production, and extra cellular matrix protein secretion studies.

2.5. Variable Serum Conditions

Assay media was made to have the same composition as culture media without phenol red indicator (1X MEM with 1% (v/v) of P/S, 1% (v/v) fungizone, 0.1 mg/mL L-Glutamine with varying FBS compositions 10, 5, 3, 1, 0 % (v/v)). Assay media was chosen without phenol red to use the same media that would be used with fluorescence imaging in later experiments to reduce fluorescence background. Serum levels were selected to compare previously published concentrations for proliferation and morphology studies.[14, 23, 38-41] VICs were seeded onto TCPS 24 well plates at 15,000 cells/cm^2 with media containing one of the five different FBS concentrations. At days 1, 3, 7 and 9 assay media was removed and cells were treated with 0.5 mL of 0.25% (w/v) trypsin for 15 minutes and wells were rinsed with 0.5 mL of DPBS solution. Cell solution was diluted in 20 mL of DPBS and analyzed with a Coulter Counter (Z2, Beckman Coulter, Miami, FL) between 10 and 22 µm. Four samples per media treatment group were used.

2.6. Proliferation

Five samples of each substrate formulation were loaded into flat bottom non-TCPS 96 well plates (3370, Corning, Lowell, MA). Samples were covered with 200 µL of ultra pure water and sterilized through exposure to UV radiation for 30 minutes. After removal of the water, surfaces were seeded with VICs at a density of 15,000 cells/cm^2 in assay

media with 10% (v/v) FBS. Cellular proliferation was assessed after 1,2,4 and 7 days using the CyQuant Direct Cell Proliferation Assay (Invitrogen, Carlsbad, CA) as per the manufacturer's instructions. Cells were stained with the two part stain solution which stains nucleic acids of all cells and suppresses the fluorescence of cells with compromised membranes. The fluorescently labeled cells were imaged on an inverted microscope (Eclipse TS-100, Nikon, Melville, NY) with a mercury light source (X-Cite Series 120, Lumen Dynamics, Mississauga, Ontario). One 10x magnification image per sample was captured with a 14.2 Color Mosaic camera (Diagnostic Instruments Inc. Sterling Heights, MI) and processed using Spot software (Diagnostic Instruments Inc). Automated image analysis to determine cell numbers (automated cell counting) was performed with Cell Profiler software (Broad Institute, Cambridge, MA).

Following fluorescent imaging, cells were lifted using a 0.25% (w/v) trypsin solution with a 30 minute incubation. Cell/trypsin solutions were retained and wells were washed with 100 µL of DPBS to remove any remaining adherent cells. Cell/trypsin and wash solutions were combined for analysis by flow cytometry (C6, Accuri Cytometers, Ann Arbor, MI). Forward and side scatter gates were set to exclude debris and 30 µL of cell suspension was passed through the cytometer. The data was analyzed with FCS Express software (Version 4, De Novo, Los Angeles, CA). The gating for flow cytometry was determined using a control experiment comparing stained VICs treated with 70% v/v methanol/water with untreated VICs, Appendix Figure 3-11.

2.7. Immunocytochemistry (ICC) for Phenotypic and ECM Protein Production

Three samples of each substrate formulation were loaded into a flat bottom non-tissue culture polystyrene 96 well plates (3370, Corning, Lowell, MA). Samples were covered with 200 μL of ultra pure water and sterilized through exposure to UV radiation for 30 minutes. VICs were seeded onto substrates at 25,000 cells/cm^2 in assay media with 3% (v/v) FBS. After 7 days of culture, cells were fixed with formalin for 30 min and washed twice with phosphate buffered saline (PBS). Cells were then permeabilized with 0.01% (v/v) Tween20 for 15 min. Permeabilized cells were washed twice with PBS followed by a block with a 3 wt% bovine albumin serum(BSA)/PBS for 1 hour. Samples were incubated with primary antibodies for phenotypic markers or extra cellular matrix proteins for in a 3wt% BSA solution. Antibodies used for phenotypic expression were mouse α-smooth muscle actin (αSMA, ab7817, 1:100, AbCam, Cambridge, MA) and rabbit core binding factor-1 (CBFa-1, CBFA11-A, 1:100, Alpha Diagnostic, San Antonio, TX) identified aVIC or obVIC. Antibodies used to identify ECM associated proteins included collagen-I (1:100, ab90395, AbCAM) and elastin (1:100, ab21610, AbCAM). After a 90 minute incubation with primary antibody solution and cells were washed twice with PBS. One set of secondary antibodies was used for both the phenotypic markers and ECM components, goat anti-mouse AlexaFluor 488 (1:75, A11001, ex 495 / em 519, Invitrogen) and donkey anti-rabbit AlexaFluor 647 (1:75, A31573, ex 650 / em 665, Invitrogen) in a 3wt% BSA solution. Following incubation for 90 minutes in the secondary antibody solution, cells were counter stained with DAPI in PBS (1:1000, Invitrogen) for 5 minutes. Samples where then removed from the 96 well plate and mounted on coverglass using mounting media (Fluoromount, F4680-25ML,

Sigma-Aldrich, St. Louis, MO) and sealed with clear nail polish. Staining controls to insure non-specific binding of the secondary antibodies was performed on substrates with and without VICs.

Samples were imaged on a Zeiss Axioskop 2 MOT microscope (Standort Göttingen - Vertrieb Deutschland) with Plan-Apochromat 63x oil 1.4 NA objective (Zeiss) and a Nuance Multispectral Imaging System FX Camera (Cambridge Research and Instrumentation, CRI, Hopkinton, MA). Images were captured and analyzed using Nuance Software (3.0.1, CRI). Quantification of the fluorescence in the images required comparison to control standards of cells incubated with primary, secondary antibody, and DAPI separately to remove background, auto-fluorescence of cells fixed to surfaces, and assign a reference spectrum to each stain. Phenotypic staining resulted in αSMA stained green (λ =519 nm), CBFa-1 stained in far red (λ =655 nm), and nucleus stained blue (λ = 461 nm). ECM production staining resulted in collagen-I stained green (λ =519 nm), elastin stained in far red (λ =655 nm), and nucleus stained blue (λ = 461 nm).

2.8. Sulfanted Glycosaminoglycans (sGAG) Production

Four samples of each substrate formulation were loaded into flat bottom non-tissue culture polystyrene 96 well plates (3370, Corning, Lowell, MA). Samples were covered with 200 µL of ultra pure water and sterilized through exposure to UV radiation for 30 minutes. VICs were seeded onto substrates at 25,000 cells/cm^2 in assay media with 3% (v/v) FBS. Briefly, at 2 day and 7 day media was removed and retained for testing. Cells were washed with DPBS and digested with papain extraction reagent as specified by manufacturer for 3 hours at 65° C. Digested extract was centrifuged at 10,000g for 10

minutes and the supernatant was retained for assay. Quantification of sGAG was determined by testing the media and the digested extract separately using the Blyscan sGAG Kit (B1000, Biocolor, Carrickfergus, UK) at days 2 and 7. Assay was performed according to manufacturer's protocol. Dye reagent was added to test solution, and incubated for 30 minutes on a mechanical shaker. The sGAG-dye precipitate was concentrated by centrifugation. The supernatant was then removed and the sGAG-dye precipitate was resuspended using the dissociation reagent and absorbance was measured at 656 nm using a plate reader (M2, Molecular Devices, Sunnyvale, CA). Total sGAG is calculated by the sum of cell culture media and extract.

2.9. Statistical Analysis

Nanoindentation, variable serum conditions, proliferation, phenotypic expression, sGAG production, and ECM protein secretion results were analyzed using the Tukey-Kramer one-way nonparametric analysis of variance (ANOVA) with values of $p < 0.05$ considered statistically significant. All analysis were done with InStat 3 (GraphPad Software, La Jolla, CA). All data are presented as mean ± standard deviation.

3. Results

3.1. Nanoindentation

The mechanical properties of the substrate surfaces were characterized with nanoindentation. Table 3-2 displays the maximum load values obtained to reach a 4000 nm depth in each sample.

Table 3-2. Maximum load applied to reach a depth of 4000 nm

	Max Load (mN)
3% DEGDMA	0.45 ± 0.02
19% DEGDMA	3.17 ± 0.16
25% DEGDMA	6.02 ± 1.57
33% DEGDMA	24.62 ± 3.37

Figure 3-1 shows the reduced modulus (E_r) for each material formulation. Evaluation by nanoindentation display a three order of magnitude increase in material properties (E_r = 6.5 – 1,500 MPa) between the 3 and 33 wt% DEGDMA formulations. Differences between formulations were found to be significant with $p < 0.01$. The standard deviation of the E_r of the 3% DEGDMA sample was found to be within in the signal noise and displayed as zero.

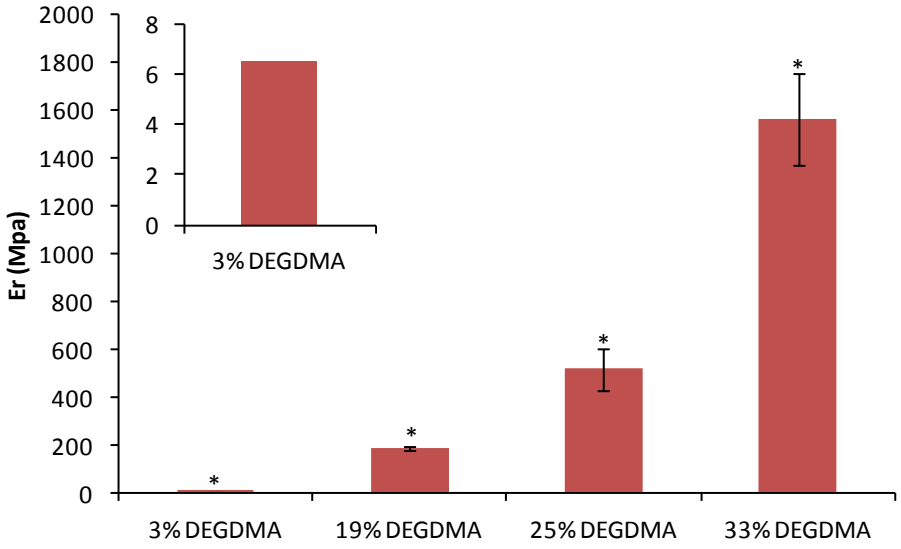

Figure 3-1. Reduced Modulus (Er) nOM / DEGDMA formulations determined by nanoindentation. Tissue culture polystyrene (TCPS) was also measure using the same nanoindenter setup (Er = 30.6 ± 10.9 GPa). * p<0.01

3.2. Variable Serum Conditions

In order to minimize effects of changes in cell number over time in all further experiments, studies to determine the minimum serum concentration necessary to maintain viability and morphology were conducted. Additionally, when many cell types density reaches higher levels intercellular signaling slows growth but, VICs at higher confluency begin to exhibit obVIC characteristics.[11, 16, 23, 42] Cell number and spreading were assessed for up to nine days in media containing 0, 1, 3, 5, or 10% FBS. As shown in Figure 3-2, the number of cells attached was independent of serum concentration, with a reduction in cell attachment observed only with 0% FBS media. Throughout the rest of the study a statistically significant increase in the cell number was observed for the positive control (10% FBS) at each time point ($p<0.05$). In media with 1, 3, and 5% FBS, no increase in the cell number was detected, while a decrease in cell number occurred under 0% FBS conditions.

Figure 3-3 shows brightfield microscopy of VICs which revealed the changes in the morphology of the cells over the course of the experiment. Cell number increase in 10% FBS to a confluent culture at 7 days with an aligned and spindle shaped morphology (Figure 3-3 a2-a4). The 3% FBS appears to allow cells to attach and spread on the surface without a significant change in morphology over the course of the study (Figure 3-3 d1 – d4). Cells in 1% FBS attach to the surface, but as compared to cells in 3% FBS media did not spread to the same extent (Figure 3-3 c1 – c4). A limited number of cells to attached with 0% FBS media and all cells detached by day 3 (Figure 3-3 d1 – d2).

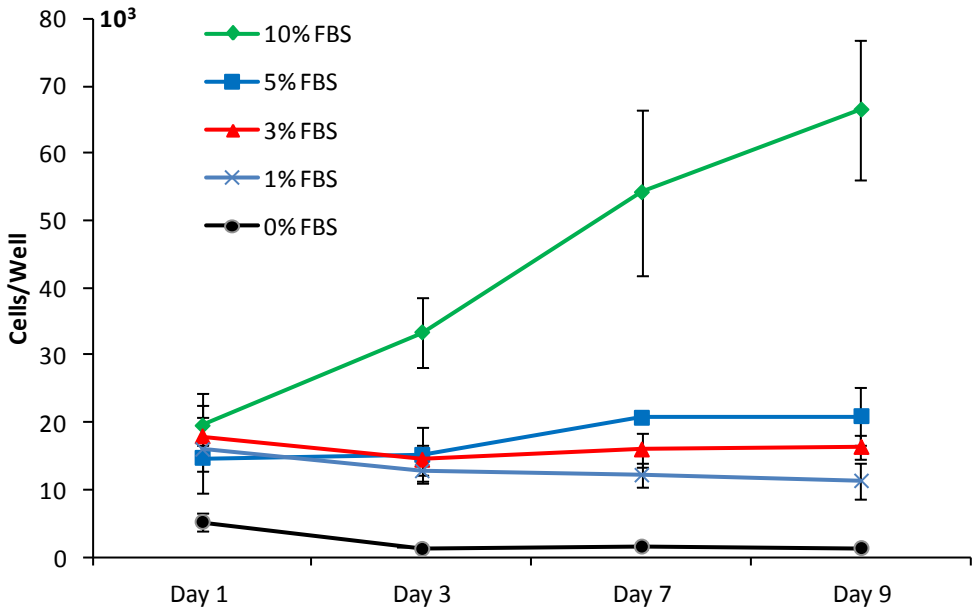

Figure 3-2. Cell number as a function of FBS concentration over a 9 day culture period with no media changes. No significant differences were found between the different time points for cells cultured under reduced serum conditions (5,3,1 % FBS), n=4

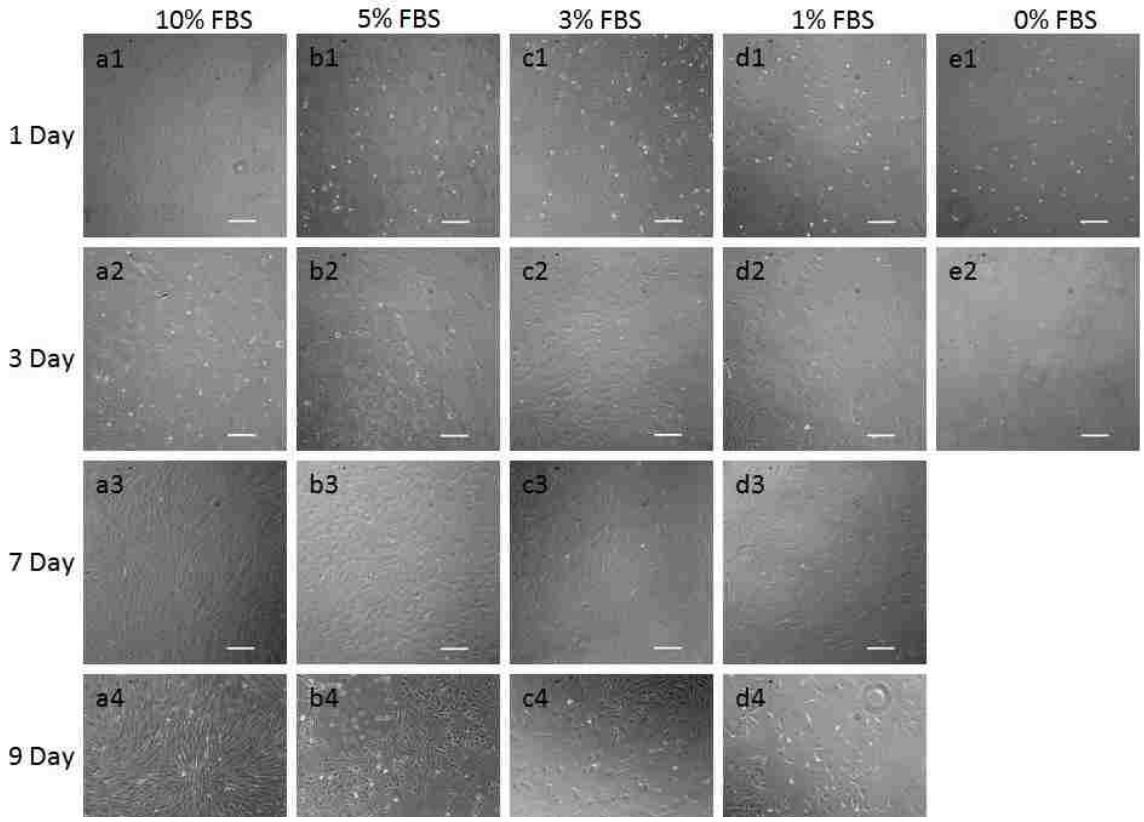

Figure 3-3. Brightfield imaging of VICs cultured in varying levels of FBS over a period of 9 days without media changes. VICs cultured in 10% FBS grew to a confluent culture within the nine day observation period with morphology representing smooth muscle cells aligned and spindle shaped (a1 – a4). VICs grown in 5% FBS attach and spread then begin to retract processes by the ninth day (b1 – b4). The VICs in 3% FBS attach and spread on the surfaces without significant changes in morphology (c1 – c4). VICs in 1% FBS attach to the surface but do not show the same level of spreading as compared to VICs in higher concentrations of FBS (d1 – d4). A limited number of VICs attach and extend processes, by the 3rd day in culture no apparent cells are attached to the surface cultured in 0% FBS (e1 – e2).

3.3. Cell Proliferation on Substrates

Cell number was determined under normal culture conditions (10% FBS) 1, 2, 4 and 7 days after seeding on varying stiffness substrates. The number of VICs was measured with three different methods (flow cytometry, fluorescence microscopy with computer analysis and by manual counting). Results are presented in Figure 3-4. It was determined by all three methods that the stiffness of the underlying substrate had no statistically significant impact on the attachment or the cell number at each timepoint. This data

suggests that the stiffness of the substrate does not influence the rate of the proliferation of VICs when incubated under normal culture conditions.

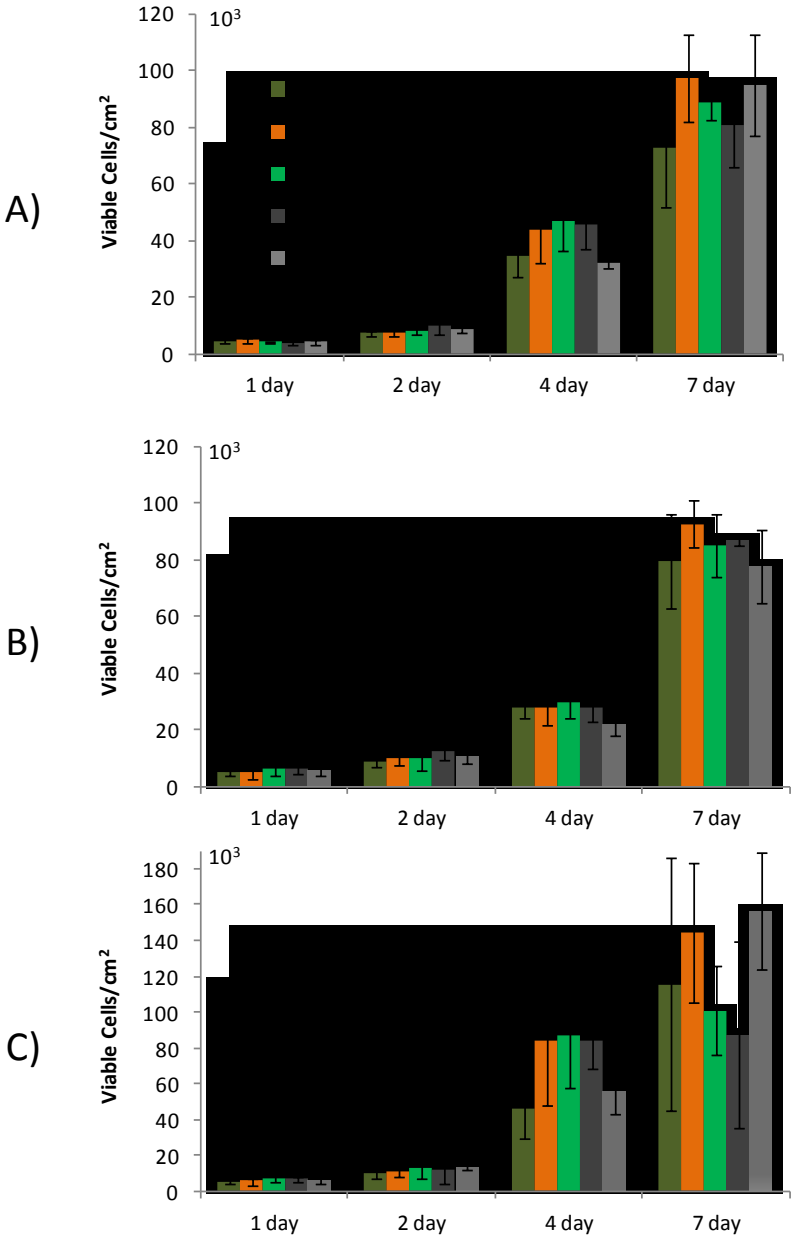

Figure 3-4. Number of viable cells stained with CyQuant Direct Cell Proliferation assay measured with 3 different methods A) flow cytometry, and fluorescence microscopy followed by B) automated and C) manual analysis. n=4

3.4. Phenotypic Expression

The phenotype marker αSMA was selected as the marker for the desired aVIC phenotype and the transcription factor CBFa-1 was used for the identification of the obVIC. Results presented in Figure 3-5 show no statistical significant difference in αSMA expression levels between formulations and the TCPS control, indicating that stiffness alone does not affect expression of αSMA. Representative images of phenotypic ICC staining can be seen in Figure 3-5. VICs cultured on the three stiffest materials (Figure 3-6 B - D) showed distinctive αSMA stress fiber organization. The VICs on the softest material had little stress fiber organization (Figure 3-6 A).

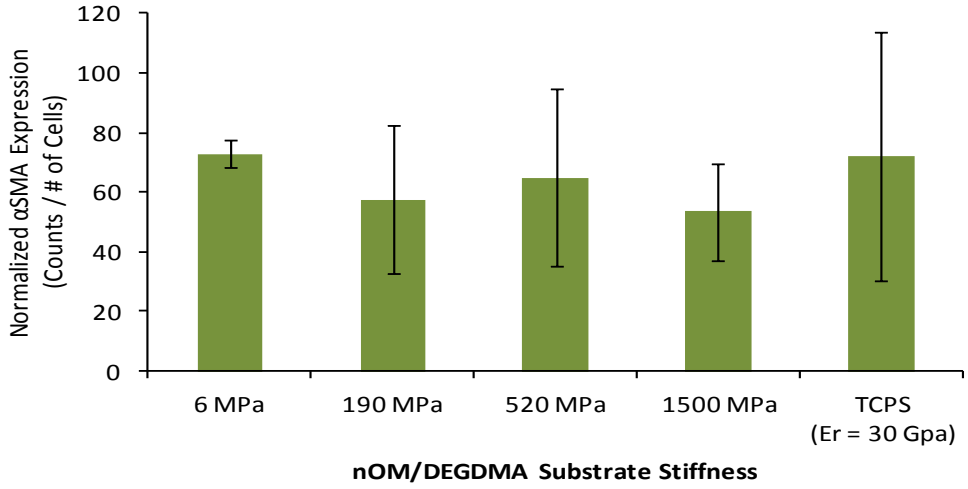

Figure 3-5. Alpha smooth muscle actin expression (αSMA) per cell by VICs cultured on the various rigidity nOM / DEGDMA substrates normalized by cell number. There is no statistical difference in αSMA expression between the formulation or the tissue culture polystyrene control (TCPS). n=3

The staining of CBFa-1 was found at barely detectable levels above the background sporadically on the different substrates as shown in Appendix Figure 3-12. There were not significant levels to confidently quantify the expression levels with the spectral imaging techniques used.

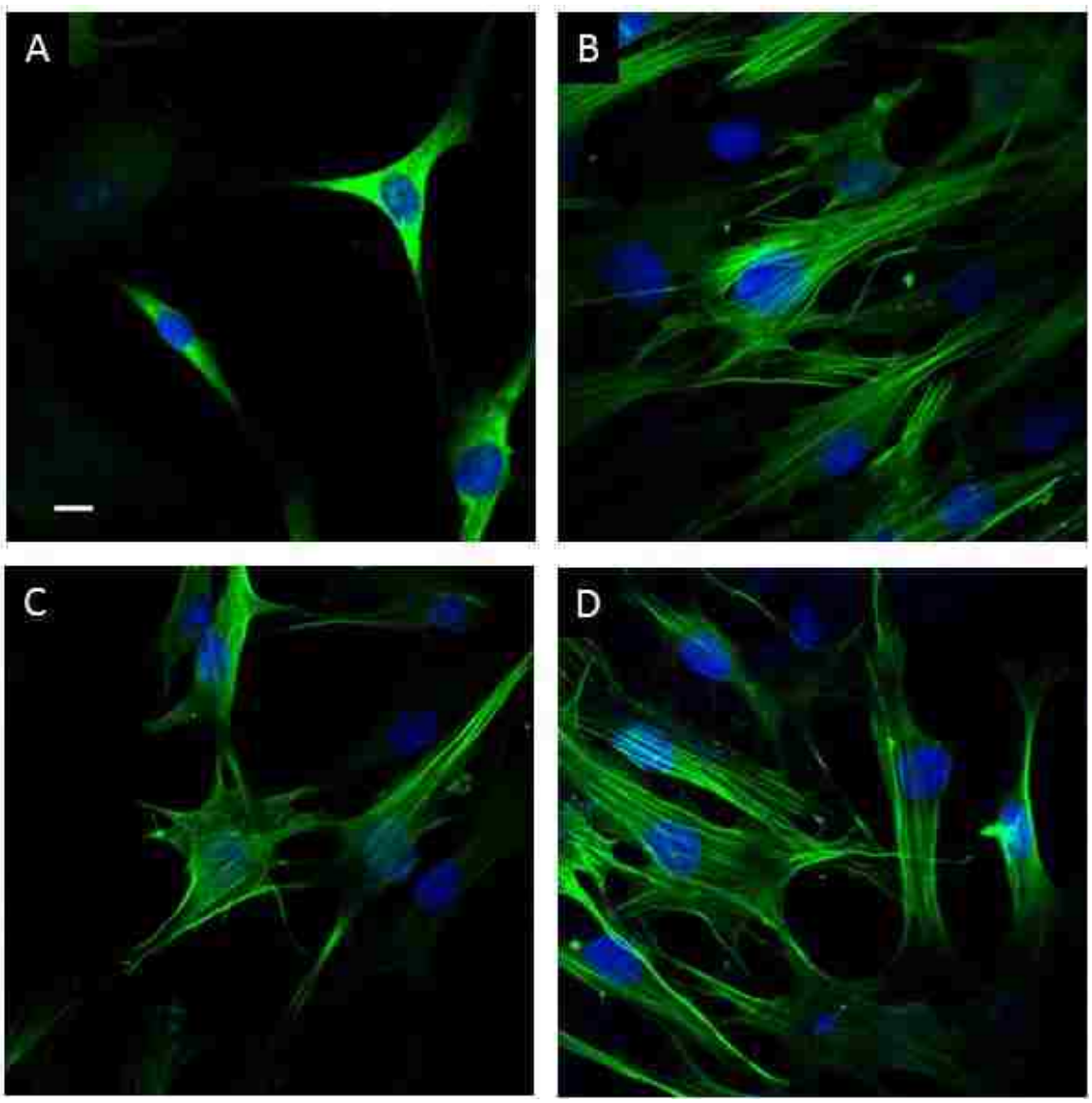

Figure 3-6. Immunocytochemistry stain VIC phenotypic staining after 7 days in culture in reduced serum conditions. A) 6 MPa, B) 186 MPa, C) 500 MPa, D) 1,500 MPa. Green = α-smooth muscle actin, Red = Core Binding Factor 1, Blue = DAPI, Scale Bar = 10 µm

3.5. ECM Production: Sulfated Glycosaminoglycans

The sGAG content after 2 and 7 days of culture in reduced serum conditions (3% FBS) are shown in Figure 3-7. A significant increase in the amount of sGAG produced was observed on all formulations between day 2 (~1.5 µg/well) and day 7 (~12 µg/well). No significant difference was found in sGAG production on the different formulations at either time point ($p>0.05$). Reduced serum culture conditions ensured that there was not an increase in the number of VICs over the experiment, as determined in the variable serum condition experiments presented earlier, Figure 3-2.

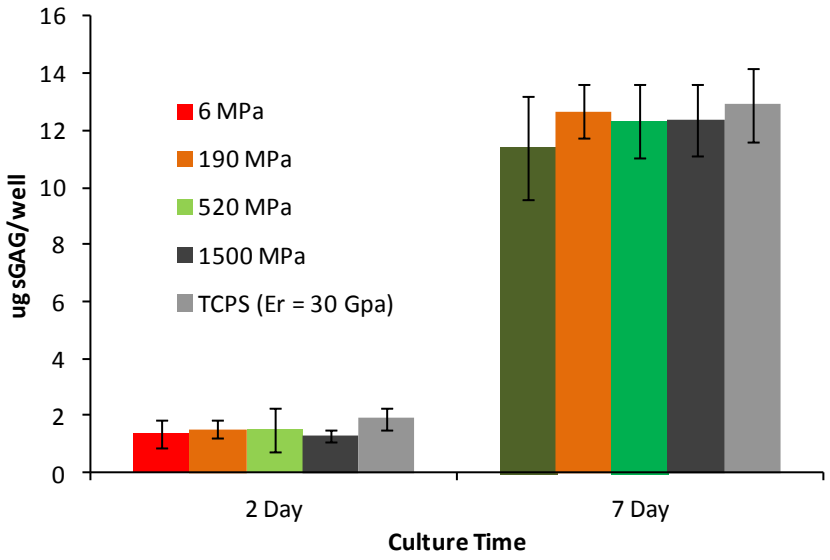

Figure 3-7. Total sulfated glycosaminoglycans (sGAG) content of valvular interstitial cells (VICs) cultured on the varying stiffness substrates. No significant difference was observed between the different substrates or the tissue culture polystyrene control at day 2 or day 7. n=4

3.6. ECM Production: Collagen-I and Elastin Expression

The amount of collagen-I and elastin was quantified using spectral imaging after 7 days of culture. There was no difference in the normalized expression of collagen-I between any of the nOM / DEGDMA formulations and TCPS control (Figure 3-8). However, the cells on the 6 MPa substrate did show a significant ($p<0.05$) increase in elastin production over the 520 and 1,500 MPa substrates (Figure 3-9). Figure 3-10 shows representative images of collagen-I and elastin staining counter stained with DAPI.

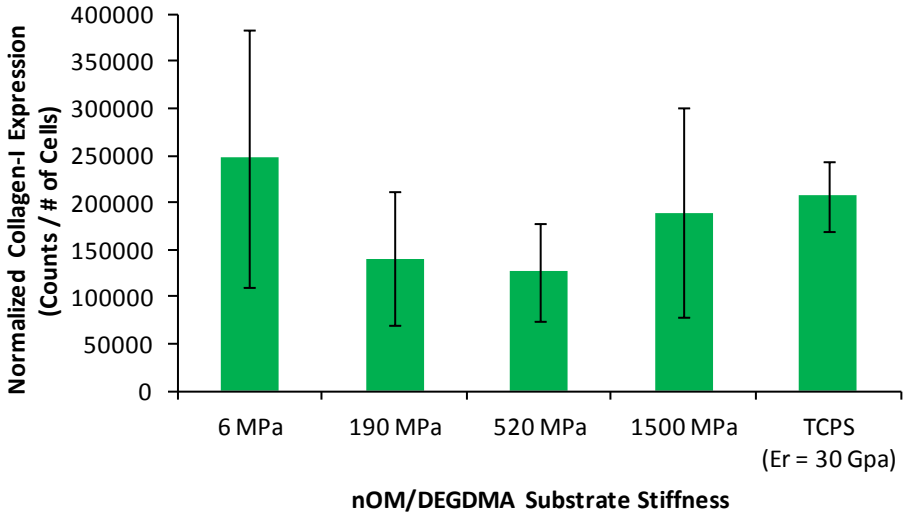

Figure 3-8. Collagen-I expression (Col-I) of valvular interstitial cells (VICs) cultured on substrates of varying rigidity. Change in the rigidity of the VIC culture substrate has no statistical difference of the expression of Col-I after culture for 7 days in reduced serum conditions. n=3, $p > 0.05$

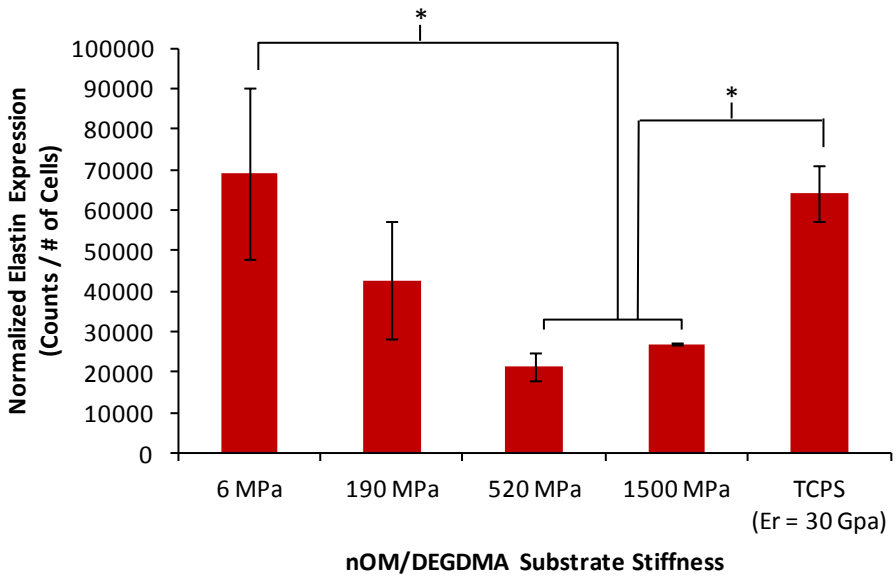

Figure 3-9. Elastin expression determined by ICC staining and spectral imaging quantification. Change in the rigidity of the VIC culture substrate is inversely proportional to the expression of elastin after culture for 7 days in reduced serum conditions. A significant upregulation of elastin expression was observed of the 6MPa substrates over the 520 and 1,500 MPA substrates. Although tissue culture treated polystyrene (E_r = 30.62 ± 10.87 GPa) is stiffer than the 1500 MPa substrates, the difference in the surface contributes to the change in elastin expression. n=3, * p<0.05

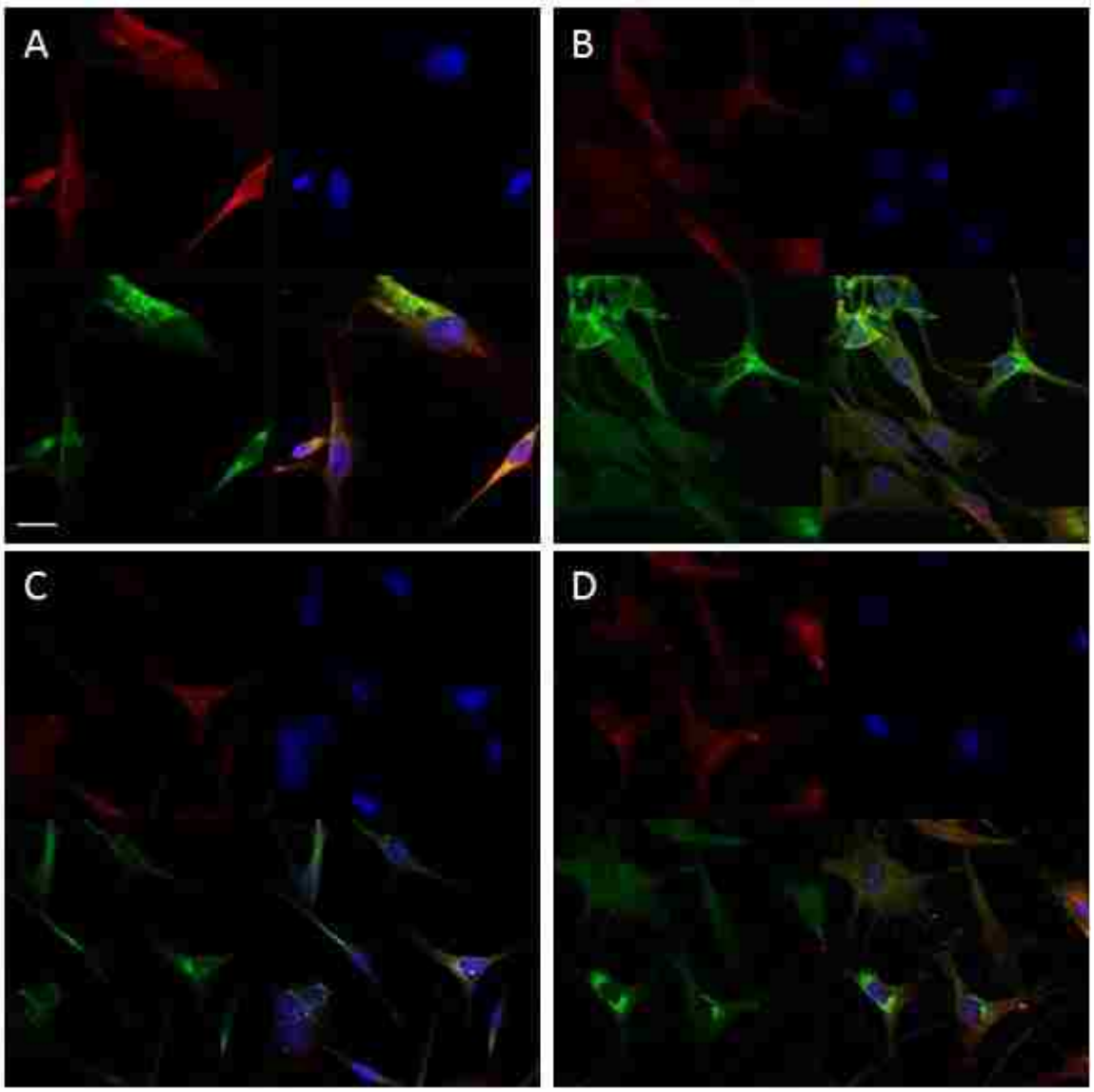

Figure 3-10. Immunocytochemistry stain VIC ECM Production staining 7 days culture in reduced serum conditions. A) 6 MPa, B) 190 MPa, C) 520 MPa, D) 1500 MPa. Red = Elastin (upper left), Green = Collagen I (lower left), Blue = DAPI (upper right), Merged (lower right), Scale Bar = 20 µm

4. Discussion

The work presented here shows the isolated effect of substrate stiffness on the phenotypic expression on VICs as examined by rate of proliferation and expression of phenotypic markers αSMA and CBFa-1. In addition, the production of sGAG, collagen-I, and elastin was also assessed. These studies utilized substrates, nOM / DEGDMA, which allowed for varying bulk modulus from 20 to 5,000 kPa with similar surface features.

Nanoindentation is a technique that samples the mechanical properties of small volumes of a material within microns of the surface. This technique is well suited for the study of materials that will directly interact with cells adhered to the surface. When cells are adhered to a surface, the cytoskeleton of the cell produces shear stress on the material. These cell induced stresses can propagate into the material 50 μm from the surface.[43] Therefore, any of the material that is greater than 50 μm from the surface will not have an effect on the cells. Nanoindentation allows for the sampling of the material's properties that is relevant to cells adhered surface.

The observed trend of increasing stiffness with an increase in DEGDMA content is the same as previously observed in compression testing of bulk materials. Bulk compression testing showed an increase from 25 to 4,700 kPa with an increase of 3 to 33 wt% DEGDMA crosslinker. Nanoindentation of the materials found an increase from 6 to 1,500 MPa with increase of 3 to 33 wt% DEGDMA. The two order of magnitude difference of the moduli measurements between the bulk material testing and nanoindentation is attributed to the difference of sample volume analyzed and the type of modulus examined. In polymeric materials, small volumes versus bulk material may have very different properties due to cyclization and, void volumes and differences in

sampling methods.[33, 36, 44] Bulk compressive modulus also measures the combined properties of plastic and elastic modulus, where nanoindentation only measures the elastic (reduced) modulus. In the bulk material, a larger increase is seen between the 3, 19 and 25 wt% materials (160% increase) than with nanoindentation (86% increase). The sharp increase in the material modulus that is observed in bulk material testing between the 19 and 25 wt% DEGDMA materials is not observed when the material is tested using nanoindentation. In the bulk material, this transition is contributed to the change of how DEGDMA contributes to the overall mechanics. In the lower DEGDMA content materials, DEGDMA crosslinks polymer chains of primarily nOM. The higher DEGDMA content substrate, DEGDMA becomes a significant part of the polymer backbone. The lack of this sharp transition observed with nanoindentation between the 19 and 25 wt% DEGDMA materials suggest that in small volumes and only the elastic modulus, the role DEGDMA plays in the polymer backbone is not as profound as in the bulk. Nanoindentation demonstrated that the modulus of a material at a cellular level is not the same as the bulk measurements.

In the native valve, VICs occupy the environments that are primarily composed of elastin and collagen.[15, 45] Direct measurement of individual fibers of elastin and collagen by atomic force microscopy has yielded measured elastic moduli of 1 and 200 – 7500 MPa, respectively. The nanoindentation results of nOM / DEGDMA networks shows that these polymer substrates are appropriate for modeling the majority of the native ECM of the VICs on the cellular level.

To be able to isolate the impacts of substrate rigidity on various cell functions it is important to be able to control cell density during a study. If population's numbers

change, results would be difficult to interpret because of alterations in cell-cell signaling over the course of the experiment.[46] Experimentation started to determine the minimum serum concentration necessary support VIC viability but limit proliferation. The cell number and morphology were evaluated over nine days in media with varying concentrations of serum. It has been previously demonstrated that cells under varying serum conditions (1 - 10% FBS) have limited changes in the phenotypic expression based on expression of activated marker, αSMA, after several culture passages.[38]

The quantification of the VICs under normal, reduced and depleted serum conditions allowed for the determination of the minimum serum conditions to arrest cell growth over an extended cultured time. Representative bright field microscopy images show that cells cultured in 3% FBS (Figure 3-3 c1 – c4) allow for cell spreading greater than seen with the 1% FBS (Figure 3-3 d1 – d4). Cells under 3% FBS maintained the spread morphology throughout the extent of the study with no statistical change in cell number. These results suggest that 3% FBS is the minimum serum concentration to isolate the impact of an underlying substrate without convolution by changes in cell density.

The results of VIC proliferation on the substrates of varying rigidity contrasts with that of Yip *et al.* Yip studied VICs cultured on collagen gels of varying thickness (10 μm and 2.5 mm) mounted on TCPS, which where modeled to have moduli of 2,000 and 6,000 N/m, respectively.[23] Yip *et al.* found that the VICs cultured on the compliant collagen gels had a significantly higher rate of proliferation than that of cells on the stiffer gels. The collagen gels were characterized as having similar collagen fiber diameters and limited changes in the individual sample stiffness over course of the experiment. However, significant degradation of some of the gels was observed. The

combination of the different thickness of collagen gels and the degradation over the culture period may have presented the cells with unstable surface chemistry. The thin gels used (10 μm), may have allowed the underlying TCPS to affect cell adhesion. In this study, therefore, it is difficult to assume that the variation of gel stiffness is the only property influencing cell function. The newly introduced substrates composed of nOM / DEGDMA have been developed to overcome the problems of variation in substrate surface properties over a range of moduli. The results of shown in Figure 3-4 show that even with a three order magnitude change in substrate rigidity no significant difference is seen in cell numbers between substrate formulations. Combining the results from Yip *et al.* and VICs cultured on nOM / DEGDMA substrates suggests that it may be the difference in substrate chemistries inducing the changes in cell numbers between substrates and not the stiffness of the substrate.

A simple viability assay was used to fluorescently stain viable cells to determine the number of cells on each substrate by three different methods (flow cytometry, automated image analysis and manual image analysis). Each method has its advantages and disadvantages. Manual fluorescent image analysis has long been used to quantify cell number as it is inexpensive and easily implemented. The use of image analysis software is a higher throughput method, capable of analyzing entire images quickly and accurately. Image analysis software relies on the acquisition of representative images of samples to be able to quantify cell numbers and the implication of correct algorithms. The software analysis of images relies on a combination of size, intensity ratio (foreground/background) and sharpness of objects edge to determine number of cells in an image. The software applies the same algorithm to each image consistently analyzing

the images. The manual method of verification relies on the same basic principles of object identification as the software. However, instead of a mathematical determination of object identification it is completely based on operator judgment. Flow cytometry is a high throughput/high accuracy method that is capable of analyzing entire samples. However, flow cytometry only works on suspensions of cells and not cells adhered to a surface. Requiring that cells be lifted from surfaces before analysis by either enzymatic digestion or mechanical contact. Results from the three different methods were compared to determine consistency in the analysis methods.

All of three methods used to analyze the number of cells on the substrates resulted in observation of the same trends throughout the study. The standard deviation for all methods increases with culture time, but the increase is more dramatic with the methods associated with image analysis (Figure 3-4, (B) computer or (C) manual). The manual analysis of the microscopy images has the greatest standard deviation. The large standard deviation is associated with the clustering of cells as cell density increased. This comparison shows that computer image analysis is the preferred method of analysis as it is capable of analyzing entire populations and is accurate due to automation. Automated image analysis can also provide additional information regarding varying cell densities across a single substrate.

Spectral imaging was selected as the method to analyze the phenotypic markers (αSMA, CBFa-1) and ECM production (collagen-I, elastin) as it directly measures the target.[47, 48] Spectral imaging lowers the detection limit of target over that of an RGB image, as the spectrums of each stain are used as standards to separate the contribution of stain versus background. Separation of each spectrum allows for the detection and

quantification of multiple stains on the same sample. However, the technique requires a lower limit of target that is dependent on sample preparation and stain used making it highly dependent on the accuracy of the control spectrums.

The VICs have characteristics of fibroblasts, smooth muscle cells, myofibroblasts and osteoblasts.[19, 38, 49] Native VICs in an adult healthy valve are predominantly fibroblast like, known as the quiescent phenotype (qVIC)[16]. The transition to aVIC phenotype is marked by the expression of α-Smooth Muscle Actin (αSMA) and stress fiber formation.[16, 17] The aVIC is the desired phenotype for tissue engineering applications as it is associated with higher rates of ECM synthesis and proliferation *in vivo*.[14] The expression level of αSMA was not impacted by the stiffness of the substrate (Figure 3-5), indicating that VICs cultured on all of the substrates showed that all of the VICs were of the aVIC or obVIC phenotype. Our αSMA expression results compliment the work by Benton *et al.* which found that expression of αSMA on fibronectin coated PEG hydrogels (modulus of 100 kPa) compared with TCPS did not change. It was only when Benton *et al.* used a different protein, fibrin, was an increase in αSMA expression observed on TCPS over the PEG hydrogels.[14]

Although the αSMA expression was consistent across the surfaces structural changes within the VICs were observed. As can be seen in Figure 3-6, stress fibers of αSMA were diffuse on 6 MPa substrates and more distinct in all other treatment groups. The difference in stress fiber organization is most likely due to the substrates' ability to resist the shear stress the cells create.[38, 50] As the focal adhesions and stress fibers are assembled, there is a continuous cycle of tension and alignment producing varying levels

of stress fiber organization.[19] The stiffer nOM / DEGDMA substrates resist the cell induced shear stress allowing for greater stress fiber organization.

It has been shown that environmental conditions can cause the aVIC to differentiate into the obVIC while still expressing αSMA.[14] The osteoblastic phenotype has been associated with the stiffing of the AV and that a stiffer culture substrate would upregulates the obVIC.[22] Expression of CBFa-1 was detectable but not quantifiable in the positive control (Appendix Figure 3-12) which dictates the calculation of expression levels. However, expression was not detectable at significant levels on any of the substrates to allow for quantification of expression using the spectral imaging technique. The low amounts of CBFa-1 observed suggest that additional factors in either the culture media or bound to substrate are required to promote the obVIC phenotype and that simply culturing VICs on stiff substrates does not induce the obVIC. This conclusion is supported by the work of Benton *et al.* which found that only after the addition of fibrin to either TCPS or PEG hydrogels was there a considerable increase in the levels of CBFa-1 expressed after 6 days of culture. The previous work combined with the results presented here show that substrate rigidity is not the dominating effect on cell phenotype but still may play a role as a moderator of cell sensitivity to soluble factors.

Glycosaminoglycans are linear chains of disaccharides repeat units that serve structural as well as cellular signaling compounds.[51] It was found that out of the two primary classes of GAGs present in the AV (sulfated and hyaluron) VICs incorpurate, 90% sGAG and 10% hyaluronan into the ECM.[41] The dimethylmethylene blue (DMMB) assay was selected to easily and quickly assess the total amount of sGAG produced by VICs into the matrix.[41] Previously, Gupta *et al.* showed that VICs mechanical

environment affects the amount as well as type of GAGs produced. Gupta *et al.* found that VICs cultured in collagen gels constrained to produce stain as the cells contracted the gel increased the incorporation of total GAGs into the surrounding matrix over that of VICs cultured in unconstrained gels. No direct relationship between the stiffness of the substrate and the production of sGAG was found in studies using nOM / DEGDMA substrates. The differences observed between this study and the work by Gupta *et al.* can be attributed to several factors. The use of the collagen gel for a scaffold offers the advantage of easily fabricating an environment composed of natural materials, but may introduce additional variables that could in fact be affecting the behavior of the VICs. To introduce the variable mechanical environments Gupta *et al.* strained the collagen gel, which may change the cell environment as the collagen fibers are strained the fibers will align and change the microenvironment of the cell.[52].

For the goal of tissue engineering, it is important to induce VICs to produce the primary structural proteins of the native AV ECM, collagen and elastin. Collagen-I makes up the bulk of the collagen present in the valve and is critical to allow the valve to resist the tension placed on it during normal function.[24] Previous *ex vivo* studies has shown that VICs in native ECM will upregulate the production of collagen when place under strain, which has led to the investigation of the role of substrate rigidity in ECM production.[53] This phenomenon was investigated with an *in vitro* model where VICs were cultured on flexible substrates coated with collagen-I. When the substrates were placed under increasing levels of strain, the production of collagen increased as well.[24] Placing a material under stress will increase the rigidity of the material, but it also affects the surface properties of a material, including alignment of collagen fibers. In these studies

where the cell culture substrate is strained to produce changes in material mechanics, it is difficult to discern if it is the increase in material rigidity or other changes in the material are inducing certain cell functions. Additionally, the rate at which a material is stained can influence the response of VICs, which raises the question of if the synthesis of collagen was due to the resulting stiffness of the material or the rate at which the strain was applied.[54, 55] Comparison of the results of previous studies and the results presented here suggests that it was the changes in the surface that were induced by the stretching that caused the change in the level of collagen expression. This hypothesis is further supported by the work of Shah *et al.* and Benton *et al.* with degradable PEG based hydrogels and TCPS, where levels of collagen expression were only impacted by the addition of exogenous soluble signals.[10, 40]

Elastin is necessary in the valve to maintain the collagen structures and allows for the recoil of the valve during normal function. However, it has proved difficult to induce the production of elastin *in vitro* and *in vivo*.[1, 6] A major discovery by Masters *et al.* and Shah *et al.* found that culture media supplemented additional hyaluronic acid (HA, 3 µg/mL) upregulated VIC elastin production.[6, 10] Shah *et al.* used VICs encapsulated in degradable hydrogels of HA / PEG. As the gels degraded releasing HA, the expression of elastin increased.[10] Although mechanical testing was not performed, mass loss and gel dissolution occurred of the hydrogels even with the production of ECM components by the VICs. This suggests that mechanical rigidity of the three dimensional structure decreased over the course of the study.[56] Combining this with our elastin production results presented in Figure 3-9 suggests that the significant increase in the amount of elastin produced seen by Shah *et al.* was a compound effect between the HA stimulation

and the decreased rigidity of the gel due to degradation. It is possible that VICs increase the amount of elastin produced on softer substrates because the modulus was similar to that of elastin fibers which are primary found in the ventricularis.

While results are encouraging, there are some limitations to this study. Quantification of the protein expression by ICC spectral imaging allowed for the direct analysis of expressed proteins associated with phenotypic expression and ECM secretion. However, expression of proteins must be at a high enough level to be able to confidently distinguish the fluorescence associated with desired protein over that of the background. Use of quantifiable real time-polymerase chain reaction (RT-PCR), could be used to supplement the spectral imaging results, as it is capable of detecting small changes in levels of mRNA. It should be noted however, that mRNA expression does not directly correlate to protein expression, due to the time for cells to produce the proteins as well as regulation pathways associated with protein expression. The results presented here could be supplemented with RT-PCR to obtain a more sensitive analysis of expression. In addition, this study was limited to only analysis of the sGAG produced by the VICs, this does not examine hyaluronic acid expression that could be affected by the rigidity of the substrate. Fluorophore-assisted carbohydrate electrophoresis (FACE) could be used to analyze all the different classes of GAGs to develop a complete picture of GAG production. Only a single type of collagen production was evaluated, this limits the study as it does not examine the regulation effects of the changes in type of collagen produced.

5. Conclusion

Cell culture substrates fabricated from nOM / DEGDMA were utilized with a three order magnitude increase in the reduced modulus (E_r) to determine the isolated impact of substrate rigidity on the proliferation, phenotype and ECM production of VICs. Nanoindentation was employed to determine the material stiffness at the cell-substrate interface, finding that the nOM / DEGDMA substrates utilized of varied from 6 to 1,500 MPa, covering the majority of micro mechanical environment experienced by VICs in native tissue.[57] To properly test VICs for proliferation, phenotype and ECM production it was desired to find a minimal media serum level that allowed for VIC viability and spreading while limiting proliferation. It was found that media supplemented with 3% (v/v) serum allowed for efficient cell adhesion, limited proliferation, and did not significantly affect the morphology of the cells. It was found by three different methods that the rigidity of the culture substrate did not have a significant difference in the proliferation of VICs. Through immunocytochemistry staining of phenotype marker αSMA, no difference was found between the levels of expression after 7 days of culture. The marker for the diseased osteoblastic phenotype was not detectable. Phenotypic evaluation concluded that all surfaces produced aVICs, while obVICs were not a significant portion of the VIC populations. Production of the major ECM components sGAG and collagen-I had no statistical difference between the different substrate rigidities. However, softer substrates (E_r = 6 MPa) had significantly higher levels of elastin produced over the stiffer substrates (E_r = 500, 1500 MPa). The results of these studies offer the ability to separate out the independent impact of substrate rigidity on VIC functions. It was found that the substrate rigidity only affected the production of

elastin with no detectable difference in the proliferation, phenotype, or production of other ECM components.

6. Appendix

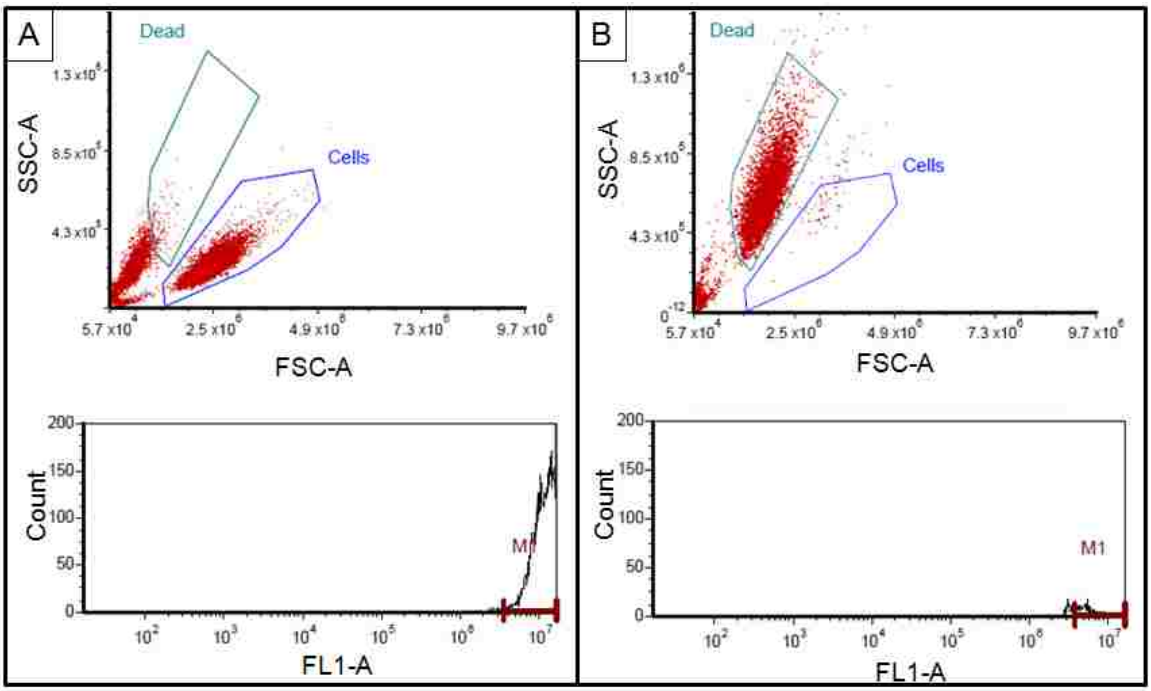

Figure 3-11. Flow cytometry analysis of VICs untreated (A) and incubated with 70% v/v Methanol/water (B) stained with CyQuant Direct Cell Proliferation Assay. The 2 part assay stains DNA fluorescent green, cells with compromised membranes the fluorescent signal is suppressed as seen in the comparison of the FL1-A histograms between (A) and (B).

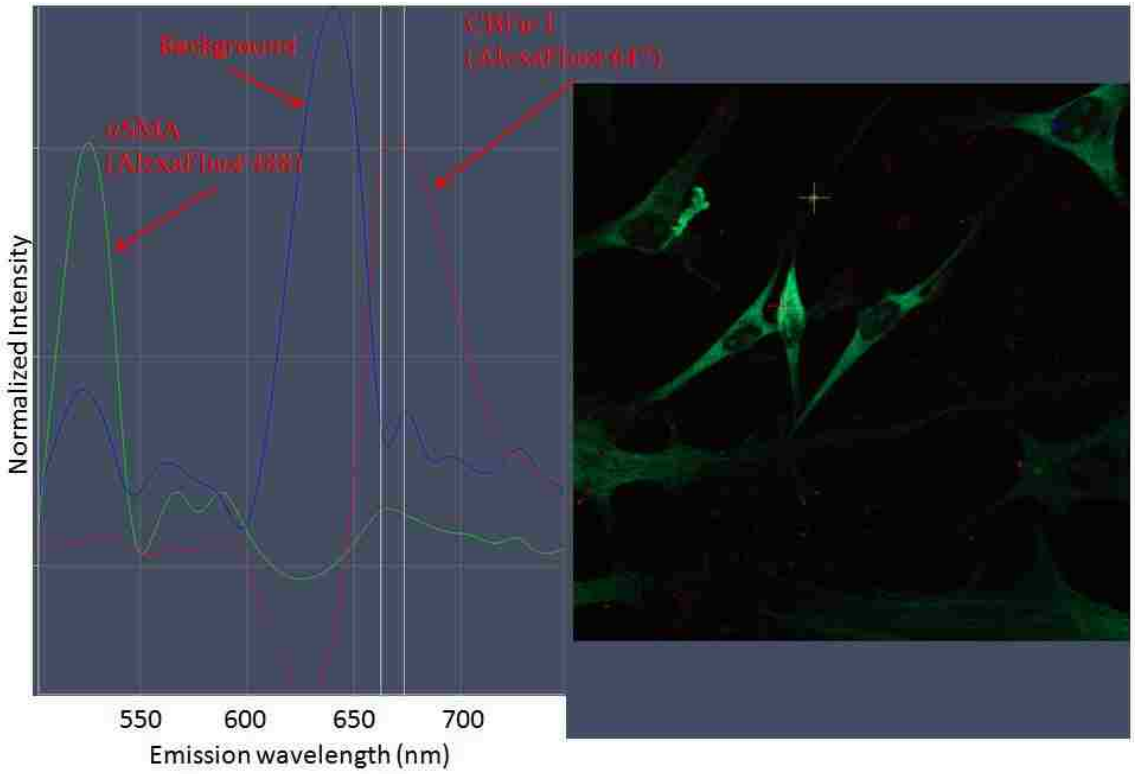

Figure 3-12. Emission spectra of αSMA positive and a single CBFa-1 positive VIC verifying the ICC staining method

7. References

1. Flanagan, T. C.; Pandit, A., Living artificial heart valve alternatives: A review. *Eur Cell Mater* **2003,** 6, (July-December Cited November 21, 2003), 28-45.

2. Nkomo, V. T.; Gardin, J. M.; Skelton, T. N.; Gottdiener, J. S.; Scott, C. G.; Enriquez-Sarano, M., Burden of valvular heart diseases: A population-based study. *Lancet* **2006,** 368, (9540), 1005-1011.

3. Butcher, J. T.; Mahler, G. J.; Hockaday, L. A., Aortic valve disease and treatment: The need for naturally engineered solutions. *Adv Drug Deliver Rev* **2011,** 63, (4-5), 242-268.

4. Sacks, M. S.; Schoen, F. J.; Mayer, J. E., Bioengineering challenges for heart valve tissue engineering. *Annu Rev Biomed Eng* **2009,** 11, (1), 289-313.

5. Butcher, J. T.; Nerem, R. M., Porcine aortic valve interstitial cells in three-dimensional culture: Comparison of phenotype with aortic smooth muscle cells. *J Heart Valve Dis* **2004,** 13, (3), 478-485.

6. Masters, K. S.; Shah, D. N.; Leinwand, L. A.; Anseth, K. S., Crosslinked hyaluronan scaffolds as a biologically active carrier for valvular interstitial cells. *Biomaterials* **2005,** 26, (15), 2517-2525.

7. Leask, R. L.; Jain, N.; Butany, J., Endothelium and valvular diseases of the heart. *Microsc Res and Techniq* **2003,** 60, (2), 129-137.

8. Lincoln, J.; Lange, A. W.; Yutzey, K. E., Hearts and bones: Shared regulatory mechanisms in heart valve, cartilage, tendon, and bone development. *Dev Biol* **2006,** 294, (2), 292-302.

9. Michael, S. S.; Merryman, W. D.; David, E. S., On the biomechanics of heart valve function. *J Biomech* **2009,** 42, (12), 1804-1824.

10. Shah, D. N.; Recktenwall-Work, S. M.; Anseth, K. S., The effect of bioactive hydrogels on the secretion of extracellular matrix molecules by valvular interstitial cells. *Biomaterials* **2008,** 29, (13), 2060-2072.

11. Proudfoot, D.; Skepper, J. N.; Hegyi, L.; Bennett, M. R.; Shanahan, C. M.; Weissberg, P. L., Apoptosis regulates human vascular calcification in vitro : Evidence for initiation of vascular calcification by apoptotic bodies. *Circ Res* **2000,** 87, (11), 1055-1062.

12. Yip, C. Y. Y.; Chen, J.-H.; Zhao, R.; Simmons, C. A., Calcification by valve interstitial cells is regulated by the stiffness of the extracellular matrix. *Arterioscl Throm Vas* **2009,** 29, (6), 936-942.

13. Osman, L.; Yacoub, M. H.; Latif, N.; Amrani, M.; Chester, A. H., Role of human valve interstitial cells in valve calcification and their response to atorvastatin. *Circulation* **2006,** 114, (1_suppl), I-547-552.

14. Benton, J. A.; Kern, H. B.; Anseth, K. S., Substrate properties influence calcification in valvular interstitial cell culture. *J Heart Valve Dis* **2008,** 17, (6), 689-699.

15. Misfeld, M.; Sievers, H. H., Heart valve macro- and microstructure. *Phil Trans R Soc B* **2007,** 362, (1484), 1421-1436.

16. Liu, A. C.; Joag, V. R.; Gotlieb, A. I., The emerging role of valve interstitial cell phenotypes in regulating heart valve pathobiology. *Am J of Pathol* **2007,** 171, (5), 1407-1418.

17. Cushing, M. C.; Liao, J.-T.; Jaeggli, M. P.; Anseth, K. S., Material-based regulation of the myofibroblast phenotype. *Biomaterials* **2007,** 28, (23), 3378-3387.

18. Merryman, D. W., Mechano-potential etiologies of aortic valve disease. *J Biomech* **2010,** 43, (1), 87-92.

19. Tomasek, J. J.; Gabbiani, G.; Hinz, B.; Chaponnier, C.; Brown, R. A., Myofibroblasts and mechano-regulation of connective tissue remodelling. *Nat Rev Mol Cell Biol* **2002,** 3, (5), 349-363.

20. Hinton, R. B., Jr; Lincoln, J.; Deutsch, G. H.; Osinska, H.; Manning, P. B.; Benson, D. W.; Yutzey, K. E., Extracellular matrix remodeling and organization in developing and diseased aortic valves. *Circ Res* **2006,** 98, (11), 1431-1438.

21. Lester, W. M.; Damji, A. A.; Gedeon, I.; Tanaka, M., Interstitial-cells from the atrial and ventricular sides of the bovine mitral-valve respond differently to denuding endocardial injury. *In Vitro Cell Dev-An* **1993,** 29A, (1), 41-50.

22. Mohler, E. R.; Gannon, F.; Reynolds, C.; Zimmerman, R.; Keane, M. G.; Kaplan, F. S., Bone formation and inflammation in cardiac valves. *Circulation* **2001,** 103, (11), 1522-1528.

23. Yip, C. Y. Y.; Chen, J.-H.; Zhao, R.; Simmons, C. A., Calcification by valve interstitial cells is regulated by the stiffness of the extracellular matrix. *Arterioscler Thromb Vasc Biol* **2009,** 29, (6), 936-942.

24. Ku, C.-H.; Johnson, P. H.; Batten, P.; Sarathchandra, P.; Chambers, R. C.; Taylor, P. M.; Yacoub, M. H.; Chester, A. H., Collagen synthesis by mesenchymal stem

cells and aortic valve interstitial cells in response to mechanical stretch. *Cardiovasc Res* **2006,** 71, (3), 548-556.

25. Nemir, S.; West, J. L., Synthetic materials in the study of cell response to substrate rigidity. *Ann Biomed Eng* **2010,** 38, (1), 2-20.

26. Pedron, S.; Peinado, C.; Bosch, P.; Benton, J. A.; Anseth, K. S., Microfluidic approaches for the fabrication of gradient crosslinked networks based on poly(ethylene glycol) and hyperbranched polymers for manipulation of cell interactions. *J Biomed Mater Res A* **2011,** 96A, (1), 196-203.

27. Brown, X. Q.; Ookawa, K.; Wong, J. Y., Evaluation of polydimethylsiloxane scaffolds with physiologically-relevant elastic moduli: Interplay of substrate mechanics and surface chemistry effects on vascular smooth muscle cell response. *Biomaterials* **2005,** 26, (16), 3123-3129.

28. Wong, J. Y.; Leach, J. B.; Brown, X. Q., Balance of chemistry, topography, and mechanics at the cell-biomaterial interface: Issues and challenges for assessing the role of substrate mechanics on cell response. *Surf Sci* **2004,** 570, (1-2), 119-133.

29. Rehfeldt, F.; Engler, A. J.; Eckhardt, A.; Ahmed, F.; Discher, D. E., Cell responses to the mechanochemical microenvironment--implications for regenerative medicine and drug delivery. *Adv Drug Delivery Rev* **2007,** 59, (13), 1329-1339.

30. Kannurpatti, A. R.; Anseth, J. W.; Bowman, C. N., A study of the evolution of mechanical properties and structural heterogeneity of polymer networks formed by photopolymerizations of multifunctional (meth)acrylates. *Polymer* **1998,** 39, (12), 2507-2513.

31. Yoo, S. H.; Kim, C. K., Effects of various diluents included in the resin matrices on the characteristics of the dental composites. *Polym-Korea* **2009,** 33, (2), 153-157.

32. Meriç, G.; Dahl, J. E.; Ruyter, I. E., Cytotoxicity of silica-glass fiber reinforced composites. *Dent Mater* **2008,** 24, (9), 1201-1206.

33. Tranchida, D.; Piccarolo, S.; Loos, J.; Alexeev, A., Accurately evaluating young's modulus of polymers through nanoindentations: A phenomenological correction factor to the oliver and pharr procedure. *Appl Phys Lett* **2006,** 89, (17).

34. Oliver, W. C.; Pharr, G. M., An improved technique for determining hardness and elastic-modulus using load and displacement sensing indentation experiments. *J Mater Res* **1992,** 7, (6), 1564-1583.

35. Clifford, C. A.; Seah, M. P., Quantification issues in the identification of nanoscale regions of homopolymers using modulus measurement via afm nanoindentation. *Appl Surf Sci* **2005,** 252, (5), 1915-1933.

36. Kaufman, J. D.; Klapperich, C. M., Surface detection errors cause overestimation of the modulus in nanoindentation on soft materials. *J Mech Behav Biomed* **2009,** 2, (4), 312-317.

37. Johnson, C. M.; Hanson, M. N.; Helgeson, S. C., Porcine cardiac valvular subendothelial cells in culture - cell isolation and growth-characteristics. *J Mol and Cell Cardiol* **1987,** 19, (12), 1185-1193.

38. Cushing, M. C.; Liao, J.-T.; Anseth, K. S., Activation of valvular interstitial cells is mediated by transforming growth factor-[beta]1 interactions with matrix molecules. *Matrix Biol* **2005,** 24, (6), 428-437.

39. Cushing, M. C.; Jaeggli, M. P.; Masters, K. S.; Leinwand, L. A.; Anseth, K. S., Serum deprivation improves seeding and repopulation of acellular matrices with valvular interstitial cells. *J Biomed Mater Res-A* **2005,** 75A, (1), 232-241.

40. Benton, J. A.; Fairbanks, B. D.; Anseth, K. S., Characterization of valvular interstitial cell function in three dimensional matrix metalloproteinase degradable peg hydrogels. *Biomaterials* **2009,** 30, (34), 6593-6603.

41. Gupta, V.; Werdenberg, J. A.; Blevins, T. L.; Grande-Allen, K. J., Synthesis of glycosaminoglycans in differently loaded regions of collagen gels seeded with valvular interstitial cells. *Tissue Eng* **2007,** 13, (1), 41-49.

42. Rajamannan, N. M.; Subramaniam, M.; Rickard, D.; Stock, S. R.; Donovan, J.; Springett, M.; Orszulak, T.; Fullerton, D. A.; Tajik, A. J.; Bonow, R. O.; Spelsberg, T., Human aortic valve calcification is associated with an osteoblast phenotype. *Circulation* **2003,** 107, (17), 2181-2184.

43. Mehrotra, S.; Hunley, S. C.; Pawelec, K. M.; Zhang, L.; Lee, I.; Baek, S.; Chan, C., Cell adhesive behavior on thin polyelectrolyte multilayers: Cells attempt to achieve homeostasis of its adhesion energy. *Langmuir* **2010,** 26, (15), 12794-12802.

44. Wong, S. C.; Lee, H.; Qu, S. Y.; Mall, S.; Chen, L., A study of global vs. Local properties for maleic anhydride modified polypropylene nanocomposites. *Polymer* **2006,** 47, (21), 7477-7484.

45. Merryman, D. W.; Shadow Huang, H.-Y.; Schoen, F. J.; Sacks, M. S., The effects of cellular contraction on aortic valve leaflet flexural stiffness. *J Biomech* **2006,** 39, (1), 88-96.

46. Chester, A. H.; Taylor, P. M., Molecular and functional characteristics of heart-valve interstitial cells. *Phil Trans R Soc B* **2007,** 362, (1484), 1437-1443.

47. Taylor, P. M.; Allen, S. P.; Yacoub, M. H., Phenotypic and functional characterization of interstitial cells from human heart valves, pericardium and skin. *J Heart Valve Dis* **2000,** 9, (1), 150-158.

48. Taylor, C. R.; Levenson, R. M., Quantification of immunohistochemistry—issues concerning methods, utility and semiquantitative assessment ii. *Histopathology* **2006,** 49, (4), 411-424.

49. Rabkin, E.; Aikawa, M.; Stone, J. R.; Fukumoto, Y.; Libby, P.; Schoen, F. J., Activated interstitial myofibroblasts express catabolic enzymes and mediate matrix remodeling in myxomatous heart valves. *Circulation* **2001,** 104, (21), 2525-2532.

50. Fletcher, D. A.; Mullins, R. D., Cell mechanics and the cytoskeleton. *Nature* **2010,** 463, (7280), 485-492.

51. Raman, R.; Sasisekharan, V.; Sasisekharan, R., Structural insights into biological roles of protein-glycosaminoglycan interactions. *Chem Biol* **2005,** 12, (3), 267-277.

52. Pins, G. D.; Christiansen, D. L.; Patel, R.; Silver, F. H., Self-assembly of collagen fibers. Influence of fibrillar alignment and decorin on mechanical properties. *Biophys J* **1997,** 73, (4), 2164-2172.

53. Xing, Y.; He, Z.; Warnock, J. N.; Hilbert, S. L.; Yoganathan, A. P., Effects of constant static pressure on the biological properties of porcine aortic valve leaflets. *Ann Biomed Eng* **2004,** 32, (4), 555-562.

54. Weinberg, E.; Shahmirzadi, D.; Mofrad, M., On the multiscale modeling of heart valve biomechanics in health and disease. *Biomech Model Mechanobiol* **2010,** 9, (4), 373-387.

55. Butcher, J. T.; Markwald, R. R., Valvulogenesis: The moving target. *Philos Trans R Soc Lond B* **2007,** 362, (1484), 1489-1503.

56. Chen, J.; Chen, J.; Xu, Z., Rheological and biological characteristics of hyaluronic acid derivative modified by polyethylene glycol. *J Wuhan Univ of Technol* **2008,** 23, (5), 617-621.

57. Guthold, M.; Liu, W.; Sparks, E.; Jawerth, L.; Peng, L.; Falvo, M.; Superfine, R.; Hantgan, R.; Lord, S., A comparison of the mechanical and structural properties of fibrin fibers with other protein fibers. *Cell Biochem Biophys* **2007,** 49, (3), 165-181.

Chapter 4 : Conclusions and Future Directions

1. Conclusions

Aortic valve disease is of major clinical importance in the United States, affecting approximately 100,000 people each year.[1, 2] The lack of sustainable treatments has led researchers to develop a living tissue substitute for diseased tissue. The stiffening of the AV in disease states has encouraged researchers to develop *in vitro* cell culture platforms, which are a model capable of revealing the phenotypic patterns of cells during health and disease of the AV. While invaluable information has been gathered on the response of VICs to the stiffness of the supporting substratum, many have been obscured by a variety of complicating substrate factors. Most notably, the change in surface features over a physiologically relevant range has complicated results.

Tissue engineering of the aortic heart valve (AV) has the potential to be the next generation of therapies for replacing or repairing diseased and damaged valves. However, after initial success of tissue scaffolds in animal models, it became clear that a greater understanding of the cellular biology of the primary cell population of the AV, valvular interstitial cells (VICs), was needed.[3] Inducing VICs to produce structural extra cellular matrix (ECM) components of AVs is a multifaceted problem. The plastic phenotype of the VICs has to be modulated along with induction of ECM production.[4] A proper balance between the physical properties of the substrate and soluble signaling factors is extremely important to direct VIC functions for AV tissue engineering applications.[3, 5]

Maintaining this balance between the material and soluble factors is convoluted by limitations imposed by current cell culture platforms. For example, isolating effects of substrates rigidity on VIC biology from those imparted by differences in substrate chemical composition and topographical features has been difficult.[6, 7] We sought to

develop a new cell culture platform that is capable of exhibiting a wide range of physiologically relevant moduli without significant variation in the surface. In this work, we developed a culture platform using n-octyl methacrylate (nOM) / diethylene glycol dimethacrylate (DEGDMA) that would allow for the systematic evaluation of substrate modulus on VIC biologic functions while maintaining a consistent surface.

The material platform composed of varying amounts of nOM and DEGDMA, which produced a substrate with a range covering three orders of magnitude. Differences in modulus in the bulk polymer (25 – 5,000 kPa) as well as on the surface (6 – 1,500 MPa) were seen. Analysis of the surface indicated that the wettability (contact angle of 90°), topography (R_{rms} of 17 ± 6 nm), chemical composition (~70% aliphatic carbon) and total amount of protein adsorbed (~18 μg BSA/cm^2) varied little over this entire range of moduli. This platform will potentially enable studies of cellular biology associated with initiation and progression of diseases outside the AV, that are characterized by a stiffening of the tissue, including liver fibrosis[8] and many cancers.[9]

The successful fabrication of the nOM / DEGDMA substrates allowed for the first evaluation of the impact of rigidity on VICs without complications from changes in the topography and chemical composition of the surface. For example, protein markers for the activation of VICs (αSMA) showed no significant variation ($p>0.05$). The marker of disease-state, core binding factor-1 (CBFa-1), was barely detectable on any of the materials, indicating that rigidity alone was not enough to produce a diseased phenotype. No significant difference ($p>0.05$) was found in the production of sulfated glycosaminoglycans and collagen-I, on any of the materials. Softer materials, however, yielded a significantly greater expression of elastin ($p<0.05$).

We have successfully demonstrated that an easily fabricated cell culture platform of nOM / DEGDMA could be used for cell culture studies. The substrates have a large range of physiologically relevant moduli in the bulk polymer as well as on the surface. The materials maintained similar chemical and topographical features across the entire range. This enabled us to perform the first analysis of the phenotypic expression of VICs with isolated impact of substrate rigidity. The results obtained will be used to further the understanding of the regulations of phenotypic transitions of the VICs as well as design three-dimensional scaffolds for the engineering of AV tissue.

The successful development of the base platform allows for the advancement of surface modification to probe the events at the material/VIC interface. This understanding will in turn provide the foundation of engineering VIC encapsulated constructs that mimic healthy AV tissue. Below we present our vision of those parameters that need to be defined in addition to modulus to form an effective material/VIC interface. They include surface topography, relative hydrophobicity, and functionalization. Optimizing these features along with modulus will enable more effective engineered tissues.

2. Future Directions

2.1. Nanotopography – Preliminary Studies to Support Future Work

The objective of this section is to identify material platforms with defined substrate stiffness and topography that direct tissue formation from the VICs. Many methods have been used to generate micron to nanometer scale topography for tissue engineering applications, including but not limited to shadow masks, photolithography, electron beam, and focused ion beam lithography directly on a cell culture substrates.[10-12] These

methods can be used to fabricate a stamp to use in lithography to increase the number of substrates that can be fabricated. In this method, the surface features of a stamp are transferred to a substrate by mechanical contact with an uncured monomer solution followed by photo or thermal induced crosslinking. Ultraviolet nanoimprint lithography (UV-NIL) was chosen as it is both a high throughput and high fidelity method, which avoids the use of additional heat for curing that causes problems of stamp destruction due to thermal expansion. [13] The UV-NIL process allows for the generation of materials with feature sizes down to ~10 nm. The small feature size is possible because the use of low viscosity monomer solutions do not require heat for mold filling. Without the additional heat temperature gradients and differences in thermal expansion between the stamp / substrate are avoided.[14]

By combining the rigidity-controlled network of poly(nOM-co-DEGDMA) with topographical features produced using UV-NIL, a new multi-functional substrate can be fabricated. The new platform will be used to simultaneously determine the impact of variation of both ordered surface topography and substrate compliance on the cellular functions of VICs. The fabrication of substrates entails a number of steps. Working stamps were fabricated from the master mold by solvent casting of a thin fluoropolymer film (Figure 4-1A, 1 and 2), Dupont Teflon AF 2400 (2,2-bistrifluoromethyl-4,5-difluoro-1,3,-dioxole (PDD) and tetrafluoroethylene (TFE)) in perfluorinated solvent (FC40, 3M) at 165°C and -22 inHg for 6 hours.[13, 15] Polydimethlysiloxane (Sylgard 184, Dow) was also evaluated as a potential working mold material, but was discarded when swelling of the mold was observed upon application of the nOM / DEGDMA monomer solution. The fluoropolymer mold overcomes many of the problems associated with using

a rigid mold for UV-NIL, including mass transport/variable pattern filling and the need for surface treatment to allow mold release.[14, 16] The fluoropolymer mold helps to reduce mass transport/variable pattern filling, as it is a flexible film that is capable of conforming to any long-range undulations. The fluoropolymer mold is easily released from the resulting cured material because of its low surface energy of 15.6 dyne/cm.[15] The low surface energy has the added benefit for biological applications, as it will help limit possible surface contamination of the final substrate with the stamp materials. A photo-curable solution of monomers, nOM and DEGDMA, is placed over the fluoropolymer working mold (Figure 4-1A, 3 and 4). The rigidity of the substrate is independently controlled by the ratio of the photo curable monomers. Figure 4- 4B, shows the fabrication method utilized to generate free standing nOM / DEGDMA substrates with nanotopography on the surface. Using this method, it is possible to generate cell culture substrates with tunable rigidity and surface topography as shown in Figure 4-2.

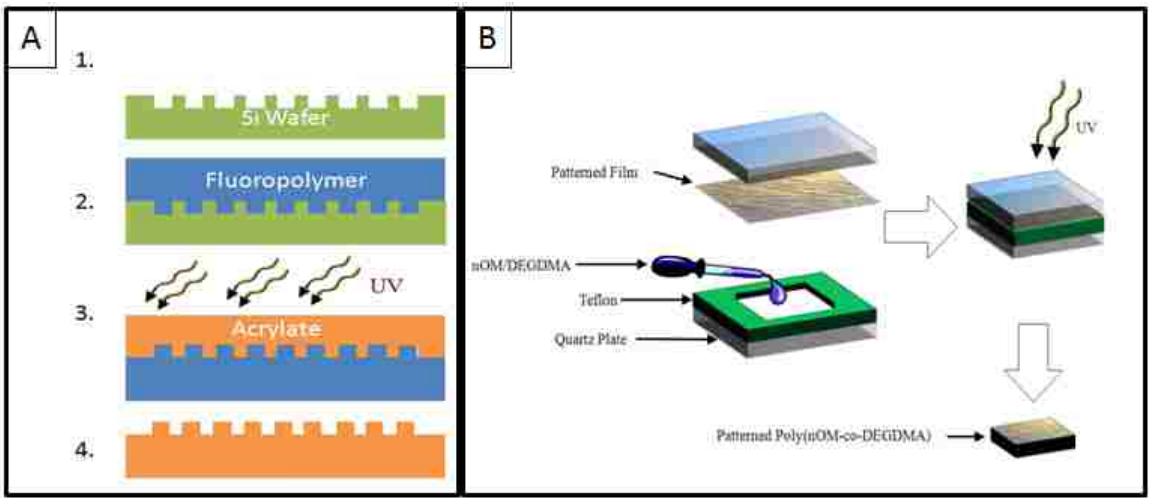

Figure 4-1. Schematic illustration of ultra violet nanoimprint process (UV-NIL). A thin film on a silica wafer is patterned using interferomatric lithography(A1), a fluoropolymer working stamp is solvent casted on to the patterened silica wafer (A2), then a acrylate monomer solution is poured over the working stamp and cured with UV (A3), the acrylate is easily removed from the working mold because of the low surface energy of the working stamp. Placing the working fluoropolymer stamp in the quartz mold can be used to generate freestanding sub-micro patterned substrates (B)

The results in Figure 4-2 show that the majority of the pattern from the master stamp (A) is transferred to the working fluoropolymer stamp (B) and finally to a UV cured nOM/DEGDMA substrate. The variable filling of the master stamp with the fluoropolymer solution as well as incomplete filling of the fluoropolymer stamp with nOM/DEGDMA monomer solutions results in the hill and valley effect seen. These results demonstrate the feasibility of creating submicron topography features on a freestanding cell culture substrate. Optimization of the solvent casting of the fluoropolymer by determining the rate at which the solvent is evaporated. The rate is easily controlled by varying temperature and pressure. These variations in the process will help to eliminate mass transfer problems that result in undulations in the final substrate.

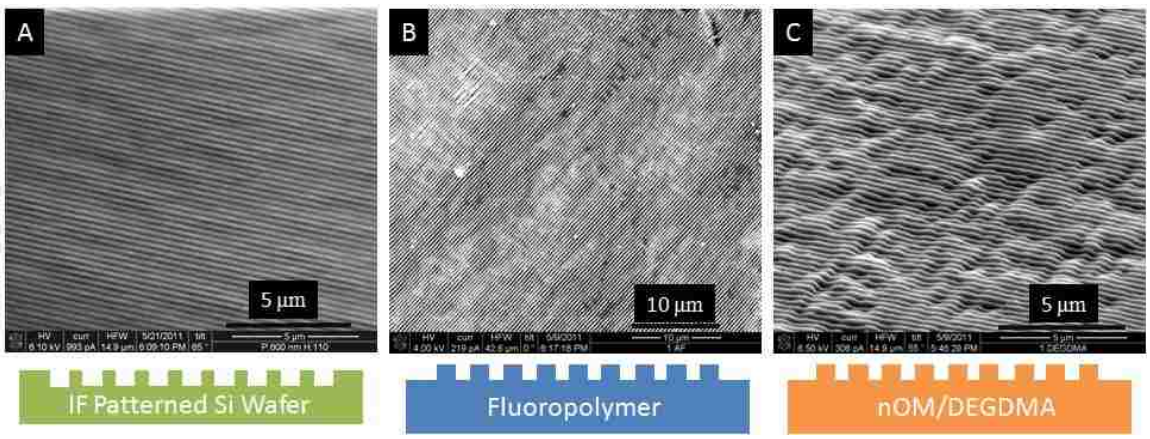

Figure 4-2. Scanning Electron Microscopy Images of the (A) master stamp, (B) working AF stamp, (C) nOM/DEGDMA patterned substrates. Optimization of the process will help to eliminate mass transfer problems that result in undulations in the final substrate

The nOM / DEGDMA platform has proved to be capable of adding sub-micron ordered surface topography. Optimization of the imprinting process could produce substrates with ordered topography and moduli control. The combined impact of surface

rigidity and topography moves the field closer to mimicking the native in vivo environment.

2.2. Chemical Surface Modification

A significant dependence of the chemical surface that is presented to the VICs on the phenotypic and ECM secretion has been observed.[17, 18] Non-specific protein adsorption from serum onto synthetic substrates is the simplest method for promoting cell adhesion. The adsorption of serum components is dependent on the substrates wettability and topography.[19, 20] Non-specific protein adsorption of the nOM/DEGDMA substrates can be modulated using chemical treatments. For example, the contact angle can be decreased using an oxygen plasma to add hydroxyl groups.[21] The surface could also be made more positive by treatment with a weak aqueous acid.[22] This would result in a decrease in the contact angle with the protonation of the surface.

Specific control of the VICs could be achieved by the adsorption of specific native ECM components such as fibronectin, collagen, heparin and hyaluron. All of these ECM components have shown to influence both phenotypic markers and ECM secretion of VICs.[17, 18, 23] Surface adsorption is a viable option for the use of nOM/DEGDMA because of limited surface variation, which exists over the range of modulus. This would remove the variability of protein adsorption conformation that exists with other materials and can be verified by time of flight mass spectrometry.[19]

Modification of the surfaces by either specific ECM components or nonspecifically adsorbed serum proteins allows an additional method to direct the cell function of VICs. Controlling nonspecific protein adsorption onto the surfaces is attractive as it could allow

for the same control offered from specific protein adsorption without the need to purchase expensive animal derived proteins.

2.3. Further Valvular Interstitial Cell Expression Characterization

To investigate the impact of the substrate features on ECM production and phenotypic expression, additional quantified methods can be used. Quantitative reverse transcriptase-polymerase chain reaction (RT-qPCR) can be used to measure mRNA expression of markers associated with activation, α-smooth muscle actin (αSMA), disease (CBFa-1) and ECM proteins (pro-collagen, elastin) of VICs. Cells are lysed and mRNA is isolated using an mRNA isolation kit (Qiagen) followed by reverse transcription (Improm II-Reverse transcription kit, Promega) the cDNA is then amplified using qPCR. Sybr Green provides the fluorescent signal when bound to dsDNA, this is an indication of the concentration of the dsDNA in solution in situ during the PCR procedure. The control gene for these experiments will be GAPDH which is associated with glycolysis.[24] This allows for determination of the fold change of expression of the mRNA of interest as compared to the control gene. The use of qPCR for the quantification of expression is attractive method as it samples an entire population of cells. RT-PCR could provide additional level of understanding of the phenotypic gene expression and ECM secretion by testing for specific marker genes. The reliance on mRNA allows the technique to be much more sensitive to small changes in expression levels then immunocytochemistry staining.

The discovery of the activated VIC (aVIC) cell surface markers such as vascular endothelial growth factor receptor 2(VEGFR2) and angiotensin II Type 1 (AT1), could

allow for the quantification of phenotypic expression levels without destruction of the cell population prior to analysis.[3] Using flow cytometry instead of immunocytochemistry staining or RT-PCR offers rapid analysis of entire populations of VICs cultured on various substrates. The identification of the osteoblastic-like VICs (obVICs) could also be performed by assaying for the expression of receptor activator for nuclear factor ligand (RANKL).[3] Utilization of flow cytometry could allow for analysis of entire populations to generate a greater understanding of the transition of between the different VIC phenotypes.

The AV is composed of primarily type I collagen, but type III collagen (25%) also makes up a significant portion of the valve. In diseased AV the production of both type I and III collagens is shown to vary. [25] The changes in the ratio of type I to type III collagen production could either be a byproduct of signaling pathways in disease or the rigidity of the surrounding matrix. Evaluation of both the production of type I and III collagens could give insight into the role of rigidity in the regulation of the type of ECM produced by the VICs.

3. References

1. Nkomo, V. T.; Gardin, J. M.; Skelton, T. N.; Gottdiener, J. S.; Scott, C. G.; Enriquez-Sarano, M., Burden of valvular heart diseases: A population-based study. *Lancet* **2006,** 368, (9540), 1005-1011.

2. Butler, D. L.; Goldstein, S. A.; Guldberg, R. E.; Guo, X. E.; Kamm, R.; Laurencin, C. T.; McIntire, L. V.; Mow, V. C.; Nerem, R. M.; Sah, R. L.; Soslowsky, L. J.; Spilker, R. L.; Tranquillo, R. T., The impact of biomechanics in tissue engineering and regenerative medicine. *Tissue Eng Part B* **2009,** 15, (4), 477-484.

3. Butcher, J. T.; Mahler, G. J.; Hockaday, L. A., Aortic valve disease and treatment: The need for naturally engineered solutions. *Adv Drug Deliver Rev* **2011,** 63, (4-5), 242-268.

4. Liu, A. C.; Joag, V. R.; Gotlieb, A. I., The emerging role of valve interstitial cell phenotypes in regulating heart valve pathobiology. *Am J of Pathol* **2007,** 171, (5), 1407-1418.

5. Sacks, M. S.; Schoen, F. J.; Mayer, J. E., Bioengineering challenges for heart valve tissue engineering. *Annu Rev Biomed Eng* **2009,** 11, (1), 289-313.

6. Pedron, S.; Peinado, C.; Bosch, P.; Benton, J. A.; Anseth, K. S., Microfluidic approaches for the fabrication of gradient crosslinked networks based on poly(ethylene glycol) and hyperbranched polymers for manipulation of cell interactions. *J Biomed Mater Res A* **2011,** 96A, (1), 196-203.

7. Brown, X. Q.; Ookawa, K.; Wong, J. Y., Evaluation of polydimethylsiloxane scaffolds with physiologically-relevant elastic moduli: Interplay of substrate mechanics and surface chemistry effects on vascular smooth muscle cell response. *Biomaterials* **2005,** 26, (16), 3123-3129.

8. Wells, R. G., The role of matrix stiffness in hepatic stellate cell activation and liver fibrosis. *J Clin Gastroenterol* **2005,** 39, (4), S158-S161.

9. Nemir, S.; West, J. L., Synthetic materials in the study of cell response to substrate rigidity. *Ann Biomed Eng* **2010,** 38, (1), 2-20.

10. Norman, J.; Desai, T., Methods for fabrication of nanoscale topography for tissue engineering scaffolds. *Ann Biomed Eng* **2006,** 34, (1), 89-101.

11. Curtis, A.; Wilkinson, C., Topographical control of cells. *Biomaterials* **1997,** 18, (24), 1573-1583.

12. Curtis, A.; Wilkinson, C., Nantotechniques and approaches in biotechnology. *Trends in Biotechnol* **2001,** 19, (3), 97-101.

13. Khang, D.-Y.; Lee, H. H., Sub-100 nm patterning with an amorphous fluoropolymer mold. *Langmuir* **2004,** 20, (6), 2445-2448.

14. Schift, H., Nanoimprint lithography: An old story in modern times? A review. *J Vac Sci Technol B* **2008,** 26, (2), 458-480.

15. Khang, D. Y.; Kang, H.; Kim, T.; Lee, H. H., Low-pressure nanoimprint lithography. *Nano Lett* **2004,** 4, (4), 633-637.

16. Guo, L. J., Nanoimprint lithography: Methods and material requirements. *Adv Mater* **2007,** 19, (4), 495-513.

17. Cushing, M. C.; Liao, J.-T.; Anseth, K. S., Activation of valvular interstitial cells is mediated by transforming growth factor-[beta]1 interactions with matrix molecules. *Matrix Biol* **2005,** 24, (6), 428-437.

18. Masters, K. S.; Shah, D. N.; Leinwand, L. A.; Anseth, K. S., Crosslinked hyaluronan scaffolds as a biologically active carrier for valvular interstitial cells. *Biomaterials* **2005,** 26, (15), 2517-2525.

19. Wong, J. Y.; Leach, J. B.; Brown, X. Q., Balance of chemistry, topography, and mechanics at the cell-biomaterial interface: Issues and challenges for assessing the role of substrate mechanics on cell response. *Surf Sci* **2004,** 570, (1-2), 119-133.

20. Horbett, T. A.; Waldburger, J. J.; Ratner, B. D.; Hoffman, A. S., Cell adhesion to a series of hydrophili–hydrophobic copolymers studies with a spinning disc apparatus. *J Biomed Mater Res* **1988,** 22, (5), 383-404.

21. Owen, M. J.; Smith, P. J., Plasma treatment of polydimethylsiloxane. *J Adhes Sci Technol* **1994,** 8, (10), 1063-1075.

22. Briggs, D.; Brewis, D. M.; Konieczo, M. B., X-ray photoelectron spectroscopy studies of polymer surfaces. *J Mater Sci* **1976,** 11, (7), 1270-1277.

23. Cushing, M. C.; Liao, J.-T.; Jaeggli, M. P.; Anseth, K. S., Material-based regulation of the myofibroblast phenotype. *Biomaterials* **2007,** 28, (23), 3378-3387.

24. Benton, J. A.; Kern, H. B.; Anseth, K. S., Substrate properties influence calcification in valvular interstitial cell culture. *J Heart Valve Dis* **2008,** 17, (6), 689-699.

25. Eriksen, H. A.; Satta, J.; Risteli, J.; Veijola, M.; Väre, P.; Soini, Y., Type i and type iii collagen synthesis and composition in the valve matrix in aortic valve stenosis. *Atherosclerosis* **2006,** 189, (1), 91-98.